Campylobacter concisus impairs colonic epithelial sodium channel function and aggravates epithelial barrier dysfunction via mucosal immune activation

Dissertation to obtain the academic degree of
Doktor der Naturwissenschaften (Dr. rer. nat.)

submitted to the Department of Biology, Chemistry, Pharmacy
Freie Universität Berlin

by
Praveen Kumar Nattramilarasu

from Berlin

May 31 2021

This dissertation was carried out from October 9, 2017 to May 31, 2021 under the supervision of Prof. Dr. med. Jörg-Dieter Schulzke in the Medical Clinic for Gastroenterology, Infectiology and Rheumatology, Clinical Physiology/Nutritional Medicine, Charité - Universitätsmedizin Berlin, Campus Benjamin Franklin.

1st reviewer:
Prof. Dr. med. Jörg-Dieter Schulzke

Charité - Universitätsmedizin Berlin
Medical Clinic for Gastroenterology, Infectiology and Rheumatology,
Clinical Physiology/ Nutritional Medicine,
Campus Benjamin Franklin
Hindenburgdamm 30
12203 Berlin
Tel. : +49 (0) 30 450 514548
E-Mail: joerg.schulzke@charite.de

2nd reviewer:
Prof. Dr. Petra Knaus

Freie Universität Berlin
Department of Biology, Chemistry and Pharmacy,
Institute of Chemistry and Biochemistry,
Signal Transduction
Thielallee 63
14195 Berlin
Tel. : +49 (0) 30 838 52935
E-Mail: knaus@zedat-fu-berlin.de

Date of defense: 13.09.2021

Acknowledgement:

Performing this work would not have been possible without the help of several people. I thank all of them for their advice and valuable suggestions, which resulted in the successful completion of my doctoral thesis.

First of all, I thank my thesis advisor Prof. Dr. Jörg-Dieter Schulzke for the creation of this exciting research topic and giving me the opportunity to work in his research group. The door to Prof. Schulzke's office was always open whenever I ran into a trouble spot in my experiments or had questions about my research. On a special note, I thank PD Dr. Roland Bücker, who supervised my work. Without his support, this doctoral thesis would not have been a reality. With them, I would like to thank Prof. Dr. Petra Knaus for her valuable suggestions at thesis committee meetings and the supervision of the work.
I thank the fellow doctoral students and colleagues in the research group for providing a friendly working atmosphere. Of note, I would like to thank Anja Fromm, In-Fah Maria Lee, Britta Jebautzke and Claudia Heldt for the excellent technical assistance.

I extend my gratitude to our collaborative research partner Dr. Hans Nielsen from Denmark for providing us with the *Campylobacter concisus* strain used in this study. A special thanks to our collaborative partners in Berlin, PD Dr. Markus M. Heimesaat and Prof. Dr. Stefan Bereswill, and their research group members for their valuable support in conducting animal experiments. I also extend my gratitude to Prof. Dr. Michal-Ruth Schweiger at Cologne for the RNA sequencing and Oliver Nagel for his contribution to analyze the sequencing data through his technical expertise in Bioinformatics.

I sincerely thank the funding partners of the research, DFG and BMBF PAC-Campy consortium. A special thanks to PD Dr. Rita Rosenthal and Prof. Dr. Dorothee Günzel for organizing several events of the graduate school TJ-Train DFG-GRK2318, which was much useful for the progress of this work. With that, I am delighted to thank Prof. Dr. Michael Fromm for his motivation and inspiring ideas.

At last, I would like to thank my mother Dr. Menaka for her moral support in difficult circumstances. I thank all my family members and friends for their extended support. With all these supports, I am confident that I will have an excellent research career in future.

Table of Contents

1. Introduction

1.1. Intestinal epithelium and tight junctions

The epithelium is a thin continuous protective layer of tissue lining the skin, gut, internal organs, and blood vessels throughout the human body. The intestinal epithelium is composed of a single layer of columnar epithelial cells, which forms a physical barrier to prevent the entry of luminal content, harmful pathogens, and antigens into the body. The small and large intestines differ both in their function and anatomy. The epithelium of the small intestine is folded with crypts of Lieberkühn and possesses striated microvilli, whereas the large intestine has crypts but lacks villi (Bowcutt et al., 2014).

A continuous network of different membrane proteins, which form the junctional complex, links the epithelial cells to one another. The transmission and freeze-fracture electron micrographs of the junctional complexes are represented in Figures 1A and 1B. The epithelial junctional complex comprises tight junction (TJ), adherens junction (AJ), and desmosomes, which is depicted in the schematic representation in Figure 1C. The adherens junctions and desmosomes stabilize cell-cell contacts and convey signals for communication across the neighboring cells (Shen et al., 2009), while the primary function of TJ is to create a paracellular barrier between the fluid compartments above and under the epithelial cells (Schneeberger and Lynch, 1992). Ultrastructural analyses by freeze-fracture electron microscopy (FFEM) visualized TJ proteins as an anastomosing network in intercellular connections (Farquhar and Palade 1963; Staehelin et al., 1969) and gap junctions as interlinking proteins of the adjacent epithelial cells (Staehelin, 1972). Since TJs are the principal components of the intercellular epithelial junctions in modulating the barrier function, different TJ proteins, their structure, and functions are briefly discussed in the following sub-sections.

1.1.1 Occludin and tricellulin

Occludin (65 kDa) is the first transmembrane membrane protein characterized in both epithelial and endothelial TJs (Furuse et al., 1993). It has been shown in earlier studies that occludin was not directly linked to the barrier-forming property of the TJs by *in vitro* and *in vivo* experiments

(Saitou et al., 2000; Yu et al., 2005). The transepithelial electrical resistance (TER), which is a direct measure of the barrier function, was not altered in the epithelia of different intestinal segments in homozygous and heterozygous occludin knockout mice (Schulzke et al., 2005). This pointed against a paracellular barrier function of occludin in the intestinal epithelia. However, it was later discovered that occludin plays a crucial role in the maintenance of the intestinal TJ barrier to the passage of macromolecules, as occludin depletion in the *in vitro* and *in vivo* experiments resulted in a selective increase in the flux of macromolecules (Al-Sadi et al., 2011).

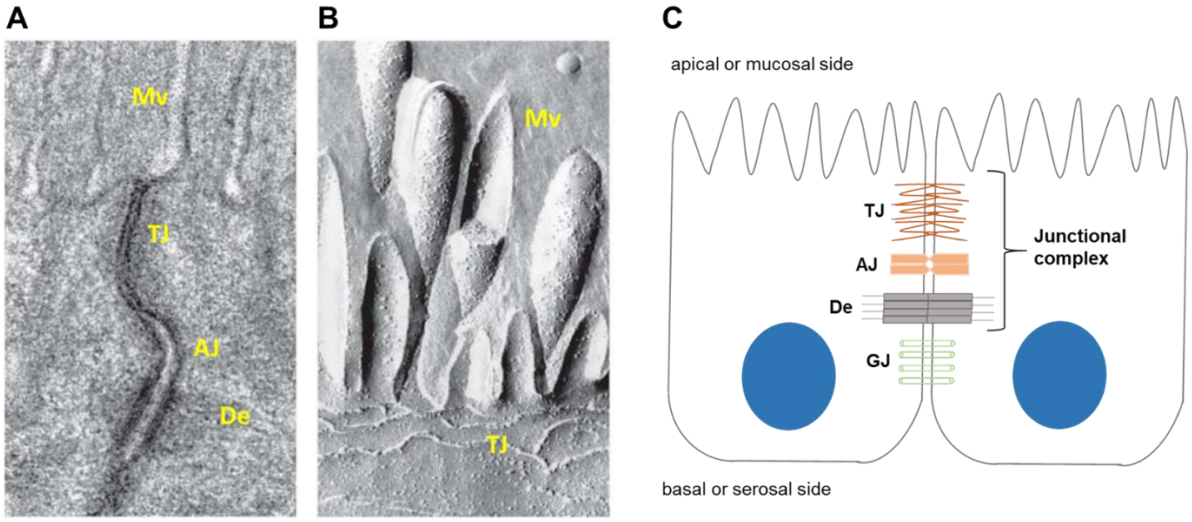

Figure 1. The intercellular junctional complex of the intestinal epithelium. (A) Transmission electron micrograph of tight junction (TJ), adherens junction (AJ), and desmosomes (De) in the intercellular junctions between two villous enterocytes of intestinal epithelial cells. The tight junctions are localized below the microvilli (Mv) (modified from Shen et al., 2011). (**B)** Freeze-fracture electron micrograph with apical Mv and TJ strands in intestinal epithelial cells (modified from Shen et al., 2011). (**C)** Schematic representation of TJ, AJ, and De in the junctional complexes of intestinal epithelial cells. Gap junctions (GJ) are located below the desmosomes.

The TJ proteins in the opposing membranes of two adjacent cells laterally associate with each other to form paired TJ strands (Tsukita et al., 2001), which are referred to as bicellular TJs (bTJs). As bTJs approach the tricellular contact regions, they form tricellular tight junctions (tTJs), in which the central area is vertically oriented and contains three pairs of central sealing elements (Staehelin, 1973). Tricellulin was ascertained as a novel TJ protein localized in tricellular TJ (Ikenouchi et al., 2005). It was proposed that the TJ protein tricellulin might be directly involved in the lateral association of central sealing elements to make TJs functionally

continuous at the tricellular cell contact points and thereby form a stable epithelial barrier at tTJ (Ikenouchi et al., 2005). This was confirmed by *in vitro* experiments, which depicted that tricellulin forms a paracellular barrier to macromolecules in tTJ (Krug et al., 2009). Later, it was discovered that the angulin family of proteins, angulin-1 and angulin-2, recruits tricellulin to tricellular cell contacts (Masuda et al., 2011; Higashi et al., 2013). Hence, the angulins and tricellulin synergistically function to seal the central tube of the tricellular contacts and prevent the entry of luminal antigens and harmful pathogens into the intestinal mucosa.

1.1.2 Claudins

Claudins are integral membrane proteins of bTJ and form the backbone of the TJ strands. The molecular weight of claudins is in the range of 20-27 kDa, and each claudin comprises four transmembrane domains, two extracellular loops designated as ECL-1 and ECL-2, an intracellular loop, and intracellularly located C- and N-terminal ends (Furuse et al., 1998). The C-terminal ends of the claudins were shown to bind the PDZ domains of the cytoplasmic scaffolding proteins zonula occludens-1 (ZO-1), ZO-2, and ZO-3 (Itoh et al., 1999). However, the longer C-terminal ends differ in the claudins with different PDZ binding domains to ZO-1 (Krause et al., 2008). In mammals, 27 different claudins have been characterized to date (Günzel, 2017), of which 14 variants are established in the human intestine (Günzel and Yu, 2013). The claudins are expressed in varying degrees in different intestinal segments (Chiba et al., 2008, Luettig et al., 2015). Although the structure and function of the intestinal claudins are not completely characterized so far, they were broadly classified into two categories: i) sealing claudins (claudin-1, -3, -4, -5, -8, -11, -14, and -19), which seals the epithelial TJ; ii) channel-forming claudins (claudin-2, -10a, -10b, -12, -15, and -17), which form channels across the TJ for selective passage of ions and/or water (Günzel and Fromm, 2012). Furthermore, the channel-forming claudins exhibit specific selectivity and form channels either to anions, cations, or both cations and water. The anion-selective claudins are claudin-10a and claudin-17 (Günzel et al., 2009; Krug et al., 2012). The cation-selective claudins include claudin-10b, claudin-12, and claudin-15 (Alexandre et al., 2007; Fujita et al., 2008; Günzel et al., 2009; Tanaka et al., 2016). Claudin-2 and claudin-15 exhibit selectivity for both water and cations (Amasheh et al., 2002; Rosenthal et al., 2010; Tamura et al., 2011; Rosenthal et al., 2020).

The junctional adhesion molecule (JAM) also belongs to the group of transmembrane proteins. The JAM, occludin, tricellulin or MARVEL (Myelin and lymphocyte and related proteins for vesicle trafficking and membrane link) D2 and MARVEL D3 exhibit distinct but overlapping functions. Therefore, they are classified under a single family of tight junction-associated MARVEL proteins abbreviated as TAMPs (Raleigh et al., 2010). More importantly, the TJ proteins bind to the intracellular scaffold proteins ZO-1, ZO-2, and ZO-3, which in turn are linked to the actin cytoskeleton proteins (Van Itallie and Anderson, 2014). The interactions among the different TJ proteins also play a crucial role in maintaining the integrity of the epithelial barrier. The interactions between the proteins present within a cell membrane are defined as cis-interactions, whereas the interactions between the membrane proteins of the opposing cells are defined as trans-interactions (Krause et al., 2008). Furthermore, TJ proteins facilitate the polarization of the epithelial cells by preventing the intermixing of transmembrane proteins between the apical and basolateral compartments, which is referred to as fence function (Mandel et al., 1993). They can also act as selective channels for the movement of ions and electrolytes, which is referred to as gate function (Mandel et al., 1993). The crosstalk of several intracellular cell signaling pathways regulates the function and assembly of TJ proteins (González-Mariscal et al., 2008). In addition, they are also regulated by different mechanisms involved in gene expression and epithelial cell differentiation (Balda and Matter, 2009). More importantly, the downregulation in the expression of TJ proteins and their subcellular redistribution represents the molecular correlate of the intestinal barrier dysfunction induced by diarrheal pathogens like *Shigella* spp., *Salmonella* spp., and *Yersinia enterocolitica* (Sakaguchi et al., 2002; Tafazoli et al., 2003; Hering et al., 2016). Besides the pathogenic invasion of the intestinal barrier with its subsequent detrimental effects, the inflammatory response from the gut mucosal immune system also plays a pivotal role in regulating the intestinal barrier function.

1.2 Regulation of the intestinal barrier function by the gut mucosal immune response

The gut mucosal immune system has evolved mechanisms to counteract pathogens and food antigens (Janeway, 2001). The surface of the intestinal epithelium is covered with mucus layers, of which the mucus layer is thicker in the large intestine compared with the small intestine (Bowcutt et al., 2014). The pre-epithelial mucus layer, which is the first line of defense in the gut wall, is secreted by goblet cells of the intestinal epithelium (Pabst, 1987). The lamina propria is the loose connective tissue layer below the epithleium, which extends from the villus

to crypts of the intestinal epithelium and forms the core region of intestinal mucosa. It hosts the body's largest population of immune cells, which include the inductor and effector immune cells (McGhee and Fujihashi, 2012). The macrophages in the lamina propria elicit an inflammatory response against the harmful pathogens and antigens, which breach the intestinal epithelial barrier from the outer mucus layer (Smith et al., 2011). However, the uncontrolled immune response of macrophages to the pathogens can be detrimental to the host epithelium by disruption of TJs.

Based on the expression of surface cell receptors, the macrophages were classified into M1- and M2-type macrophages. However, this is not true in the case of gut-resident macrophages, as they possess the hallmarks of both M1 and M2 subtypes (Mowat and Bain, 2011). M1-macrophages in the lamina propria induce epithelial barrier dysfunction by TJ modifications in the context of intestinal inflammation (Lissner et al., 2015). In response to the inflammatory stimulus, macrophages secrete the pro-inflammatory cytokines like tumor necrosis factor (TNF)-α, interleukin (IL)-1, IL-8, IL-12, and IL-6 (Duque and Descoteaux, 2014). In addition, the macrophages also maintain functional homeostasis in intestinal tissues by ameliorating inflammation through anti-inflammatory cytokines like IL-10 (Takada et al., 2010).

In response to pathogenic stimuli in the mucosal compartment, the macrophages secrete proinflammatory cytokines, which can induce epithelial barrier defects via TJ disruption. This phenomenon was described in an *in vitro* experiment with the human immunodeficiency virus (HIV), in which the supernatants from the coculture of HIV and monocyte-derived macrophages decreased TER in HT-29 cells by ZO-1 disruption and epithelial cell apoptosis (Schmitz et al., 2002). Although HIV enhances the release of TNF-α, interferon (IFN)-γ, IFN-α, and IL-1β from macrophages, TNF-α and IFN-γ were proposed as the key cytokines in modulating the epithelial barrier function (Schmitz et al., 2002). The phenomenon of enhanced cytokine release by macrophages in response to pathogenic stimuli was also evident in bacterial infections, for instance in *Campylobacter jenuni* and *Aeromonoas hydrophila*, which in turn induce epithelial barrier damage (Bücker et al., 2018; Lobo de Sá et al., 2019; Dong et al., 2018). Apart from the regulation of epithelial barrier function, the proinflammatory cytokines also modulate the ion transport functions of the intestinal epithelium.

1.3 Epithelial sodium channel (ENaC) and intestinal transport function

The epithelium maintains functional homeostasis in different segments of the small and large intestine by transport of ions and water across the mucosal and serosal sides. The sodium (Na^+) and potassium (K^+) transport across the tight epithelia in the kidney and colon is substantial for the electrolyte balance in the human body despite large variations in the diet. The absorption of Na^+ was depicted for the first time in the human colon along with chloride (Cl^-) and water transport (Levitan et al., 1962). Epithelial sodium channel (ENaC) is an amiloride-sensitive Na^+ channel localized in the apical membrane of epithelial cells in lungs, sweat glands, distal nephron, and distal colon, and absorbs Na^+ into the cells by electrogenic transport (Canessa et al., 1994). The colonic ENaC plays a pivotal role in diarrheal patients as an increase in electrogenic Na^+ absorption by ENaC compensates the loss of electroneutral Na^+ absorption by sodium-hydrogen antiporter 3 (NHE3) (Schultheis et al., 1998), and prevents loss of water into the lumen. Of note, the human colon absorbs 90% of the 1.5-2.0 L of the ileal effluent, which passes through the ileocaecal valve daily to prevent loss of water into the lumen (Debongnie and Phillips, 1978).

The electrogenic absorption of Na^+ via ENaC functions in concert with the activity of the Na^+K^+ATPase located at the basolateral membrane of colonic epithelia. The extrusion of three Na^+ ions into the serosa and intake of two K^+ from serosa into the cells through the Na^+K^+ATPase creates a negative intracellular electrical potential difference, which in turn drives the passive flow of Na^+ from the lumen into the cells via ENaC (Figure 2A). ENaC was initially reported as a tetrameric channel with 2α, β, and γ subunits, whose coordinated activity is responsible for the pore formation in ENaC and the transport of Na^+ into the cell (Kosari et al., 1998; Firsov et al., 1998). However, the stoichiometry of ENaC subunits was later confirmed as 3:3:3 by Fluorescence Resonance Energy Transfer (FRET) studies (Strauschenko et al., 2004). In the large intestine, the α-ENaC is constitutively expressed, while the expression of β- and γ-ENaC genes are regulated by glucocorticoids and mineralocorticoids (Fuller et al., 2000; Amasheh et al., 2000). The adjacent localization of three different ENaC subunits in the apical membrane of colonic epithelium is depicted in Figure 2B.

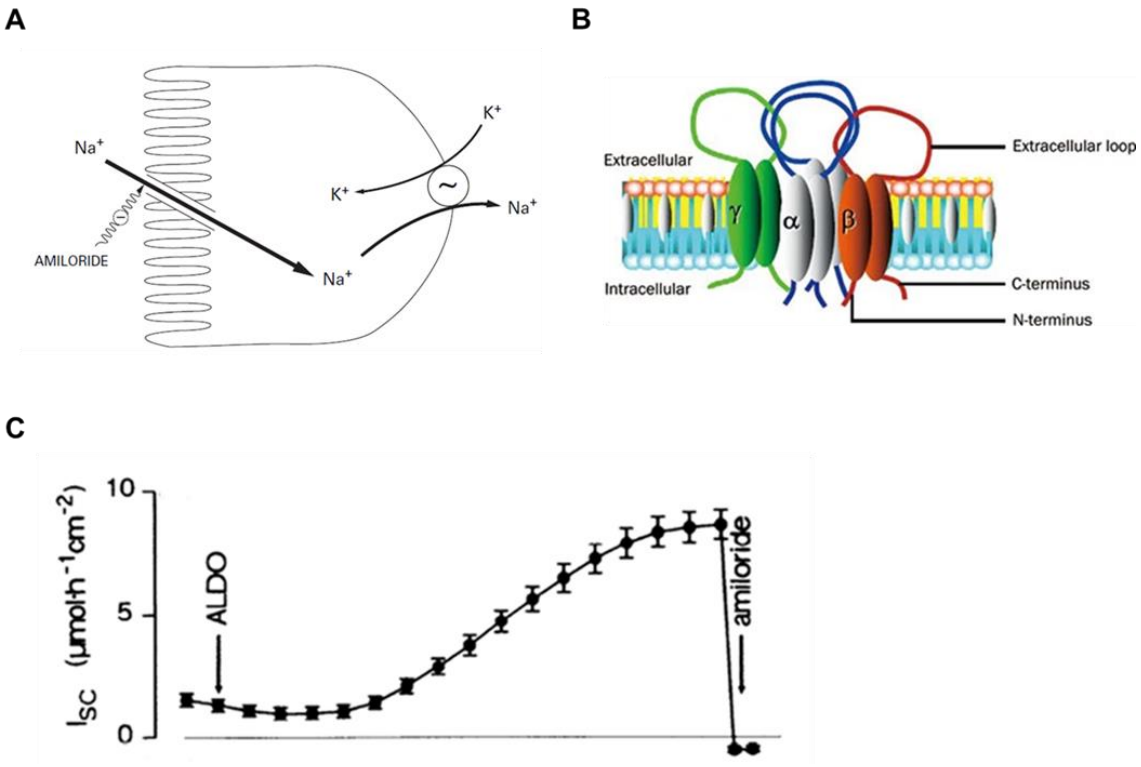

Figure 2. Epithelial sodium channel (ENaC) and electrogenic sodium absorption. **(A)** A cellular model of electrogenic sodium absorption in colonic epithelium. On the basolateral side of the epithelium, three Na^+ ions are transported from the cells to the serosal side for every two K^+ ions transported into the cells through Na^+K^+ATPase. This creates a lumen-negative electric potential difference, which in turn leads to a passive flow of Na^+ from the lumen into the cells via amiloride-sensitive ENaC in the apical side (adapted from Sandle, 1998). (**B)** ENaC subunits α, β, and γ possess two transmembrane domains, a large extracellular loop and an intracellular C-terminal and N-terminal ends (adapted from Sun et al., 2011). **(C)** Amiloride-sensitive Na^+ absorption via ENaC in the rat distal colon measured in the Ussing chambers. The tissues of the distal colon are mounted in the Ussing chamber and stimulated with aldosterone (ALDO) for 8 h, which increases the short-circuit current (I_{sc}) as a result of an increase in ENaC activity (ENaC-mediated Na^+ absorption). ENaC-blocker amiloride is added at a concentration of 100 µM to the mucosal side of the tissue, as a result of which I_{sc} drops to its basal value. The difference in I_{sc} after amiloride treatment at the mucosal side (ΔI_{sc}) reflects the ENaC activity (adapted from Fromm et al., 1993)

ENaC activity is regulated by the mineralocorticoid aldosterone at the genomic level. The effect of aldosterone in the regulation of ENaC in tissues is divided into three phases: - i) a latent phase (30-90 min after aldosterone stimulation) with receptor binding, translocation, and gene activation, ii) an early phase of increasing Na^+ transport (30 min-4 h after aldosterone stimulation) accompanied by an increase in tissue conductance, iii) a phase with a continued rise in Na^+ transport rate (4-12 h after aldosterone stimulation) with further increase in tissue conductance after stimulation of the basolateral Na^+K^+ATPase (Benos et al., 1995). Amiloride

is a potassium-sparing diuretic drug used in the clinics, which is also used for the molecular analysis of Na^+ entry into the cells in tight epithelium (Benos, 1982). The potential difference of the epithelial membranes was first reported in Ussing chambers by voltage-clamp technique (Schoen and Candia, 1978), which formed a basis for the experimental measurements of ion fluxes in the Ussing chamber (Fossat and Lahlou, 1982). The voltage-clamp technique in Ussing chambers was then used to measure Na^+ transport by ENaC in the distal colon of rats by an increase in short-circuit current (I_{sc}) 8 h after aldosterone (3 nM) stimulation (Fromm et al., 1993).

Amiloride blocks ENaC by binding to the extracellular domain of the α-ENaC pore and thereby prevents Na^+ absorption from the intestinal lumen into the cells (Schild et al., 1997; Kieber-Emmons et al., 1999). The aldosterone-dependent increase and subsequent decrease in I_{sc} after ENaC blockade by amiloride is depicted in Figure 1C. The aldosterone-mediated increase in ENaC activity in the distal colon was accompanied by transcriptional upregulation of regulatory β- and γ-ENaC subunits (Epple et al., 2000). In addition to aldosterone, butyrate and glucocorticoid were also ascertained as important mediators of increased colonic ENaC activity (Bergann et al., 2009a; Zeissig et al., 2006; Zeissig et al., 2007a). In the pathophysiology of inflammatory bowel diseases (IBD), the malfunction of ENaC is mediated by proinflammatory cytokines like IL-1β and TNF-α (Barmeyer et al., 2004; Amasheh et al., 2004). In the IL-$2^{-/-}$ mouse model, the colitis with clinical and morphological similarities to ulcerative colitis (UC) exhibited a defective Na^+ absorption via ENaC in the distal colon despite an intact epithelial barrier function (Barmeyer et al., 2003). A recent study demonstrated that IL-13, a Th-2 cytokine that is implicated in the pathogenesis of UC, induced ENaC dysfunction in the colonic epithelium, which is in turn modulated by intracellular mitogen-activated protein kinase (MAPK) signals (Dames et al., 2015). Therefore, the functional ENaC activity induced by corticoid hormones and butyrate in the colonic epithelium are negatively regulated by certain proinflammatory cytokines via intracellular MAPK signaling.

Besides ENaC, the membrane protein Down-regulated in adenoma (DRA) is an absorptive ion transport channel. The gene expression of DRA was first ascertained in mucosal epithelia of colon tissues and was inhibited in adenomas and adenocarcinomas (Schweinfest et al., 1993). The mutation in the DRA gene caused congenital chloride diarrhea (Höglund et al., 1996). DRA was later identified as a Na^+-independent electroneutral chloride (Cl^-)/bicarbonate (HCO_3^-)

exchanger in the apical membrane of HEK 293 cells with active Cl^- absorption and HCO_3^- secretion (Melvin et al., 1999). In addition, it was also found to act in concert with NHE3 to absorb NaCl in the colon (Melvin et al., 1999). NHE3 is characterized as a major Na^+ absorptive channel in the intestine (Bookstein et al., 1994), which is localized in the surface of epithelial cells of the proximal colon (Dudeja et al., 1996). The different isoforms of NHE, namely NHE1, NHE2, and NHE3 have been later identified in the crypt epithelial cells of the rat distal colon (Rajendran et al., 2001).

Apart from the absorptive functions of the intestinal epithelium, the secretion of ions also plays an important role in maintaining intestinal homeostasis. Cl^-, HCO_3^- and K^+ constitute the major ions secreted into the intestinal lumen via a transcellular route through ion transport channels, which differ in their molecular structures and intrinsic biophysical properties (Schulzke et al., 2014). A recent study demonstrated that Cl^- secretion was carried out by colonocytes of both, crypt and surface epithelial cells expressing the apical cystic fibrosis transmembrane conductance regulator (CFTR), whereas K^+ secretion was carried out by goblet cells (Linley et al., 2014). This defies the ancient concept of absorption and secretion in the intestinal epithelium, which proposed that the surface epithelial cells are responsible for the absorptive function and crypt epithelial cells exclusively carry out the secretory functions (Welsh et al., 1982).

The Cl^- secretion into the lumen via CFTR is also regulated by Cl^- uptake into the cell from the serosal side via Na^+-coupled Cl^- co-transport by $Na^+K^+2Cl^-$ co-transporter 1 (NKCC1), which is in turn regulated via K^+ extrusion through basolateral intermediate-conductance calcium (Ca^{2+})-activated K^+ channel (IK) (Field, 2003; Rajendran and Sandle, 2018). Furthermore, the Na^+ absorption in ENaC and NHE3 are also regulated indirectly via IK channels, as it maintains the low intracellular Na^+ levels by modulating the activity of Na^+K^+ATPase to create a negative membrane potential for Na^+ absorption from the lumen into the cell (Rajendran and Sandle, 2018). The regulation of Cl^- secretion and Na^+ absorption through different transmembrane ion channels is depicted in Figure 3. Furthermore, the intracellular messengers like cyclic adenosine monophosphate (cAMP), cyclic guanosine monophosphate (cGMP), Ca^{2+}, and protein kinase C (PKC) either activate or regulate the Cl^- secretion into the lumen (Schulzke et al., 2014).

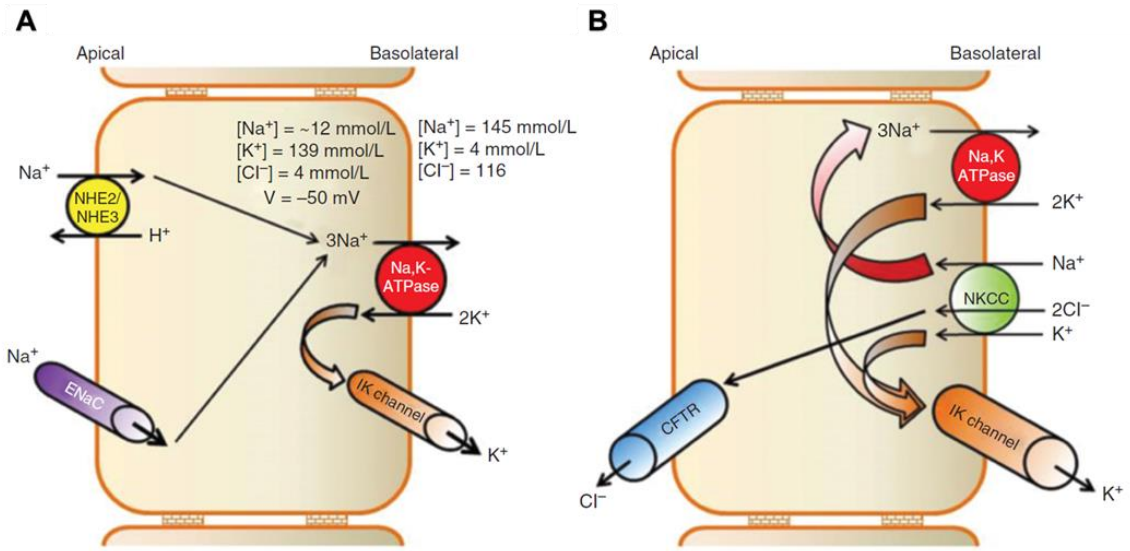

Figure 3. The regulation of sodium absorption and chloride secretion in the colonic epithelia through different transmembrane ion channels. (A) Under basal conditions, the Na^+K^+ATPase acts in concert with basolateral intermediate-conductance calcium (Ca^{2+})-activated potassium channel (IK) channels, which synergistically increases the intracellular potassium (K^+) and decreases sodium (Na^+) to create a negative membrane potential of -50 mV. This in turn drives the Na^+ absorption via epithelial sodium channel (ENaC) and sodium-proton exchanger isoform 2/3 (NHE2/3). **(B)** The apical chloride (Cl^-) exit into the lumen via cystic fibrosis transmembrane conductance regulator (CFTR) is regulated by basolateral Cl^- uptake by $Na^+K^+2Cl^-$ co-transporter 1 (NKCC1). The Cl^- uptake via NKCC1 tends to depolarize cells, which is counter-balanced by K^+ exit through the IK channel. This in turn creates the electrical gradient for the sustained Cl^- secretion via CFTR (modified from Rajendran and Sandle, 2018).

To briefly sum up the transport functions, the coordinated activity of ENaC with the other ion transport channels in the large intestine is responsible for the electrolyte balance, and thereby maintains the functional homeostasis. Diarrhea results from imbalances in intestinal absorption and secretion, and different regulatory events influence the malfunction in intestinal absorption and secretion. For instance, activation of adenylate/guanylate cyclase occurs by enterotoxic pathogens like *Vibrio cholerae* or *Escherichia coli*, which enhances the Cl^- secretion accompanied by loss of Na^+ and water into the lumen, the phenomenon which is referred to as enteric tears (Cooke, 1998). The mechanisms of infectious diarrhea with a special focus on *Campylobacter* spp.-induced diarrhea are described in the following section.

1.4 Diarrheal mechanisms in human campylobacteriosis

Based on pathophysiological mechanisms exhibited by *Campylobacter* spp. in the context of infectious diarrhea, diarrhea has been broadly classified into the secretory, the malabsorptive, and the leak flux diarrhea, which was recently reviewed (Lobo De Sá et al., 2021a). Secretory diarrhea induced by *Campylobacter* spp. was ascertained to exhibit a pathomechanism similar to cholera toxin (CT) with intraluminal fluid accumulation in rat ileal loop model, and an increase in intracellular cAMP levels in Chinese hamster ovary (CHO) cells by *Campylobacter jejuni* enterotoxins (Ruiz-Palacios et al., 1983; Wassenaar, 1997). Although the enterotoxic property of *C. jejuni* was depicted through functional assays (McCardell et al., 1984), the existence and functionality of *C. jejuni* enterotoxin remained elusive as the sonicates of *C. jejuni* and *Campylobacter coli* were not enterotoxic to CHO cells (Waldström et al., 1983). A recent *in vivo* study on the physiological effects of *C. jejuni* in the human colon identified that the colon biopsy of infected patients lacked active Cl^- secretion as basal I_{sc} was unchanged along with controls (Bücker et al., 2018), which confirmed that *C. jejuni* does not induce secretory diarrhea with a pathomechanism similar to CT.

Concerning malabsorptive diarrhea induced by *Campylobacter* spp., downregulation of different ion transporters and channels were reported to date only in the large intestine (Lobo de Sá et al., 2021a). In colon biopsies of IBD patients, the malabsorption in the surface epithelium was attributed to defective Na^+ transport via ENaC in the non-inflamed regions of the colon (Sandle et al., 1990). The absorptive transport functions were inhibited by *C. jejuni* in Caco-2 cells with fluid accumulation and cell dome formation, which indicated that malabsorption plays a pivotal role in *Campylobacter*-induced diarrhea (MacCallum et al., 2005). In the *in vivo* studies, transcriptional downregulation of CFTR is also accompanied by downregulation of another absorptive ion channel, DRA, in the colon mucosae of *C. jejuni*-infected patients, which indicated a compromised electroneutral Cl^- absorption (Bücker et al., 2018). More importantly, *C. jejuni* inhibits the functional ENaC activity in the human colon with downregulation of regulatory ENaC subunits (β, γ) and an increase in the release of epithelial proinflammatory cytokines (Bücker et al., 2018). Therefore, Na^+ malabsorption by ENaC dysfunction was confirmed as one diarrheal pathomechanism of *C. jejuni*. In addition to ENaC, Na^+/K^+-ATPase localized in the basal membrane of the colonic epithelial cells was also inhibited after *C. jejuni* infection (Kanwar et al., 1994). However, the differential regulation of NHE by *Campylobacter* infections has not been reported to date, although the expression and

function of NHE were regulated by different infections as reviewed in a previous study (Gurney et al., 2017).

Leak flux diarrhea is characterized by a passive flow of water and solutes into the intestinal lumen mainly via the paracellular route. This might result from barrier dysfunction induced by perturbation in the epithelial TJs or apoptotic leaks in epithelia (Schulzke et al., 2009). The term "leak flux mechanism" describes the epithelial barrier dysfunction by TJ perturbations and epithelial apoptosis or other cell death mechanisms, which in turn leads to loss of water and solutes from the circulation into the intestinal lumen (Figure 4). For instance, cytokines like TNF-α can induce epithelial apoptosis (Gitter et al., 2000), and cause diarrhea by the leak flux mechanism. In the context of infectious diarrhea, leak flux mechanism with epithelial barrier defects was first demonstrated in HIV enteropathy (Stockmann et al., 1998). Later, the bacterial infections of *Y. enterocolitica* and *Arcobacter butzleri* were also found to exhibit the leak flux diarrheal pathomechanism (Hering et al., 2011; Hering et al., 2016; Bücker et al., 2009). This was also evident in the diarrheal pathogenesis of *Campylobacter* spp. (Nielsen et al., 2011; Bücker et al., 2017; Bücker et al., 2018).

Taken together, the watery type of *Campylobacter*-induced diarrhea can result from either the malfunctions in intestinal secretion and absorption or from the leak flux pathomechanism. The epithelial leaks induced by *Campylobacter* spp. can result in the influx of bacterial enterotoxins and/or antigens or the transmigration of bacteria from the lumen into the mucosa. This can in turn aggravate the immune response of mucosal immune components leading to a vicious circle of intestinal epithelial barrier dysfunction and immune activation (*leaky gut* phenomenon), which is depicted in Figure 4.

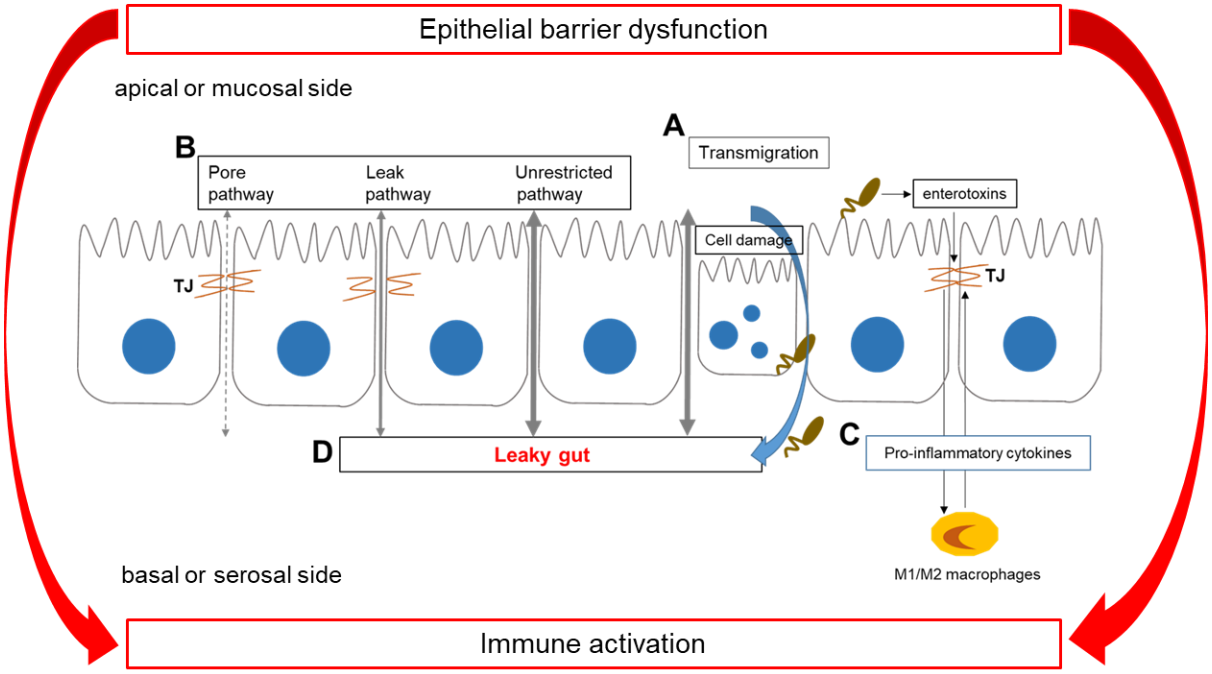

Figure 4. The leak flux pathomechanism with the vicious circle of epithelial barrier dysfunction and mucosal immune activation (*leaky gut* concept) in human campylobacteriosis (modified from Lobo de Sá et al., 2021a). It comprises the following events. **(A)** Bacterial passage by transcellular translocation through transcytosis or paracellular transmigration via cleavage of tight junction (TJ) proteins by secreted enterotoxins e.g., zonula occludens toxin (ZOT) without any changes in the permeability for water and solutes. **(B)** Opening of leak pathway (permeability for solutes < 100 Å) by direct interaction of bacteria with the epithelium and disruption of TJ. Opening of the unrestricted pathway (permeability for solutes > 100 Å) through detrimental effects on the epithelium by cell damage induced by bacteria. **(C)** The contribution of proinflammatory cytokines from subepithelial immune cells (M1/M2 macrophages) can aggravate the bacterial-induced TJ disruption and results in diarrhea by opening of the pore pathway (permeability for solutes < 6 Å), leak pathway or unrestricted pathway, all of which is described as leak flux pathomechanism of diarrhea. **(D)** The luminal antigen influx via the opening of the leak pathway and unrestricted pathway can potentiate the epithelial barrier dysfunction (*leaky gut* phenomenon).

1.5. *Campylobacter concisus*

Campylobacter concisus is a Gram-negative, asaccharolytic, rod-shaped, and motile bacterium first identified in the periodontal pockets of patients with severe gingival inflammation (Tanner et al., 1981; Tanner et al., 1985). It was later found that *C. concisus* exhibit a chemotactic response to formate, which enables the bacterium to colonize plaque-laden periodontal pockets (Pastor and Gibbons, 1986). It was also proposed in the same study that hydrogen (H_2) can be a possible chemo-attractant to *C. concisus*. A holistic approach to characterize the subgingival microflora of periodontal pockets found an increase in *C. concisus* colonization in the diseased

microflora of periodontitis patients (Moore et al., 1985). Moreover, *C. concisus* was increasingly isolated from active inflammation sites of periodontal pockets (Tanner et al., 1987). However, no clear correlation was established between the colonization of *C. concisus* in the oral cavity of periodontal patients and its corresponding pathogenesis. *Campylobacter concisus* was resistant to tetracycline treatment, whereas the other bacteria like *Wolinella recta, Bacteroides gracilis* (now *Campylobacter gracilis*) and *Eikenella corredens* in the oral lesions were susceptible to tetracycline (Tanner et al., 1987). Interestingly, *C. concisus* was also detected in extra-oral sites and was found to be mainly associated with gastroenteritis and diarrhea as discussed below.

1.5.1 *Campylobacter concisus* in extra-oral human diseases

The first non-oral isolation of *C. concisus* was reported in a patient with diabetic foot ulcer with the underlying condition of osteomyelitis (Johnson and Finegold, 1987). Since the infection in foot ulcer was polymicrobial and *C. concisus* was eradicated following cefoxitin treatment for foot ulcer, the pathogenicity of *C. concisus* in the context of foot ulcer or osteomyelitis was dispensable. Interestingly, *Campylobacter* spp. characterized with electrophoretic techniques and immunotyping identified 22 different strains of *C. concisus* from patients with gastrointestinal disorders (Falsen et al., 1987; Vandamme et al., 1989). Furthermore, *C. concisus* was increasingly detected in the feces of patients with gastrointestinal disorders, which implied the association of *C. concisus* with gastroenteritis (Vandamme et al., 1989; Maher et al., 2003). Moreover, *C. concisus* was ascertained as one of the frequent non-*C. jejuni*/*C. coli* *Campylobacter* spp. isolated from the stools of diarrheal children (Lindblom et al., 1995). In another clinical epidemiology study, two different strain types of *C. concisus* were identified in the feces of diarrheal immunocompromised patients (Aabenus et al., 2002). However, no statistical differences were found between the isolation rates of *C. concisus* in the feces of healthy and diarrheal patients (Van Etterijck et al., 1996). Therefore, it has been difficult to elucidate the role of *C. concisus* in the pathophysiology of acute infectious diarrhea.

A clinical study with a large cohort of diarrheal patients to compare the clinical manifestations of *C. concisus* and *C. jejuni*/*C. coli* infections in patients, identified that majority of *C. concisus*-infected patients presented prolonged diarrhea (> 2 weeks) compared with *C. jejuni*-infected patients (Nielsen et al., 2012). Furthermore, *C. concisus*-infected patients presented only a mild fever with low plasma C-reactive protein (CRP) and fecal calprotectin levels compared with *C.*

jejuni-infected patients (Nielsen et al., 2012; Nielsen et al., 2013), which indicates that *C. concisus* infection does not induce a severe enteric or systemic inflammation, unlike *C. jejuni*/*C. coli*. *Campylobacter concisus* was also found to exhibit pathogenic properties in colonic epithelial cells *in vitro* with TJ modifications and cellular apoptosis (Nielsen et al., 2011; Man et al., 2010a). A recent case study reported *C. concisus* in a pulmonary abscess of an immunocompromised patient who underwent allogeneic stem cell transplantation. However, this was later concluded as an endogenous infection under immunosuppressive conditions (Hagemann et al., 2018). Since two different phenotypically indistinguishable groups of *C. concisus* strains were identified in feces of diarrheal patients (Aabenhus et al., 2002), the genetic heterogeneity of *C. concisus* was characterized using amplified fragment length polymorphism (AFLP), which classified *C. concisus* into four genetically distinct taxonomic groups i.e., genome species (GS) (Aabenhus et al., 2005). Out of the four GS, the majority of the strains belonged to GS1 and GS2 subtypes, in which GS2 was predominantly associated with fever, gut inflammation, chronic diarrhea, and bloody stools (Aabenhus et al., 2005). A recent study with a complete genome characterization indicated that the *C. concisus* strains classified under GS2, possess larger bacterial genome size, and higher guanine (G) plus cytosine (C) content in the genome (Wang et al., 2017). This indicates that GS2 *C. concisus* strains might possess additional virulence factors, for instance, extrachromosomal plasmids or enterotoxins to exert their pathogenicity in different diseases.

1.5.2. Virulence factors of *Campylobacter concisus*

The first evidence of the virulence factors attributed to *C. concisus* rooted in a clinical study in Italy, which identified unusual *Campylobacter* spp. from stool samples of children with enteritis. *Campylobacter concisus* was found to be one of the major atypical *Campylobacter* spp., which induced the elongation of CHO cells in a mechanism similar to *C. jejuni* subsp. *doylei* (Musmano et al., 1998). Later, different virulence factors associated with *C. concisus* were determined in the context of diarrheal pathogenesis and intestinal barrier dysfunction.

1.5.2.1 Hemolysin

A hemolytic protein, phospholipase A2 (PLA2), was identified as one of the potential virulence factors in *C. concisus* that caused stable vacuolating and cytolytic effects on CHO cells (Istivan et al., 1998). Furthermore, PLA2 was delineated as a membrane-bound hemolysin and enhanced

hemolytic activity of the strains corresponding to both of the sub-categories: GS1 and GS2 of *C. concisus* (Istivan et al., 1998; Istivan et al., 2004). The hemolytic activity of PLA2 was detected in clinical isolates of *C. concisus* obtained from children with enteritis and induced hemolysis in human and rabbit erythrocytes (Istivan et al., 2004). This was confirmed by contact hemolysin assays, in which the crude suspensions and the pellets of *C. concisus* show similar hemolytic activity to erythrocytes. Interestingly, *C. concisus* strains had shown a strong cell-associated hemolytic activity to human and rabbit erythrocytes when compared with *C. jejuni* and *C. coli* (Istivan et al., 2004).

Further investigations to elucidate the possible genes associated with the membrane-bound hemolytic activity resulted in the identification of the complete *pldA* gene that encodes PLA2 in *C. concisus* (Istivan et al., 2008). The *pldA* gene of the human-hosted *C. concisus* shares a similarity of more than 98% to the *pldA* of classical zoonotic diarrheal pathogen *C. coli*. Since the hemolytic activity of *C. concisus* by PLA2 was similar to other pathogenic *Campylobacter* spp., *C. concisus* was thought to be a possible enteropathogen (Istivan et al., 2008). An assessment of *in vitro* pathogenesis indicated that the two genetically distinct groups of *C. concisus*, GS1 and GS2, exhibit a different pathogenic mechanism to cause intestinal diseases in humans as reviewed earlier (Kalischuk and Inglis, 2011). GS2 isolates found in diarrheic patients showed higher levels of invasion and translocation in colonic epithelial T84 cell monolayers, whereas GS1 isolates were predominantly detected in non-diarrheic patients and exhibited an increased apoptotic fragmentation, IL-8 induction and/or carriage of toxin genes (Kalischuk and Inglis, 2011).

1.5.2.2 Enterotoxins

The enterotoxins secreted by *C. concisus* might play a pivotal role in the diarrheal pathogenesis of *C. concisus*. In 2005, a Danish study observed cytolethal distending toxin (CDT)-like effect on Vero cells by fecal isolates of *C. concisus* from diarrheal patients (Engberg et al., 2005). However, CDT-like effect was also detected in fecal *C. concisus* isolates from healthy individuals, and no clear phenotypic and genotypic differences were observed between *C. concisus* isolates from diarrheal patients and healthy carriers (Engberg et al., 2005). Hence, this study proposed further investigations on other virulence factors of *C. concisus*, which might contribute to diarrheal pathogenesis. Different epidemiological studies in Australia identified a

higher prevalence of *C. concisus* in fecal samples and mucosal biopsies of IBD patients compared with non-IBD and healthy controls (Man et al., 2010b; Zhang et al., 2010; Mahendran et al., 2011), although the prevalence of oral *C. concisus* isolates did not vary much between the group of IBD patients and healthy controls. However, the ectopic oral *C. concisus* colonization and oral microbiota dysbiosis should be elucidated in future studies for a better understanding of IBD pathogenesis (Qi et al., 2021).

To unravel the pathogenetic potential of *C. concisus* in the context of IBD and to delineate the virulence factors conferred by *C. concisus*, the secreted proteins of *C. concisus* were characterized in a strain isolated from the cecal biopsy of a Crohn's disease (CD, a subgroup of IBD) patient (Kaakoush et al., 2010 and Kovach et al., 2011). The secretome analysis revealed that *C. concisus* possesses several putative virulence factors like adhesin, hemolysin, S-layer-RTX protein and outer membrane protein (OMP)-18, which are present in other *Campylobacterales* (Kaakoush et al., 2010). Of note, zonula occludens toxin (ZOT) was also found to be secreted by *C. concisus*. ZOT is a diarrheal toxin first identified in *V. cholerae* (Fasano et al., 1991), which was known to induce an increase in intestinal permeability and promote transient TJ changes in the intestinal epithelium (Schmidt et al., 2007). However, proteomic analysis revealed that *C. concisus* ZOT had only four conserved domains with that of *V. cholerae* ZOT (Kaakoush et al., 2010). Interestingly, three different polymorphisms in ZOT genes (zot^{808T}, $zot^{350\text{-}351AC}$ and $zot^{Multiple}$) were detected in oral *C. concisus* isolates from IBD patients (Mahendran et al., 2013). In contrast to the transient epithelial barrier dysfunction induced by *V. cholerae* ZOT, zot^{808T} in *C. concisus* strain P14UCO-s1 from an UC patient induced prolonged intestinal epithelial barrier dysfunction *in vitro* through apoptosis induction (Mahendran et al., 2016).

Based on the pathogenic mechanisms of the diverse *C. concisus* strains, they are broadly classified into two different pathotypes: i) Adherent and Invasive *C. concisus* (AICC) and ii) Adherent and Toxinogenic *C. concisus* (AToCC). While AICC strains attach, invade the intestinal epithelial cells and survive intracellularly by subverting autophagy, AToCC strains attach to the intestinal epithelium and could translocate through the paracellular pathway by enterotoxin-mediated cleavage of TJ to enter the intestinal mucosa (Kaakoush et al., 2014a). A schematic representation of different virulence factors of *C. concisus* available and their corresponding pathogenic potential is depicted in Figure 5.

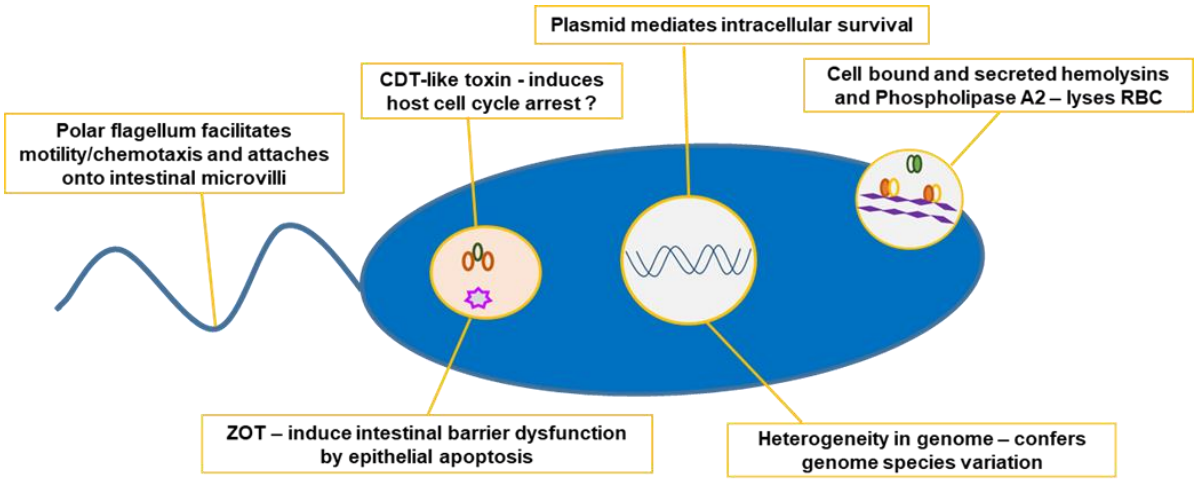

Figure 5. Schematic representation of different virulence factors of *Campylobacter concisus* and their pathogenic potentials. CDT – cytolethal distending toxin, RBC – red blood cells, and ZOT – zonula occludens toxin (modified from Kaakoush et al., 2014a).

In addition to ZOT, exotoxin-9 homologous to exotoxins of gram-positive bacteria was also identified in different strains of *C. concisus*, and the DNA levels of exotoxin-9 were elevated in fecal samples of CD patients (Kaakoush et al., 2014b). A molecular epidemiological study discerned that 57% of *C. concisus* strains from IBD patients and healthy volunteers had exotoxin-9 DNA regardless of the isolation sites and genome species types, GS1 or GS2 (Kirk et al., 2018). In parallel, a comparative genomic study of *C. concisus* strains from patients with different gastrointestinal manifestations demonstrated that ZOT and exotoxin-9 positivity were higher in CD patients compared to collagenous colitis and UC patients (Gemmell et al., 2018). In oral *C. concisus* strains from active CD patients, a novel gene *csep1* encoding *C. concisus*-secreted protein 1 (Csep1), a protein homologous to *Staphylococcus aureus* enterotoxin B was detected (Liu et al., 2018). The same study has also reported a novel pathogenic island in the extra-chromosomal plasmid pICON in the oral *C. concisus* strains of relapsed CD patients (Liu et al., 2018). Furthermore, the presence of multiple novel plasmids in the complete genomes of 16 different *C. concisus* strains was ascertained in a recent study, of which the plasmid pSMA1 was associated with severe UC patients independent of the geographical origin of the strains (Liu et al., 2020).

1.5.2.3 Lipopolysaccharide

Apart from the enterotoxins and hemolytic activity, the clinical isolates of *C. concisus* induced an increase in the surface expression of pattern recognition receptor (PRR) Toll-like receptor (TLR)-4 in colonic epithelial cells, which might enhance the inflammatory response to the endotoxin lipopolysaccharide (LPS) of enteric pathogens or commensal bacteria (Ismail et al., 2013). This can in turn induce a pronounced epithelial barrier dysfunction in IBD patients. A novel lipooligosaccharide (LOS) determinant was identified in *C. concisus* strains, which lacks a phosphate and phosphoethanolamine sialic acid substitution in oligosaccharide moiety in contrast to *C. jejuni* LOS (Brunner et al., 2018). Furthermore, *C. concisus* LOS provoked a moderate immune response in THP-1 cells and PBMCs compared with *C. jejuni* LOS (Brunner et al., 2018). This correlates to prolonged diarrhea with mild intestinal inflammation in *C. concisus*-infected patients compared with the acute and severe intestinal inflammation in *C. jejuni*-infected diarrheal patients (Nielsen et al., 2012).

1.6. Aim of the study

Campylobacter concisus was postulated to induce intestinal epithelial barrier dysfunction acting as leak flux pathomechanism (Nielsen et al., 2011). In addition, *C. concisus* elevates the release of proinflammatory cytokines IL-1β, IL-8, IL-12, IFN-γ, and TNF in the epithelial and immune cells (Man et al., 2010a; Kaakoush et al., 2011). This indicates that *C. concisus* induces mucosal immune activation in addition to the intestinal epithelial barrier dysfunction. However, the relative contribution of the mucosal immune activation on the overall intestinal epithelial barrier dysfunction after *C. concisus* infection, and the pattern of TJ protein changes remains unexplored. Hence, it becomes indispensable to investigate the link between the mucosal immune activation and the intestinal epithelial barrier dysfunction induced by *C. concisus*. It also remains uninvestigated if *C. concisus* influences the intestinal transport functions, even though it was established that *C. concisus* can induce intestinal epithelial barrier dysfunction through TJ modifications and epithelial apoptosis (Man et al., 2010a; Nielsen et al., 2011). Therefore, the two main objectives of the present study are:

i) To investigate the effects of *C. concisus* on intestinal transport function, mainly the Na^+ absorption via colonic ENaC using IL-$10^{-/-}$ mice *in vivo* and the HT-29/B6-GR/MR cell model *in vitro*.

ii) To investigate the regulatory influence of the immune activation by *C. concisus* on the intestinal epithelial barrier function using an *in vitro* co-culture model of HT-29/B6-GR/MR cells and THP-1-derived macrophages.

The *in vitro* and *in vivo* models employed in the study are described below in detail.

1.6.1 *In vitro* model to investigate ENaC activity in colonic epithelial cells

To examine the epithelial barrier properties *in vitro*, the intestinal cell lines HT-29 and Caco-2 are established as reliable models. Although both the cell types are derived from human colorectal carcinoma, they exhibit epithelial cell-like morphology when grown as confluent monolayers on permeable supports (Chantret et al., 1988). HT-29 cells are mucus-secreting cells with inducible chloride secretion (Morris et al., 1990; Breuer et al., 1992; Bajnath et al., 1992) and a broad expression of claudins within the TJ, which reflect the barrier property of human intestinal epithelium *in vivo* (Huet et al., 1987). HT-29 and Caco-2 cells were also employed successfully to investigate the intestinal epithelial barrier dysfunction induced by *Campylobacter* spp., *E. coli*, and *Y. enterocolitica* (Bücker et al., 2017; Nielsen et al., 2011; Troeger et al., 2007a; Hering et al., 2011). In addition, the transport functions of the intestinal epithelium, for instance, water transport was studied with Caco-2 cells (Ekemkcioglu et al., 1999; Verheyen et al., 2012), while the Cl^- secretion was determined in HT-29 cells (Kreusel et al., 1991; Epple et al., 2004). However, HT-29 and Caco-2 cells cannot be used to study the electrogenic Na^+ transport through ENaC as they lack endogenous expression of glucocorticoid and mineralocorticoid receptors, which are essential for the expression and localization of ENaC in the apical membrane of the colonic epithelium (Zeissig et al., 2006). Since the colonic epithelial cell lines do not express functional ENaC, HT-29 cells with the inducible expression of the mineralocorticoid receptor (HT-29/B6-Tet-On-MR) was established to measure aldosterone-dependent ENaC-mediated Na^+ absorption (Bergann et al., 2009a). The short-chain fatty acid butyrate was ascertained to be a necessary compound for the optimal expression of MR, as butyrate and aldosterone synergistically upregulate β- and γ-ENaC expression (Bergann et al., 2009a).

Butyrate induces upregulation of β- and γ-ENaC genes by enhanced binding of transcriptional factor Sp3 to the γ-ENaC promoter (Zeissig et al., 2007a). Stable transfection of the glucocorticoid receptor (GR) in HT-29 cells (HT-29/B6-GR) and its activation by synthetic

glucocorticoid dexamethasone enhanced the ENaC-mediated Na^+ absorption (Bergann et al., 2009b; Zeissig et al., 2006). Hence, the activation of glucocorticoid and mineralocorticoid receptors by steroid hormones and butyrate is indispensable for the expression and localization of ENaC in the apical membrane and thereby enhances Na^+ absorption via ENaC. HT-29/B6-GR/MR cells were later established with additional stable transfection of mineralocorticoid receptor (MR) in HT-29/B6-GR cells (Bergann et al., 2011). In HT-29/B6-GR/MR cells, GR activation increased the expression of MR, while GR and MR synergistically upregulate the transcription of β- and γ-ENaC genes, and enhance the localization of ENaC in the apical membrane of colonocytes (Bergann et al., 2011). The HT-29/B6-GR/MR cells have been successfully employed in previous studies to determine the regulation of ENaC function and the corresponding cell signaling pathways in response to the proinflammatory cytokine IL-13 (Dames et al., 2015). In the present study, we employed HT-29/B6-GR/MR cells to determine the effects of *C. concisus* on colonic ENaC activity and the regulatory cell signaling pathways (Nattramilarasu et al., 2020).

1.6.2 *In vitro* model to investigate tight junction changes in the colonic epithelial cells in presence of immune activation

The first research evidence of *C. concisus* to induce intestinal epithelial barrier dysfunction was reported in Caco-2 cells, in which *C. concisus* strain from a CD patient decreased TER, and induced a loss of occludin and ZO-1 from the intercellular junctions (Man et al., 2010a). This was accompanied by an elevated immune response of macrophages and epithelial cells induced by different strains of *C. concisus* (Man et al., 2010a). Moreover, a few clinical reports indicated an increase in the prevalence of *C. concisus* in the intestinal mucosae and feces of IBD patients (Man et al., 2010b; Mukhopadhya et al., 2011; Mahendran et al., 2011; Castaño-Rodríguez et al., 2017). It was also proposed that intestinal colonization of oral *C. concisus* strains in IBD patients could exacerbate inflammation and diarrhea (Ismail et al., 2012; Nielsen et al., 2016). However, it still remains unclear if the intestinal epithelial barrier dysfunction induced by *C. concisus* is linked to intestinal inflammation or the elevated immune response of macrophages. This was investigated by an *in vitro* co-culture model of HT-29/B6-GR/MR monolayers with THP-1-derived macrophages on the basal side established in a previous study (Lobo De Sá et al., 2019). As an important objective, we determined the TJ changes and apoptotic events induced by *C. concisus* in this *in vitro* co-culture model (Nattramilarasu et al., 2021).

1.6.3 *In vivo* model to investigate colonic ENaC activity and tight junction changes

Different clinical epidemiology studies had shown the association of *C. concisus* to diarrhea, gastroenteritis, and IBD (Maher et al., 2003; Ismail et al., 2012; Vandenberg et al., 2013). However, the pathogenic property of *C. concisus* has not been described to date in an *in vivo* model. Therefore, it is necessary to establish a suitable animal model to perform experimental infection studies with *C. concisus* and prove the pathogenic role of *C. concisus* in gastrointestinal diseases. The first successful colonization of *Campylobacter* spp. was achieved in the intestine of neonatal mice 2-3 weeks after intra-gastric inoculation with human *C. jejuni* isolates (Field et al., 1981). Germ-free (GF) Bagg Albino/c (BALB/c) mice were then discovered as a suitable animal model to study acute and chronic host-*Campylobacter* interactions after infection of GF BALB/c mice with *C. jejuni* by oral gavage (Yrios and Balish, 1986). The first adult mouse model to exhibit diarrheal symptoms following *C. jejuni* infection without any extensive pre-treatment or surgical procedures was established in BALB/C mice (Stanfield et al., 1987). The experimental infection of *C. concisus* was also performed for the first time in immunocompromised BALB/c mice to study the *in vivo* inflammatory effects of *C. concisus* in the intestine (Aabenhus et al., 2008). However, this resulted in a poor outcome on intestinal colonization of *C. concisus* in BALB/c mice.

The IL-10$^{-/-}$ mouse model to study bacterial pathogenesis in intestine emerged from *Helicobacter* research, which first detected urease-negative *Helicobacter* sp. in the intestine of IL-10$^{-/-}$ mice (Fox et al., 1999). Natural colonization of *Helicobacter* sp. was later reported in the intestine of specific pathogen-free (SPF) IL-10$^{-/-}$ mice, in which the experimental infection of *Helicobacter* sp. resulted in severe typhlocolitis (inflammation of cecum and colon) (Zhang et al., 2005). Although BALB/c mice were found to be a suitable model to study host-*Campylobacter* interactions *in vivo*, IL-10$^{-/-}$ mice with C57BL/6j background were found to exhibit better clinical signs and pathology with responses similar to human gastroenteritis (Mansfield et al., 2007). Yet, the clinical symptoms of conventional IL-10$^{-/-}$ mice were subtle compared to human campylobacteriosis with severe bloody diarrhea. To mimic the clinical symptoms of human campylobacteriosis, secondary abiotic IL-10$^{-/-}$ mice were generated by quintuple antibiotic treatment right after weaning. The secondary abiotic IL-10$^{-/-}$ mice infected per-orally with *C. jejuni* successfully reproduced the symptoms of human campylobacteriosis with acute enterocolitis and pronounced histopathological changes of the mouse colon mucosae

(Haag et al., 2012). Moreover, the secondary abiotic IL-10$^{-/-}$ mice infected with *C. jejuni* display pronounced LOS-induced and TLR-4-dependent innate and adaptive immune responses in the intestine (Haag et al., 2012). Since then, the abiotic IL-10$^{-/-}$ mouse model has been successfully employed in different *in vivo* studies (Alutis et al., 2014; Heimesaat et al., 2017; Bereswill et al., 2017). In recent studies, the secondary abiotic IL-10$^{-/-}$ mouse model was used to determine the barrier protective and anti-inflammatory effects on *C. jejuni* infection using the polyphenols curcumin and resveratrol as well as vitamin-D (Lobo de Sá et al., 2019; Mousavi et al., 2019; Lobo de Sá et al., 2021b). Therefore, the secondary abiotic IL-10$^{-/-}$ mice were used as the *in vivo* model to investigate *C. concisus*-induced changes in colonic ENaC activity and epithelial barrier function.

2. Materials and Methods

2.1. Materials

2.1.1 Cell lines

Name	Cell type	Depositor
HT-29/B6-GR/MR	Colorectal adenocarcinoma cell line HT-29/B6 stably transfected with glucocorticoid and mineralocorticoid receptor (Bergann et al., 2011)	Clinical Physiology/Nutritional, Medicine, Charité–Universitätsmedizin, Berlin, Germany
THP-1	Human monocyte leukemia cell line (ATCC TIB-202)	Medical Department, Division of Gastroenterology, Infectiology and Rheumatology, Charité-Universitätsmedizin, Berlin, Germany

2.1.2 Mouse model and bacterial infection

Strain	Genotype	Bacterium	Infection route	Dosage
C57BL/6	IL-10$^{-/-}$	*C. concisus*	Oral gavage	10^8 CFU/ml
C57BL/6	IL-10$^{-/-}$	*C. jejuni*	Oral gavage	10^8 CFU/ml
C57BL/6	IL-10$^{-/-}$	Commensal *E. coli*	Oral gavage	10^8 CFU/ml

CFU-colony forming unit

2.1.3 Laboratory consumables

Material	Manufacturer
Anaerobic box (2.5 L)	Thermo Fisher Scientific, Waltham, MA, USA
Cell culture filters (Millicell PCF - 3 µm pore size)	Merck Millipore, Burlington, MA, USA
Cell culture flasks (25 cm^2 (T25) and 75 cm^2 (T75))	Nunc GmbH & Co. KG, Wiesbaden, Germany
Cell scraper or pastula	Sarstedt AG & Co. KG, Nümbrecht, Germany
Columbia blood agar plates (5 % horse-blood)	Thermo Scientific Oxoid, Waltham, MA, USA
Copy film (A4)	Folex Coating GmbH, Köln, Germany
Coverslips (24 x 50 mm)	Menzel Deckgläser Thermo Scientific, Waltham, MA, USA
Cyrotubes (1.6 mL)	Sarstedt AG & Co. KG, Nümbrecht, Germany
Douncer or glass homogenizer (CXE6.1)	Carl Roth GmbH + Co. KG, Karlsruhe, Germany
Eppendorf tubes (safe seal reaction vials - 1.5 mL and 2 mL)	Sarstedt AG & Co. KG, Nüm- brecht, Germany
Falcon tubes (15 mL and 50 mL)	Corning, Inc., Corning, NY, USA
Filterpaper for Western blotting (Whatman 3 mm)	Carl Roth GmbH + Co. KG, Karlsruhe, Germany
GasPak EZ CampyPak container system sachets	BD Biosciences, San Jose, CA, USA

Material	Manufacturer
Glass pasteur pipettes	BRAND GmbH + Co. KG, Wertheim, Germany
Glass slides	Paul Marienfeld GmbH & Co. KG, Lauda-Königshofen, Germany
Injection syringe (1 mL, 10 mL and 20 mL)	Braun Melsungen AG, Melsungen, Germany
IV cannula (24 G yellow)	Becton Dickinson, Franklin Lakes, NJ, USA
Neubauer counting chamber	Brand GMBH & Co. KG, Wertheim, Germany
Parafilm (laboratory film)	Pechiney Plastic Packaging, Inc., Chicago, IL, USA
Petri plates (uncoated, 6 cm diameter)	Corning, Inc., Corning, NY, USA
Pipette tips with or without filters (0.5 µL – 1000 µL)	Sarstedt AG & Co. KG, Nümbrecht, Germany
Polyvinyldendifluoride (PVDF) transfer membrane	Thermo Fisher Scientific GmbH, Waltham, MA, USA
ProTaqs Mount Fluor (adhesive medium)	Biocyc GmbH & Co. KG., Luckenwalde, Germany
Protease-inhibitor cocktail tablets (complete mini EDTA-free)	Roche Diagnostics GmBH, Mannheim, Germany
Polyvinylidene difluoride (PVDF) membrane	Bio-Rad Laboratories, Inc., Hercules, CA, USA

Material	Manufacturer
Sterile filter (0.2 µm)	GE Healthcare, Chicago, IL, USA
Surgical scalpels (No. 11 und No. 20)	Braun Melsungen AG, Melsungen, Germany
Tuberculin needle (1 mL, 26 G x 3/8 inches)	Becton Dickinson, Franklin Lakes, NJ, USA
Well plates (12- and 96-wells)	Corning, Inc., Corning, NY, USA
Western Blot marker (Page-Ruler Plus) pre-stained protein ladd.er	Thermo Fisher Scientific GmbH, Waltham, MA, USA

2.1.4 Laboratory chemicals

Chemical	Manufacturer
0.5 M Tris-HCl buffer, pH 6.8	Bio-Rad Laboratories, Inc., Hercules, CA, USA
1 M Tris-HCl, pH 7.5	Gibco, Carlsbad, CA, USA
1.5 M Tris-HCl buffer, pH 8.8	Bio-Rad Laboratories, Inc., Hercules, CA, USA
16% Paraformaldehyde (PFA)	Electron Microscopy Sciences, Inc., Hat-field, PA, USA
1 M Tris buffer, pH 8.8	SERVA Electrophoresis GmbH, Heidelberg, Germany
1 M Tris-HCL, pH 7.5	Gibco, Carlsbad, CA, USA
4′,6-diamidino-2-phenylindole (DAPI)	Hoffmann-La Roche AG, Basel, Switzerland
Albumin standard	Thermo Fisher Scientific GmbH, Waltham, MA, USA

Chemical	Manufacturer
Aldosterone	Sigma-Aldrich, St. Louis, MO, USA
Amiloride	Sigma-Aldrich, St. Louis, MO, USA
Ammonium persulfate (APS)	Sigma-Aldrich, St. Louis, MO, USA
Bis-acrylamide 30%	Merck KGaA, Darmstadt, Germany
Biocyc, Luckenwalde, Germany	Biocyc, Luckenwalde, Germany
Bovine serum albumin (BSA) fraction V	Biomol GmbH, Hamburg, Germany
Bromophenolblue	GE Healthcare, Chicago, IL, USA
Calcium chloride ($CaCl_2$)	Merck KGaA, Darmstadt, Germany
Carbachol (Carbamyl choline chloride)	Sigma-Aldrich, St. Louis, MO, USA
Carbogen	Linde plc, Dublin, Ireland
Chemiluminescence solution	
Super Signal West Pico Plus stable peroxide &	Thermo Scientific, Waltham, MA, USA
Super Signal West Pico Plus luminol enhancer	Thermo Scientific, Waltham, MA, USA
Dexamethasone	Sigma-Aldrich, St. Louis, MO, USA
Dextran (4 kDa)	Serva Electrophoresis GmBH, Heidelberg, Germany
Dimethylsulfoxide (DMSO)	Riedel-de Haën AG, Seelze, Germany
Disodium hydrogen phosphate (Na_2HPO_4)	Carl Roth GmbH + Co. KG, Karlsruhe, Germany
Dithiotheritol (DTT)	Merck KGaA, Darmstadt, Germany
Ethanol -100%	Sigma-Aldrich, St. Louis, MO, USA
Ethanol - 80%	Sigma-Aldrich, St. Louis, MO, USA
Ethylene diamine tetraacetic acid (EDTA)	Merck KGaA, Darmstadt, Germany

Chemical	Manufacturer
Ethylene glycol tetraacetic acid (EGTA)	Merck KGaA, Darmstadt, Germany
Fetal calf serum (FCS)	Gibco, Carlsbad, CA, USA
Fluorescein (332 Da)	Sigma-Aldrich, St. Louis, MO, Germany
Fluorescein isothocyanate (FITC)	Merck KGaA, Darmstadt, Germany
G418-BC	Invitrogen AG, Carlsbad, CA, USA
Gentamycin	Gibco, Carlsbad, CA, USA
Glucose	Merck KGaA, Darmstadt, Germany
Glycerol	SERVA Electrophoresis GmbH, Heidelberg, Germany
Glycine	Carl Roth GmbH + Co. KG, Karlsruhe, Germany
Goat serum	Gibco, Carlsbad, CA, USA
HEPES	Sigma-Aldrich, St. Louis, MO, USA
Hormone-free FCS (h-f FCS)	Sigma-Aldrich, St. Louis, MO, USA
Hygromycin B	Biochrom GmbH, Berlin, Germany
Leupeptin (protease inhibitor)	Sigma-Aldrich, St. Louis, MO, USA
Liquid nitrogen	Linde plc, Dublin, Ireland
Magnesium chloride ($MgCl_2$)	Carl Roth GmbH + Co. KG, Karlsruhe, Germany
Methanol	Sigma-Aldrich, St. Louis, MO, USA
Milk powder	Carl Roth GmbH + Co. KG, Karlsruhe, Germany
Non-essential amino acids	Merck KGaA, Darmstadt, Germany
Paraffin Paraplast Plus	Merck KGaA, Darmstadt, Germany

Chemical	Manufacturer
Penicillin/Streptomycin (P/S, 100x, P11-010)	Gibco, Carlsbad, CA, USA
Phenylmethylsulfonyl fluoride (PMSF)	Merck KGaA, Darmstadt, Germany
Phosphate-buffered saline	Gibco, Carlsbad, CA, USA
Phosphate-buffered saline (PBS) -with or without Ca^{2+} and Mg^{2+}	Gibco, Carlsbad, CA, USA
Phorbol 12-myristate 13-acetate (PMA)	Merck KGaA, Darmstadt, Germany
Polysorbate 20 (Tween-20)	Arcos Organics B.V.B.A., Fair Lawn, NJ, USA
Polyvinylpyrrolidone (PVP-40)	Sigma-Aldrich, St. Louis, MO, USA
Potassium chloride (KCl)	Carl Roth GmbH + Co. KG, Karlsruhe, Germany
Prostaglandin E_2 (PGE_2)	Cayman Chemical Company, Ann Arbor, MICH, USA
ProTaq Mount Fluor	Biocyc, Luckenwalde, Germany
RNase-free water	Merck KGaA, Darmstadt, Germany
Roswell Park Memorial Institute Medium (RPMI 1640)	Sigma-Aldrich, St. Louis, MO, USA
Sodium azide (NaN_3)	Merck KGaA, Darmstadt, Germany
Sodium bicarbonate ($NaHCO_3$)	Merck KGaA, Darmstadt, Germany
Sodium borohydride ($NaBH_4$)	Sigma-Aldrich, St. Louis, MO, USA
Sodium chloride (NaCl)	Carl Roth GmbH + Co. KG, Karlsruhe, Germany
Sodium dihyrogen phosphate (NaH_2PO_4)	Merck KGaA, Darmstadt, Germany

Chemical	Manufacturer
Sodium dodecyl sulfate (SDS)	Carl Roth GmbH + Co. KG, Karlsruhe, Germany
Sodium orthovanadate (Na_3VO_4)	Sigma-Aldrich, St. Louis, MO, USA
Sodium salt of butyrate	Merck-Schuchardt, Hohenbrunn, Germany
Tetramethylethylenediamine (TEMED)	Amresco, Inc., West Chester, PA, USA
Tetrasodium pyrophosphate ($Na_4P_2O_7$)	Sigma-Aldrich, St. Louis, MO, USA
Theophylline	TCI Deutschland GmbH, Eschborn, Germany
Tris	Carl Roth GmbH + Co. KG, Karlsruhe, Germany
Triton X-100	Sigma-Aldrich, St. Louis, MO, USA
Trypsin-EDTA	Gibco, Carlsbad, CA, USA
U0126 (ERK1/2 inhibitor)	Biogems International, Inc. Westlake Village, CA, USA
Water (Arium pro Reinstwassersystem; double distilled H_2O – dd. H_2O)	Sartorius AG, Göttingen, Germany
β-glycerophosphate or glycerol phosphate disodium salt hydrate	Sigma-Aldrich, St. Louis, MO, USA

2.1.5 Laboratory devices

Device	Manufacturer
Aspiration pump (Fisherband FB70155)	Thermo Fisher Scientific GmbH, Waltham, MA, USA
Autoclave (VX-150)	Systec GmbH, Linden, Germany

Cell culture incubator (Heracell VIOS 160i)	Thermo Fisher Scientific GmbH, Waltham, MA, USA
Centrifuge (Avanti J-25)	Beckman Coulter, Brea, CA, USA
Centrifuge (Heraeus FRESCO21, 1.5 mL – 2 mL)	Thermo Fisher Scientific GmbH, Waltham, MA, USA
Centrifuge (UNIVERSAL 320 R (15 mL - 50 mL)	Andreas Hettich GmbH & Co. KG, Tuttlingen, Germany
Chop-stick electrodes	STX2, World Precision Instruments, Sarasota, FL, USA
Confocal Laser Scanning Microscope (CLSM)	Carl Zeiss Meditec AG, Jena, Germany
Electrophoresis chamber (BioRad)	Bio-Rad Laboratories, Inc., Hercules, CA, USA
Electrophoresis power supply (BioRad Power PAC200)	Bio-Rad Laboratories, Inc., Hercules, CA, USA
Flow cytometer (Fluorescence-activated Cell Sorting; FACS) Canto II	Becton Dickinson, Franklin Lakes, NJ, USA
Fusion (FX7)	Vilber Lourmat Deutschland GmbH, Eberhardzell, Germany
Heating block (AccuBlock)	Labnet International, Inc., Corning, NY, USA

Device	Manufacturer
Incubation shaker (UNIMAX 1010)	Heidolph Instruments GmbH & Co. KG, Schwabach, Germany
Inverted microscope (Microscope Axiovert S100)	Carl Zeiss Meditec AG, Jena, Germany
Light microscope (IMT-2)	Olympus K.K., Tokyo, Japan
Magnetic beads	Merck KGaA, Darmstadt, Germany
Magnetic stirrer with heating plate (IKA-COMBIMAG RCT)	IKA-Werke GmbH, Staufen im Breisgau, Germany
Nanodrop 2000	Thermo Fisher Scientific GmbH, Waltham, MA, USA
Volt Ohm-meter (transepithelial elecrtical resistance)	Clinical Physiology/Nutritional Medicine, Charité– Universitätsmedizin Berlin, Germany
Pipetboy	Integra Biosciences AG, Zizers, Switzerland
Pipettes (10 µL, 100 µL, 1000 µL)	Eppendorf AG, Hamburg, Germany
Real-time PCR machine (ABI 7500 Fast PCR)	Applied Biosystems, Mannheim, Germany
SpectraMax photometer (SpectraMax M2)	Molecular Devices LLC, San José, CA, USA

Device	Manufacturer
Sterile work bench (HeraSafe KS)	Thermo Fisher Scientific GmbH, Waltham, MA, USA
TECAN spectrophotometer	Tecan GmbH, Maennedorf, Switzerland
Thermal cycler 2720	Applied Biosystems, Mannheim, Germany
Trans-Blot with Turbo Transfer System (semi-dry transfer)	Bio-Rad Laboratories, Inc., Hercules, CA, USA
Ultrasonication device	Hielscher Ultrasonics GmbH, Teltow, Germany
Ussing chamber (self constructed)	Clinical Physiology Nutritional Medcine, Charité–Universitätsmedizin, Berlin, Germany
UV/VIS spectrophotometer (Lambda2 UV/VIS spectrophotometer)	PerkinElmer, Inc., Waltham, MA, USA
Voltage clamp device (CVC6)	Fiebig Hard & Software, Berlin, Germany
Vortexer (34524-200)	Thermo Fisher Scientific GmbH, Breda, Netherlands
Waterbath	Köttermann GmbH & Co KG, Uetze, Germany
Weighing chamber (L2200P)	Sartorius AG, Göttingen, Germany

Gel rocker (or) shaker (Wippe WT12)	Biometra GmbH, Göttingen, Germany
Wet/Tank Blotting Systems	Bio-Rad Laboratories, Inc., Hercules, CA, Germany

2.1.6. Laboratory solutions

2.1.6.1 Cell culture media

The cell culture media, hygromycin B and gentamycin were stored in refrigerator and maintained at 2-8 ºC. PBS (without Ca^{2+} and Mg^{2+}) was stored at RT. FCS, P/S and G418 were aliquoted and freezed at -20 ºC. The cell culture experiments were carried out in a sterile workbench. The media used for the cell culture experiments and their supplements are as follows:

Cells	Medium	Supplements
HT-29/B6-GR/MR	RPMI 1640	10% FCS
		1% P/S
		500 µg/mL G418
		200 µg/mL hygromycin B
THP-1 monocytes	RPMI 1640	10% heat-inactivated FCS
		1% P/S

FCS was heat-inactivated by incubating in water bath at 56 ºC for 30 min. Hormone free (h-f) or charcoal-stripped FCS was used instead of FCS in RMPI medium for HT-29/B6-GR/MR cells stimulated by dexamethasone, butyrate and aldosterone.

2.1.6.2 Blocking solutions and buffers

Name	Composition
Blocking solution for immunofluorescence staining	1% goat serum (v/v) in PBS (with Ca^{2+} and Mg^{2+})
Blocking solution for western blotting	1% PVP-40 (w/v) in TBST 0.05% Tween-20 (v/v) in TBST
EPHO buffer	10% 10x West-Buffer (v/v) in dd. H_2O 0.1% SDS (v/v) in dd. H_2O
Lysis buffer with phosphatase inhibitors	20 mM Tris (w/v) in dd. H_2O 150 mM NaCl (w/v) in dd. H_2O 1 mM Triton X-100 (v/v) in dd. H_2O 1 mM EDTA (w/v) in dd. H_2O 2.5 mM $Na_4P_2O_7$ (w/v) in dd. H_2O 1 mM β-glycerophosphate (w/v) in dd. H_2O 1 mM Na3VO4 (w/v) in dd. H_2O 1 mM EGTA (w/v) in dd. H_2O 1 mM PMSF (w/v) in dd. H_2O 1 µg/mL Leupeptin (w/v) in dd. H_2O PMSF and Leupeptin were freshly added into the buffer before use

Ringer's or bathing solution for Ussing chambers	113.6 mM NaCl (w/v) in dd. H_2O
	21 mM $NaHCO_3$ (w/v) in dd. H_2O
	5.4 mM KCl (w/v) in dd. H_2O
	2.4 mM Na_2HPO_4 (w/v) in dd. H_2O
	1.2 mM $MgCl_2$ (w/v) in dd. H_2O
	1.2 mM $CaCl_2$ (w/v) in dd. H_2O
	0.6 mM NaH_2PO_4
	10 mM Glucose (w/v) in dd. H_2O (substrate freshly added in the solution before use)
	Solution is gassed with carbogen and adjusted to pH-7.4
Sample buffer (5x Laemmli) for western blotting	125 mM Tris-HCl (w/v) in EPHO buffer at pH-6.8
	500 mM DTT (w/v) in EPHO buffer
	50% Glycerol (v/v) in EPHO buffer
	10% SDS (v/v) in EPHO buffer
	0.001% Bromophenol blue (v/v) in EPHO buffer
Separating gel	10% or 12.5% Acrylamide (v/v) in dd. H_2O
	350 mM Tris buffer (v/v) in dd. H_2O at pH 8.8
	0.1% SDS (v/v) in dd. H_2O
	0.1% APS (v/v) in dd. H_2O
	0.1% TEMED (v/v) in dd. H_2O

Stacking or collecting gel	5.1% (v/v) in dd. H_2O bis-acrylamide 30%
	125 mM Tris-HCl (v/v) in dd. H_2O at pH 6.8
	0.1% SDS (v/v) in dd. H_2O
	0.1% APS (v/v) in dd. H_2O
	0.1% TEMED (v/v) in dd. H_2O
Tris-buffered saline with Tween-20 (TBST)	500 mM NaCl (w/v) in dd. H_2O
	200 mM Tris (w/v) in dd. H_2O
	0.1% Tween-20 (v/v) in dd. H_2O
	pH 7.3
Transfer buffer	10% 10x West-Buffer (v/v) in dd. H_2O
	10% methanol (v/v) in dd. H_2O
Whole-cell lysis buffer	150 mM NaCl (w/v) in dd. H_2O
	10 mM Tris-buffer at pH-7.5 (v/v) in dd. H_2O
	0.1% Triton X-100 (v/v) in dd. H_2O
	0.1% SDS (w/v) in dd. H_2O
	1 protease-inhibitor tablet per 10 mL of the buffer
10x West-Buffer	1.9 M Glycine (w/v) in dd. H_2O
	0.25 M Tris (w/v) in dd. H_2O
	pH 8.1-8.4

w-weight, v-volume, dd.-double distilled

2.1.7. Antibodies

2.1.7.1 Primary antibodies

The primary antibodies for western blotting (WB) are diluted using 5% BSA (w/v) in TBST supplemented with 1.2 µM NaN_3. Antibodies for immunofluorescence (IF) are diluted using blocking solution for immunofluorescence. The antibodies used and the dilution factors (DF) are as follows:

Antibody	Species	DF (WB)	DF (IF)	Manufacturer
Anti-p-ERK1/2 monoclonal	Rabbit	1:1,000	_____	Cell Signaling Technology Europe B.V., Frankfurt am Main, Germany
Anti-β-actin monoclonal	Mouse	1:10,000	_____	Cell Signaling Technology, Danvers, MA, USA
Anti-claudin-1 monoclonal	Mouse	1:1,000	_____	Invitrogen AG, Carlsbad, CA, USA
Anti-claudin-1 polyclonal	Rabbit	1:1,000	_____	Invitrogen AG, Carlsbad, CA, USA
Anti-claudin-2 monoclonal	Mouse	1:250	_____	Invitrogen AG, Carlsbad, CA, USA
Anti-claudin-2 polyclonal	Rabbit	1:1,000	_____	Invitrogen AG, Carlsbad, CA, USA
Anti-claudin-4 monoclonal	Mouse	1:1,000	_____	Invitrogen AG, Carlsbad, CA, USA
Anti-claudin-5 polyclonal	Rabbit	1:1,000	_____	Invitrogen AG, Carlsbad, CA, USA

Antibody	Species	DF (WB)	DF (IF)	Manufacturer
Anti-claudin-7 polyclonal	Rabbit	1:1,000	_____	Invitrogen AG, Carlsbad, CA, USA
Anti-claudin-8 polyclonal	Rabbit	1:1,000	1:30	Invitrogen AG, Carlsbad, CA, USA
Anti-occludin monoclonal	Mouse	1:500	_____	Invitrogen AG, Carlsbad, CA, USA
Anti-occludin polyclonal	Rabbit	1:1,000	1:100	Sigma-Aldrich, St. Louis, MO, USA
Anti-tricellulin polyclonal	Rabbit	1:50	1:50	Invitrogen AG, Carlsbad, CA, USA
Anti-GAPDH	Mouse	1:2,000	_____	Merck KGaA, Darmstadt, Germany
Anti-ZO-1 monoclonal	Mouse	_____	1:100	Becton Dickinson, Franklin Lakes, NJ, USA

DF - dilution factor; WB - western blotting; IF – immunofluorescence

2.1.7.2 Secondary antibodies

The secondary antibodies for WB are diluted using 1% milk powder in TBST. The secondary antibodies for IF are diluted using blocking solution for immunofluorescence. The secondary antibodies used in the experiments, and the DF are as follows:

Antibody	DF (WB)	DF (IF)	Manufacturer
Anti-Mouse (IgG Alexa-Fluor 594)	_____	1:400	Invitrogen AG, Carlsbad, CA, USA
Anti-Rabbit (IgG Alexa-Fluor 488)	_____	1:400	Invitrogen AG, Carlsbad, CA, USA
Anti-Mouse	1:10,000	_____	Jackson ImmunoResearch, Inc.,West Grove, PA, USA
Anti-Rabbit	1:10,000	_____	Jackson ImmunoResearch, Inc.,West Grove, PA, USA

DF - dilution factor; WB - western blotting; IF - immunofluorescence

2.1.8 Kits

Name	Manufacturer
BCA (Bicinchoninic acid assay) protein assay kit	Thermo Scientific, Waltham, MA, USA
Cell Counting Kit-8 (CCK-8) assay	Thermo Scientific, Waltham, MA, USA
Cytometric bead array **(**Human Th1/Th2/Th17 Kit)	BD Biosciences, Franklin Lakes, NJ, USA
Cytometric bead array (Flex Set IL-13 and IL-1β)	BD Biosciences, Franklin Lakes, NJ, USA
High-Capacity cDNA Archive kit	Applied Biosystems, Mannheim, Germany

*mir*Vana miRNA isolation kit	Ambion, Life Technologies, Carlsbad, CA, USA
Terminal deoxynucleotidyl transferase dUTP nick end labeling (TUNEL) assay kit	In situ Cell Death Detection Kit, Roche AG, Mannheim, Germany

2.1.9 Software

Name	Developer
Analoga Datenaufnahme (Ussing experiments)	Clinical Physiology, Charité–Universitätsmedizin Berlin, Germany
Easywin Fitting v6.0a (data acquisition – TECAN and SpectroMax M2 photometer)	Tecan Group AG, Männedorf, Switzerland
FACP Array software v3.0 (data acquisition - flow cytometry)	BD Biosciences, Franklin Lakes, NJ, USA
GraphPad Prism v5.0 (data analyses and statistics)	GraphPad software Inc., San Diego, CA, USA
ImageJ (Western blot densitometry)	Rasband, W. S., ImageJ, National Institute of Health (NIH), Bethesda, MD, USA
Ingenuity Pathway Analysis - IPA (bio-informatics predictions from RNA-Seq data)	Qiagen Silicon Valley, Redwood, CA, USA
Microsoft Office - Excel (data acquisition and evaluation)	Microsoft Corporation, Redmond, WA, USA

2.2. Methods

2.2.1. Experimental set-up to determine colonic ENaC activity *in vitro*

HT-29/B6-GR/MR cells were used to determine ENaC-mediated Na^+ absorption in colonocytes. The cells were cultured using RPMI medium in T25 flasks and maintained at 37 °C for one week in a cell culture incubator with the humidified atmosphere (95% O_2 and 5% CO_2). RPMI media were supplemented with 10% FCS, 1% P/S, 500 IU/mL G418, and 200 µg/mL hygromycin B. The cells differentiated in T25 flasks were confluent after a week. The cells were then washed with 11 ml PBS (without Ca^{2+} and Mg^{2+}), trypsinized with trypsin-EDTA, and seeded in cell culture filters (3 µm pore size) at 1 x 10^6 cells per filter. The cells were grown as polarized monolayers in the filters for ten days. The cell monolayers reach a TER of 1500-2100 $\Omega \cdot cm^2$, after which they were washed and incubated with 10% h-f FCS for 24 h. The cell monolayers were then stimulated with DBA (a combination of dexamethasone (D, 50 nM), sodium salt of butyrate (B, 2 mM), and aldosterone (A, 3 nM)) for four days as depicted in Figure 6.

The cell monolayers were maintained at 37 °C in the cell culture incubator with humidified atmosphere throughout the DBA stimulation. In parallel, bacterial cultivation was carried out. *Campylobacter concisus* (*C. concisus* strain AAuH 37 UCo-a; an oral isolate from a male Danish UC patient who underwent Ileal Pouch-Anal Anastomosis (IPAA); Kirk et al., 2018) and *C. jejuni* (*C. jejuni* WT strain 81–176) were seeded in Columbia blood agar plates (5% horse blood) and incubated for 3 days at 37 °C in 2.5 L anaerobic box. The anaerobic box was maintained in a microaerobic atmosphere (85% N_2, 10% CO_2, and 5% O_2) emanating from the gas pack sachets of BD GasPak EZ CampyPak. Owing to the fastidious nature of *C. concisus*, H_2 is a critical factor for its growth and survival (Benoit and Maier, 2018; Benoit et al., 2020). Hence, the microaerobic atmosphere was supplemented with approximately 10% H_2 (0.082 g $NaBH_4$ was dissolved in 10 mL of water to liberate H_2; Lee et al., 2014). *C. jejuni* was used as a positive control in the experiment, as ENaC function was inhibited in HT-29/B6-GR/MR monolayers by *C. jejuni* infection (Bücker et al., 2018). The translucent grey colonies of *C. concisus* and relatively thicker and white *C. jejuni* colonies were obtained from the blood agar plates with sterile inoculum loops. The bacteria were then inoculated into an antibiotic-free RPMI medium with 10% heat-inactivated FCS. The bacterial inoculated media were vortexed

briefly and subjected to incubation shaking at 220 rpm in 37 ºC for 2 h in the microaerobic atmosphere with H_2. The absorbance of the bacterial-inoculated media was recorded using Lambda2 UV/VIS Spectrophotometer at a wavelength of 600 nm. The optical density (OD) values should be in the range of 0.4-0.5 to ensure the logarithmic growth phase of bacteria. Colony-forming units (CFU) were enumerated by counting the viable bacteria in the media using Neubauer counting chamber magnified under a light microscope.

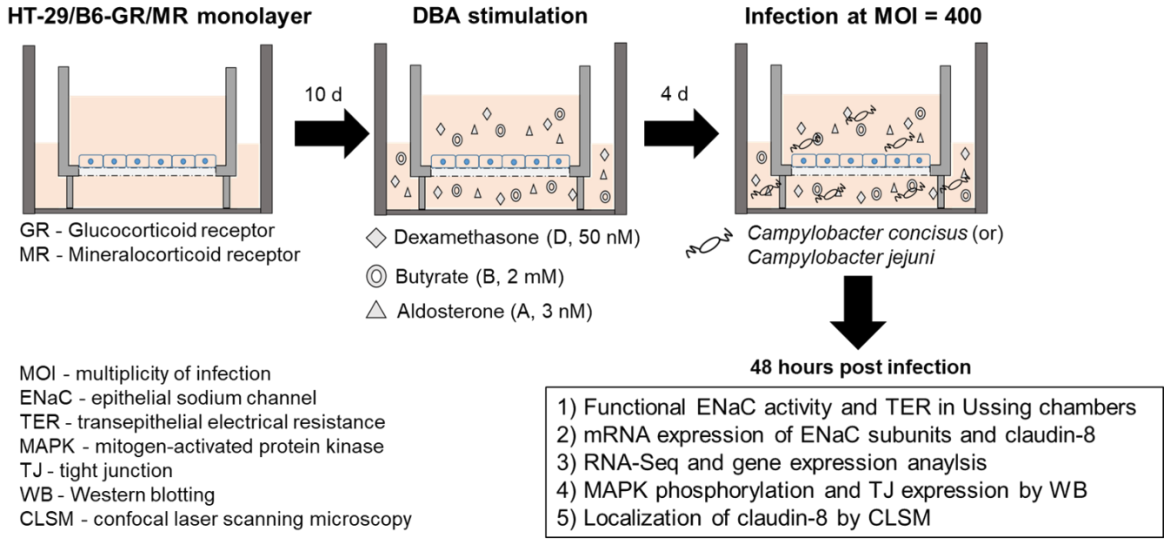

Figure 6. Study design to determine functional ENaC activity after *Campylobacter concisus* or *Campylobacter jejuni* infections with HT-29/B6-GR/MR cell model (modified from Nattramilarasu et al., 2020).

The TER values of the cell monolayers were recorded with a chop-stick electrode and a volt-ohm meter four days after DBA stimulation. Then, the cell monolayers were infected with *C. concisus* or *C. jejuni* at a multiplicity of infection (MOI) of 400 (Figure 6). MOI was calculated by dividing the CFU of bacteria by the number of HT-29/B6-GR/MR cells seeded in the filters. The cell monolayers were washed and incubated either overnight or 24 h before infection with antibiotic-free RMPI media supplemented with 10% heat-inactivated h-f FCS. After infection, the cell monolayers were maintained at 37 ºC in the microaerobic atmosphere with H_2. Forty-eight hours post infection (p.i.), the cell monolayers were used for functional and molecular analyses as described in Figure 1. Furthermore, DBA-stimulated HT-29/B6-GR/MR cells were evaluated for cytotoxicity at a MOI of 400 (refer to section 2.2.5.1). The infection dosage of *C. concisus* for HT-29/B6-GR/MR cells was optimized through cell proliferation or cytotoxicity assay at different MOI ranging from 25 to 1000 (refer to section 2.2.5.2).

2.2.1.1 Investigation of ENaC activity in colonic epithelial cell monolayers

HT-29/B6-GR/MR cell monolayers were mounted into Ussing chambers (epithelial surface area of 0.6 cm^2) 48 h after *Campylobacter* spp. infection. The Ringer's solution for Ussing chambers was maintained at a pH of 7.4. To simulate the *in vivo* conditions, the ringer solution was gassed with carbogen (95% O_2 and 5% CO_2) by bubble lift. The temperature was maintained at 37 ^oC with heated water circulating within the double-walled glass setup in Ussing chambers. The short circuit current (I_{SC}) was recorded using voltage clamp device CVC6. The cell monolayers were equilibrated in the bathing solution for 15 min to stabilize I_{SC} ($\mu A/cm^2$) and TER ($\Omega \cdot cm^2$). ENaC-dependent Na^+ transport was recorded as a decrease in I_{SC}, measured as ΔI_{SC} ($\mu A/cm^2$) 15 min after addition of ENaC blocker amiloride at a concentration of 100 µM on the apical side of the monolayers. In addition, TER values of the cell monolayers were recorded 15 min after amiloride-induced changes in I_{SC}. Amiloride was used at a concentration of 100 µM, which is ten-fold higher than the 10 µM concentration used to completely block the ENaC localized in kidney cells. 100 µM amiloride is still specific to block Na^+ transport via ENaC in the distal colon, as Na^+ transport via NHE3 in the apical membrane of the colonocytes was only affected at a concentration of 1 mM (Dames et al., 2015). The active electrogenic Cl^- secretion was measured at the end of each experiment to ensure that the epithelium is still viable at 48 h p.i. For this purpose, PGE_2 (10 µM on the basal side) and theophylline (10 mM on apical and basal sides) were used to determine cAMP-dependent Cl^- secretion in the Ussing chambers through a transient increase in I_{SC}. In addition, Ca^{2+}-dependent Cl^- secretion was determined via application of cholinergic agonist carbachol at a concentration of 100 µM on the basal side of the cell monolayers in Ussing chambers.

2.2.1.2 RNA isolation and RT-qPCR to determine the gene expression

Forty-eight hours post-*C. concisus* infection, total RNA was extracted from control monolayers and DBA-stimulated HT-29/B6-GR/MR cells using the *mir*Vana miRNA isolation kit. Before RNA isolation, the surfaces of the workbench and the pipettes were cleaned with 0.5% SDS to avoid RNase contamination. The cell monolayers on the filters were washed once using ice-cold PBS (with Ca^{2+} and Mg^{2+}), and the cells were lysed with 600 µL of the lysis buffer provided by the kit and transferred to fresh vials. The cells were then vortexed briefly and 60 µL of the RNA homogenate additive were added to the cells, and vortexed again. The cells were then incubated on ice for 10 min and 600 µL acid-phenol: chloroform was added to the cells and

vortexed again for 30-60 s. Then, the samples were centrifuged for 5 min at 10,000 × g in RT. During centrifugation the samples separate into three phases, namely an upper aqueous phase containing RNA, a middle yellowish-white interphase containing denatured proteins and DNA, and a lower organic phase. The upper aqueous phase was carefully removed without disturbing or touching the interphase and transferred to a fresh Eppendorf tube.

The aqueous phase of the samples was added with absolute ethanol at 1.25 times the total volume of the aqueous phase. The filter cartridge in the *mir*Vana miRNA isolation kit was placed on a collection tube and 700 µL of samples (lysate/ethanol mixture) were added to the filters. This was followed by a centrifugation step for 15 s at 10,000 × g, after which the flow-through was discarded. 650 µL of RNA washing solution were then pipetted into the cartridge and the samples were centrifuged for 15 s at 10,000 × g. The flow-through was discarded and the samples were washed twice with 500 µL washing solution 2/3 by centrifugation for 15 s at 10,000 × g. The residual ethanol from the washing solution was removed by centrifugation at 10,000 x g for 1 min. Then the filter cartridges were placed on fresh Eppendorf tubes and filled with 50 µL of pre-heated RNase-free water (heated at 70 ^{o}C for 1 min) and incubated at RT for 1 min. The samples were then centrifuged at a maximum speed of 17,200 × g to extract the RNA bound to filters. RNA concentration was then estimated using Nanodrop 200. RNA samples were then tested for purity using A260/280 and A260/230 ratios. The ideal A260/280 ratios for pure RNA should be in the range of 1.9-2.1. The ratio below 1.9 indicates DNA or protein contamination. The ideal A260/230 ratios should be in the range of 2.0-2.2. The ratios higher than be 2.2 indicate phenol contamination.

Reverse-transcription PCR was performed using the High-Capacity cDNA Archive Kit with an oligo (dT) primer. The reaction components were added at the concentrations specified in the kit and PCR was performed with the Thermal cycler 2720 in the following steps: 25 ^{o}C for 10 min, 37 ^{o}C for 2 h, and 85 ^{o}C for 5 min to synthesize cDNA. The gene of interest was amplified using real-time quantitative PCR machine ABI 7500 FAST PCR. TaqMan Gene Expression protocol was employed for the gene amplification with FAM dye-labelled primers [RN00580652_m1 for human ENaC α-subunit (*SCCN1A*), HS00165722_m1 for human ENaC β-subunit (*SCCN1B*), HS00168918_m1 for human ENaC γ-subunit (*SCNN1G*), HS00273282_s1 for human claudin-8 (*CLDN8*)]. GAPDH-cDNA was used as endogenous control, which was quantified using VIC reporter dyes. The differential gene expression was determined using $2^{-\Delta\Delta CT}$ method (Livak and Schmittgen, 2001). The gene expression of *C.*

concisus-infected cells was measured and presented as fold-induction. The controls were set at one-fold and the expression changes of DBA-stimulated cells and *C. concisus*-infected cells (after DBA stimulation) were determined.

2.2.1.3 RNA sequencing and gene expression analysis

Total RNA was isolated from HT-29/B6-GR/MR cell monolayers 48 h after *C. concisus* infection as described in section 2.2.1.2. RNA from controls, DBA-stimulated controls, and *C. concisus*-infected cells were sent to our collaborative research partners at "Laboratory for Epigenetics and Tumour genetics, University Hospital Cologne and Centre for Molecular Medicine Cologne, Germany". The cDNA was synthesized from the RNA using Illumina's RNA-Seq prep kit and the samples were subjected to sequencing with NovaSeq 6000 Sequencing System with quality scores of more than 80%.

Using STAR aligner version 2.7.1a in a two-pass mode (Dobin et al., 2013), the reads from RNA-Seq were sorted after mapping against human genome GRCh38 release 97. The coordinates from Ensembl annotation release 97 were utilized as a framework by first-pass read mapping. Following the first-pass read, the second-pass mapping added splice sites from the first run. The coordinates from the aforementioned Ensembl annotation with the default parameters were used to generate count tables containing gene-read coverages. The count tables with gene-read coverages were obtained through the Counts function in Bioconductor package Rsubread (Liao et al., 2019). The differential gene expression of DBA-stimulated controls and *C. concisus*-infected cell monolayers after DBA stimulation were also quantified in the form of log2-fold changes with their corresponding *P*-values using the Bioconductor package DESeq2 (Love et al., 2014). The *P*-values were adjusted by the Benjamin-Hochberg procedure. In addition to Bioconductor package Rsubread, Bioconductor package edgeR (Robinson et al., 2010) was used to estimate the gene expression changes of IL-32 in DBA-stimulated HT-29/B6-GR/MR cells after *C. concisus* infection. Counts per million (CPM) function in Bioconductor package edgeR was used to normalize the CPM and log-transformed CPM values, and mRNA expression of IL-32 was represented by CPM values (Robinson et al., 2010).

In addition to RNA-Seq data analysis, an Upstream regulator analysis was performed with bioinformatics predictions from Ingenuity Pathway Analysis (IPA) software. The upstream regulator analysis predicts the transcriptional regulators of genes whose expression or activation

was influenced by *C. concisus* infection in HT-29/B6-GR/MR cells with the information available from the existing literature and knowledge database on the diverse gene datasets, which regulate ENaC activity. The upstream regulator analysis was carried out with a special focus on transcriptional regulators targeting MAPK enzyme, extracellular signal-regulated kinase (ERK) and IL-32, which may influence ENaC activity. The upstream regulators targeting a gene can be any molecule, for instance, transcription factors, microRNAs, kinases, compounds or drugs. The overlap *P*-value and activation *Z*-score were the statistical measures computed for each potential upstream regulator. The overlap *P*-value determines whether there is a significant overlap between the dataset genes and the genes regulated by the upstream regulator. Fisher's Exact Test was used to determine the overlap *P*-value and the significance is attributed to *P*-values < 0.01. The activation *Z*-score represents the activation states of predicted upstream regulators based on a comparison with a model that assigns random regulation directions. The *Z*-score determines whether an upstream transcription regulator has significantly more "activated" predictions than "inhibited" predictions ($Z > 0$) or vice versa ($Z < 0$).

2.2.1.4 Western blotting to detect ERK phosphorylation

In parallel to the evaluation of ENaC function in Ussing chambers, DBA-stimulated HT-29/B6-GR/MR cell monolayers were assessed for activation or phosphorylation of MAPK enzyme ERK after infection with *C. concisus* and *C. jejuni*. Forty-eight hours p.i., the cell monolayers were washed twice with RPMI media supplemented with 50 µg/mL gentamycin and incubated in the same media for 3 h to kill all the residual bacteria on the cell monolayers. Then, the cell monolayers were washed twice with RPMI media supplemented with antibiotic-free and heat-inactivated 10% h-f FCS to completely remove gentamycin. After this step, the cells were stimulated with DBA and re-infected with *C. concisus* or *C. jejuni* for 5, 15, 30, 60, and 120 min to detect phosphorylation by Western blotting at different time points of infection. The cell monolayers were washed twice with ice-cold PBS (without Ca^{2+} or Mg^{2+}) after infection, and the cells were carefully removed from the monolayers using lysis buffer with phosphatase inhibitors and a complete protease inhibitor cocktail. The cells were subjected to lysis in fresh vials maintained in ice-cold conditions for 1 h with a brief vortex for every 10 min. After lysis, the cells were centrifuged at 13,000 rpm in 4 °C for 30 min. The supernatants were collected in fresh tubes and subjected to sonication with 15 pulses at brief intervals of 3 seconds for every 5 pulses. After sonication, the cells were centrifuged again at 13,000 rpm for 30 min at 4 °C.

The concentrations of the isolated proteins were estimated by the BCA protein assay kit. In BCA assay, bivalent copper ions (Cu^{2+}) are reduced to monovalent copper ions (Cu^{+}) by proteins in an alkaline environment. The reduced monovalent copper ions form violet complexes with the bicinchoninic acid. The absorbance of the violet complex was recorded at a wavelength of 562 nm using SpectraMax M2 photometer and the protein concentration was then estimated using the Easywin Fitting software embedded to the photometer.

Once the concentrations were determined, the protein lysates were diluted using the whole-cell lysis buffer and then mixed with sample buffer (5x Laemmli) in the ratio of 5:1. Bromophenol blue in the Laemmli buffer helps to visualize the protein samples when loaded into the gels, while SDS imparts a net negative charge to the proteins. The protein samples were incubated at 95 ^{o}C for 5 min in a heating block to denature the proteins. Meanwhile, the collecting and separating gels were prepared with the gel plates of 1.5 mm thickness in the electrophoresis apparatus filled with electrophoresis buffer. Once the gels were solidified, the protein samples were loaded into the gel pockets along with the Western blot marker (Page-Ruler Plus Ladder) to determine the size of the protein bands after blotting. The electrophoresis apparatus was filled using the electrophoresis buffer in which the proteins were resolved in SDS-PAGE gels at RT by applying an electric field. The proteins were separated based on size, in which the high molecular weight proteins migrate slowly and the low molecular weight proteins migrate faster to the bottom of the gel. An electric field was applied using an electrophoresis power supply. Initially, a lower voltage of 60 V was maintained for 10 min, followed by 80 V for 10 min by which the protein samples migrate the stacking gel and reach separating gel. Then, the voltage was increased to 100 V and maintained for about 90-100 min, during which the proteins were resolved in separating gels. 12.5% separating gels were used to resolve the protein samples to detect ERK phosphorylation. The resolved proteins in separating gels were electro-transferred to PVDF membranes at 100 V for 65 min using a Wet/Tank Blotting system filled with transfer buffer in ice-cold conditions. After electro-transfer, the PVDF membranes were blocked for unspecific protein signals using a blocking solution 1% PVP-40 dissolved in TBS with 0.05% Tween-20. The blocking was carried out for 1 h with a shaker at RT.

After blocking, the membranes were briefly rinsed with the TBS, and incubated with primary antibodies rabbit (Rb) anti-p-ERK1/2 and Rb anti-ERK1/2 in a shaker overnight at 4^{o}C. Mouse (M) anti-β-actin antibody was used as loading controls, and β-actin was detected in separate membranes electro-transferred with the same protein samples. Following overnight incubation

with primary antibodies, the membranes were then treated and incubated with secondary antibodies (peroxidase-conjugated goat anti-Rb or anti-M) in a shaker at RT for 2 h. The membranes were then briefly immersed in chemiluminescence solution and the bands for the proteins are detected using software embedded with the Fusion FX7 system. For densitometric analysis, the band intensities of p-ERK1/2 and ERK1/2 (total ERK1/2) blots were normalized to the β-actin intensity. The band intensities were quantified by ImageJ. Following β-actin normalization, the phosphorylation or activation of ERK was estimated by the ratio of band intensities of p-ERK1/2 to ERK1/2.

2.2.1.5 Inhibition of ERK pathway and functional ENaC changes in vitro

The changes in ENaC-dependent Na^+ transport were determined after *C. concisus*-infected HT-29/B6-GR/MR cells following ERK inhibition. For this purpose, an upstream MEK inhibitor U0126, which inhibits ERK function was used. U0126 was dissolved in DMSO at a concentration of 10 mM. The *in vitro* cell model to determine ENaC function (Figure 1) was also used in the blockade experiment. To determine ENaC activity after the ERK blockade, the experimental setup described in section 2.2.1 was followed with a few modifications. The cell monolayers were treated with the functional MEK inhibitor U0126 at a concentration of 10 µM on both apical and basal sides of the monolayers four days after DBA stimulation. Then, the cell monolayers were incubated in the humidified atmosphere (95% air/5% CO_2) for 2 h after U0126 treatment. After U0126 treatment, the cell monolayers were infected with *C. concisus* at a MOI of 400 on apical and basal sides. The cell monolayers were then transferred to the microaerobic atmosphere with H_2 in 37 ^oC. Along with infected cell monolayers, uninfected controls and controls with U0126 treatment were also maintained in the microaerobic atmosphere for 4 h. After 4 h incubation in microaerobic atmosphere, they were replaced in the humidified atmosphere (95% air/5% CO_2). Forty-eight hours p.i., ENaC-dependent Na^+ absorption (ΔI_{SC} in $\mu A/cm^2$) was determined from the cell monolayers in Ussing chambers.

2.2.2 Electrophysiological assessment of ENaC function *in vivo*

The *in vivo* effects of *C. concisus* on colonic ENaC function were examined using IL-$10^{-/-}$ mice with C57BL/6j background, which were maintained in specific-pathogen-free (SPF) condition. To ignore the beneficial effects of commensal gut bacteria lining the colon mucosae, secondary

abiotic IL-10$^{-/-}$ mice were used for *C. concisus* infection. In secondary abiotic IL-10$^{-/-}$ mice, the gut microbiota was depleted by an antibiotic cocktail of ampicillin/sulbactam (1.5 g/L), ciprofloxacin (200 mg/L), impenem/cilastatin (250 mg/L), vancomycin 500 mg/L and metronidazole (1g/L) (Heimesaat et al., 2006; Bereswill et al., 2011). The antibiotics were supplemented in autoclaved drinking water *ad libitum* for eight weeks in sterile cages. IL-10$^{-/-}$ mice were then subjected to peroral infection with *C. concisus* (*C. concisus* strain AAUH 37UCo-a; Kirk et al., 2018) or *C. jejuni* (*C. jejuni* WT strain 81-176) at 10^8 CFU in a volume of 0.3 mL PBS. Commensal *E. coli* mono-associated IL-10$^{-/-}$ mice were used as controls. The animals were euthanized by isoflurane inhalation and the colon were carefully excised six days after infection. The tissues from the distal parts of the colon were mounted into the Ussing chambers (refer scheme, Figure 7). IL-10$^{-/-}$ mice were provided by our collaborative research partners at the Institute of Microbiology, Infectious Diseases, and Immunology, Charité CBF, Berlin. The infection experiments in secondary abiotic IL-10$^{-/-}$ mice were carried out at "Forschungseinrichtung für Experimentelle Medizin, Charité-Universitätsmedizin Berlin".

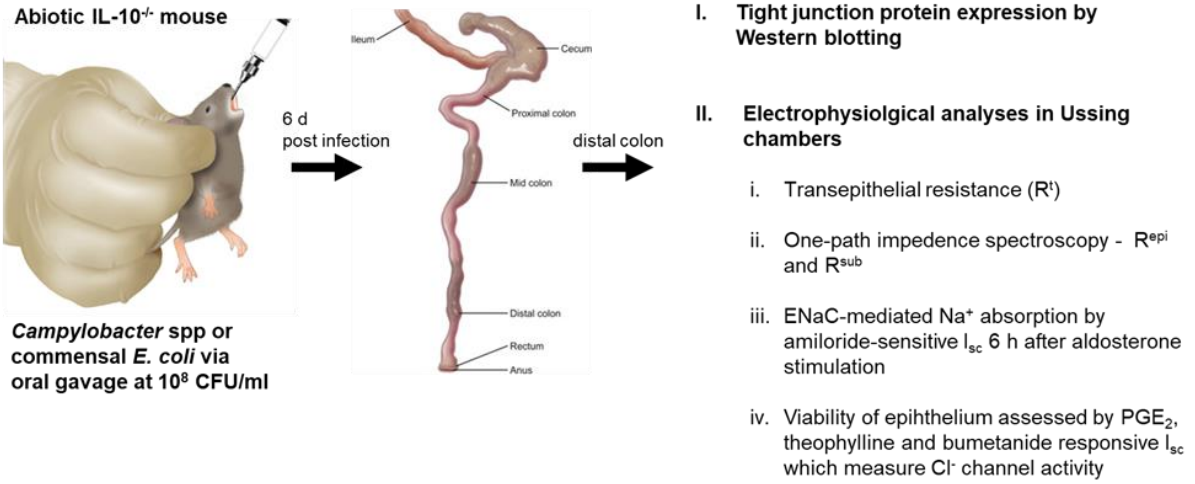

Figure 7. Workflow to assess ENaC function in colonic mucosae of secondary abiotic IL-10$^{-/-}$ mice six days after *Campylobacter* spp. infection. I_{SC} - short circuit current, R^{epi} - epithelial resistance, R^{sub} -subepithelial resistance, and PGE_2 - prostaglandin E_2. Commensal *E. coli* mono-associated IL-10$^{-/-}$ mice were used as controls (modified from Treuting and Dintzis, 2012).

The colon tissues were equilibrated for 30 min in the Ussing chambers with the Ringer's solution. TER ($\Omega \cdot cm^2$) and I_{SC} ($\mu A/cm^2$) were recorded by voltage clamp device throughout the experiment. After the equilibration step, the colon tissues were treated by mineralocorticoid

aldosterone (3 nM) in mucosal and serosal side in Ussing chambers to stimulate ENaC activity. Six hours after aldosterone stimulation, ENaC-dependent Na^+ absorption was determined as a decrease in I_{SC} (ΔI_{SC} in $\mu A/cm^2$) 15 min after addition of amiloride (100 µM), which blocks ENaC localized in the mucosal side of the colonic epithelium. At the end of each experiment, it becomes indispensable to assess the viability of the colonic tissues, as they were maintained in *ex vivo* conditions for more than 6 h. Hence, we analyzed cAMP-dependent Cl^- secretion through I_{SC} response in Ussing chambers 5 min after addition of 10 mM theophylline on mucosal and serosal sides of the tissues, and 10 µM PGE_2 on the serosal sides (Bücker et al., 2018). In addition, the inhibition of Cl^- secretion was measured by a decrease in I_{SC} through the application of bumetanide (100 µM) on the serosal side of the tissues, which inhibits Cl^- secretion through the blockade of Na-K-Cl co-transporter 1/2 (NKCC 1/2).

Although the viability of the colonic tissues was assessed at the end of each experiment, I_{SC} measurements can be influenced to different degrees by the thickness of the subepithelial layers in the tissues. Hence, we recorded the total transepithelial resistance (R^t) and subepithelial resistance (R^{sub}) of the colonic tissues by one-path impedance spectroscopy as described in previous studies (Schrifferdecker and Frömter, 1978; Fromm et al., 1985). The epithelial resistance (R^{epi}) was obtained by subtracting R^{sub} from R^t. Furthermore, the contribution of subepithelial tissue was taken into account by calculating the ratio R^t/R^{epi} (Barmeyer et al., 2016; Bücker et al., 2018) to ensure that the changes in I_{SC} accurately reflect the changes in active transport of ions through different channels of the colonic epithelium.

2.2.3 Protein isolation from mouse colon and analyses of tight junction protein expression

The colon tissues of *C. concisus*-infected IL-$10^{-/-}$ mice and controls (commensal *E. coli* mono-associated IL-$10^{-/-}$ mice) (Figure 2) were placed in cylindrical glass tubes of Douncer for homogenizing the tissues. The frozen tissues in the glass tubes were allowed to thaw down in ice for about 5 min. Then the tissues were suspended in 50-100 µL ice-cold membrane lysis buffer with a complete protease inhibitor cocktail. The tissues were homogenized in Douncer with a defined number of passes. Minimum shear stress was maintained by Douncer throughout the homogenization. The colonic tissues completely homogenized into cell suspensions were transferred into a fresh Eppendorf tube. The homogenized cell suspensions were then re-suspended about ten to fifteen times using a syringe with needles of different thicknesses,

namely tuberculin needle and IV cannula to obtain a clear homogenate. The cell suspensions were then sonicated with 15 pulses at brief intervals of 3 seconds for every 5 pulses. After sonication, the cells were centrifuged at 200 × g for 5 min at 4 °C. The supernatants were transferred to fresh vials. The supernatants in the fresh tubes were subjected to ultracentrifugation at 43,000 × g for 30 min at 4 °C. The supernatants from ultracentrifugation (solved fractions) were collected in separate vials and stored at -20 °C. The pellets were dissolved in whole-cell lysis buffer with a complete protease inhibitor cocktail. The dissolved pellets were diluted with lysis buffer and re-suspended until a clear lysate was obtained.

The protein concentration of the lysate was estimated using the BCA assay. If the protein concentrations were below par, the solved fractions were subjected to ultracentrifugation and the residual pellets were dissolved in whole-cell lysis buffer for protein estimation. 10 µg of proteins were used for SDS-PAGE gel electrophoresis and Western blotting. Proteins were resolved in SDS-PAGE gels. Electro-transfer of resolved proteins, blocking for unspecific protein signals, and incubation with primary and secondary antibodies were also performed as described in section 2.2.1.4. The primary antibodies used to detect TJ proteins in mouse colon were Rb anti-claudin-5, -7 and -8, mouse (M) anti-claudin-1, -2 and -4, M anti-occludin, and Rb anti-tricellulin. 10% separating gels were used to resolve the proteins for occludin detection and 12.5% separating gels were used for other TJ proteins. Rb anti-β-actin, M anti-β-actin, and M anti-GAPDH were used as loading controls. After this step, the membranes were incubated with secondary antibodies (peroxidase-conjugated goat anti-Rb or anti-M). The membranes were then washed, treated briefly for 1-5 min with chemiluminescence solution and the protein bands were detected using software embedded with the Fusion FX7 system. Densitometry of the blots was performed by normalizing the band intensities of TJ proteins to either β-actin or GAPDH intensities. The band intensities were estimated using ImageJ.

2.2.4. Experimental set-up to determine *Campylobacter concisus*-induced colonic epithelial barrier dysfunction and TJ changes in the presence of immune cells

To investigate the epithelial barrier dysfunction induced by *C. concisus* in the colonic epithelium under the influence of immune activation, HT-29/B6-GR/MR cells and THP-1 monocytes were used together. HT-29/B6-GR/MR cells were cultured in RPMI media for one week at 37 °C in the cell culture incubator with humidified atmosphere. The THP-1 monocytes

from the human monocyte leukemia cell line (ATCC TIB-202) were grown as suspension cells in RPMI media. After one week, the cells were centrifuged at 130 × g for 10 min at 22 ºC. The supernatant was discarded and the cell pellets were re-suspended with antibiotic-free RPMI media supplemented with heat-inactivated 10% FCS. The cell numbers were enumerated and 1.8 x 10^5 cells per mL were seeded into the individual compartments of 12-well plates. The THP-1 cells were differentiated into M1-type macrophages with the treatment of 100 nM PMA for 24-26 h.

HT-29/B6-GR/MR cells were grown as monolayers in cell culture filters (3 μm pore size) at 37 °C for 7-9 days. The cell monolayers were washed and incubated overnight with antibiotic-free RPMI media with heat-inactivated 10% FCS before infection. In parallel to HT-29/B6-GR/MR monolayers, PMA-differentiated THP-1 cells in 12-well plates were also washed and incubated overnight with antibiotic- and PMA-free RPMI media with heat-inactivated 10% FCS. After overnight incubation, HT-29/B6-GR/MR monolayers were placed on the individual compartments of 12-well plates containing THP-1-derived macrophages (Figure 8). This *in vitro* model of colonic epithelial cell monolayers with THP-1-derived macrophages on the basal side, which depicts a *leaky gut*, was adapted from a previous study (Lobo De Sá et al., 2019). In addition to the co-culture condition (HT-29/B6-GR/MR cell monolayers with THP-1-derived macrophages on the basal side), cell monolayers in monoculture condition (without THP-1 cells on the basal side) were maintained in 12-well plates.

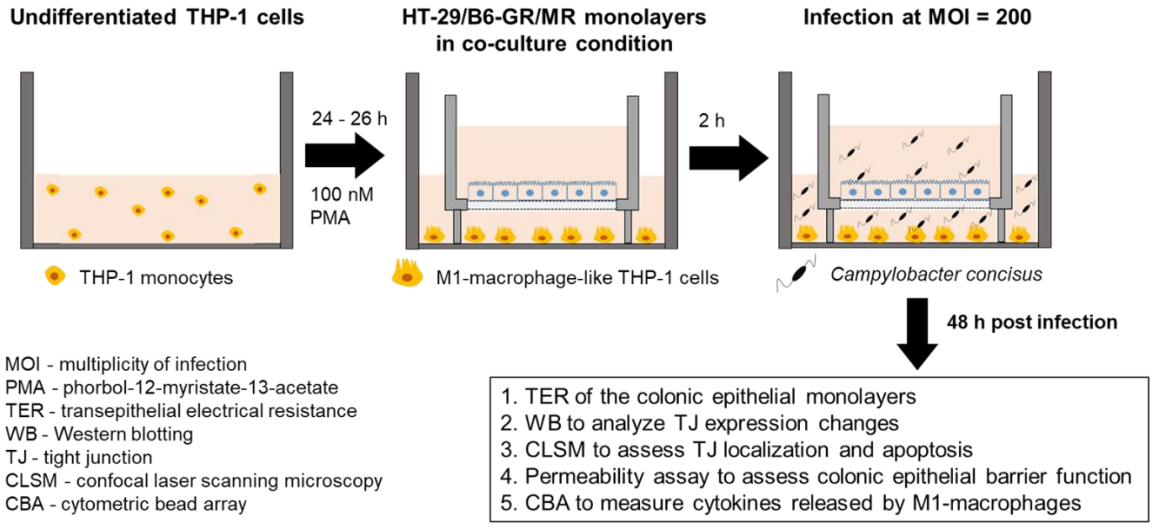

Figure 8. Study design and *in vitro* cell model to investigate colonic epithelial barrier dysfunction induced by *Campylobacter concisus* in presence of immune cells (modified from Nattramilarasu et al., 2021).

The cell monolayers maintained in co-culture condition were infected with *C. concisus* (*C. concisus* strain AAUH 37UCo-a; Kirk et al., 2018) at a MOI of 200 on the apical and basal sides (Figure 8). In parallel, the cell monolayers maintained in monoculture conditions were also infected at the same MOI to compare the epithelial barrier defects induced by *C. concisus* without THP-1-derived macrophages on the basal sides. After infection, the cell monolayers were incubated in the microaerobic atmosphere with H_2. TER of the cell monolayers was recorded in sterile conditions before infection, 24 and 48 h after infection. TJ expression and localization, epithelial apoptosis and the permeability of the cell monolayers for different macromolecules were evaluated at 48 h p.i. In addition, the cytokine release from THP-1-derived macrophages were quantified by cytometric bead array (CBA) kits.

2.2.4.1 Assessment of tight junction protein expression in colonic epithelial cell monolayers

After TER measurements at 48 h p.i, HT-29/B6-GR/MR monolayers were washed twice using PBS (with Ca^{2+}/Mg^{2+}). The proteins were extracted from controls and infected cells using whole-cell lysis buffer, the concentration was determined using BCA assay, and 15 µg of proteins from the samples were resolved using SDS-PAGE gels. The resolved proteins were electro-transferred to PVDF nitrocellulose membranes using either the Trans-Blot system or Wet/Tank Blotting system. PVDF membranes were then blocked, incubated with primary and

secondary antibodies and evaluated for specific protein bands. The primary antibodies used to analyze TJ expression in HT-29/B6-GR/MR cells were Rb anti-claudin-1, -2, -5, -7, -8, M anti-claudin-4, Rb anti-occludin, and Rb anti-tricellulin. M anti-β-actin and M anti-GAPDH were used as loading controls. Densitometry of the TJ blots was performed and the changes in the intensity of TJ protein expression were evaluated in the infected cells with respect to their controls in monoculture and co-culture conditions.

2.2.4.2 Investigation of tight junction localization in colonic epithelial cells

Forty-eight hours post-*C. concisus* infection, TJ protein localization was investigated in DBA-stimulated HT-29/B6-GR/MR monolayers or the monolayers maintained in monoculture and co-culture conditions. The cell monolayers were fixed with 2% PFA at RT for 20 min, and quenched with 25 mM glycine. Following this, the cells were permeabilized using 0.5% TritonX-100 for 7 min. The cells were then incubated with the blocking solution for 30 min at RT to prevent antibodies from binding to unspecific antigens. After blocking, the cell monolayers were incubated with primary antibodies (Rb anti-claudin-8, Rb anti-occludin, Rb anti-tricellulin, and M anti-ZO-1) for 45 min at 37 ^{o}C. The cells were washed twice with the blocking solution and incubated with the secondary antibodies for 45 min at 37 ^{o}C. After this step, the cell monolayers were again washed twice with blocking solution, once with PBS (with Ca^{2+} and Mg^{2+}), and incubated with DAPI for 20 min at RT to detect the nuclei. DAPI was diluted in the blocking solution at a concentration of 1:1000.

After staining the nuclei, the cell monolayers were washed twice with blocking solution and PBS (with Ca^{2+}/Mg^{2+}). The cell monolayers were then briefly rinsed with double distilled water and absolute ethanol. The monolayers on the filters were then dried and excised carefully from the cylindrical plastic holders to mount them on a glass slide. The monolayers were then fixed using mounting solution ProTaq Mount Fluor. The coverslips were then placed over the monolayers on the glass slides. The slides were dried briefly in dark conditions to prevent the loss of fluorescence signals. The controls and *C. concisus*-infected cell monolayers were assessed for TJ localization using confocal laser-scanning microscopy (CLSM). The individual Z-stacks of the cell monolayers were recorded using the laser scan function. We evaluated the localization of claudin-8 and occludin in bTJ and tricellulin in tTJ. Claudin-8, occludin, and

tricellulin were co-stained with ZO-1. The Pearson correlation coefficient calculated as correlation R-value by ZEN software embedded to CLSM was taken as a direct measure of the co-localization intensity of occludin/tricellulin and ZO-1.

2.2.4.3 Epithelial permeability assay to determine the barrier function of colonic epithelial cells

HT-29/B6-GR/MR monolayers infected with *C. concisus* in monoculture or co-culture conditions were evaluated for permeability to macromolecules 48 h p.i. We used fluorescent tracers of different molecular weights, fluorescein (332 Da) and fluorescein isothiocyanate (FITC)-labelled dextran (FITC-dextran; 4 kDa), to evaluate the epithelial permeability. The controls and infected cell monolayers were washed with RPMI medium supplemented with 50 µg/ml gentamycin and incubated for 2 h at 37 ^{o}C in the cell culture incubator with humidified atmosphere to kill the residual bacteria in the infected monolayers. Following the incubation step, the cell monolayers were washed and replaced with antibiotic-free RPMI media supplemented with 10% heat-inactivated FCS. 500 µL and 1500 µL of media were added on the apical and the basal sides of the monolayers respectively. The cell monolayers were then equilibrated in the cell culture incubator with the humidified atmosphere at 37 ^{o}C for 15 min. After incubation, either fluorescein (100 µM) or FITC-dextran (200 µM) was added to the cell monolayers to measure the unidirectional flux from the apical to basal sides. RPMI media on the apical and basal sides of the cell monolayers were supplemented with 200 µM unlabelled dextran (4 kDa) to measure FITC-dextran flux. 300 µL of the samples were obtained from the basal side of the cell monolayers for every 15 min up to 1 h to measure the fluorescein flux. For FITC-dextran flux measurements, the samples were obtained from the basal side every 30 min up to 2 h. An equal volume of fresh media was replaced when 300 µL was obtained from the basal side of the cell monolayers at different time points for fluorescein flux measurements. The absorbance of the fluorescent signals from fluorescein and FITC-dextran were measured using the TECAN spectrophotometer at an excitation/emission wavelength of 490/525 nm. Fluorescein and FITC-dextran fluxes were calculated over the concentration difference, from which the permeability of HT-29/B6-GR/MR cell monolayers was enumerated.

2.2.4.4 Evaluation of apoptosis in colonic epithelial cells

TUNEL assay kit was used to detect apoptosis in *C. concisus*-infected HT-29/B6-GR/MR cell monolayers in monoculture and co-culture conditions 48 h p.i. The protocol for staining apoptotic cells was followed according to the manufacturer's instructions of the TUNEL assay. Briefly, the controls and infected cell monolayers on PCF filters were washed using PBS (with Mg^{2+}/Ca^{2+}) and subjected to fixation with 2% PFA. The fixation was quenched, and the cells were permeabilized and blocked for unspecific protein signals as already described in section 2.2.4.2. After blocking, the cells were stained with the enzyme solution, the Terminal deoxynucleotidyl Transferase (TdT) provided in the TUNEL assay kit. In addition, the nuclei of the cells were stained by DAPI.

The cellular apoptosis was visualized with the green fluorescent signals of TdT in fluorescence microscope at a wavelength of 488 nm. In apoptotic cells, the green fluorescent signals of TdT co-localize with nuclei with evident DNA strand breaks. In a low power field of 150-200 cells, 5 to 8 regions were randomly picked from controls and infected cell monolayers. The number of apoptotic cells in a specific region was manually enumerated along with the total number of cells in the same region. Later, the ratio of apoptotic cells to the total number of cells was calculated in all the regions picked for epithelial apoptosis quantification.

2.2.4.5 Cytometric bead array to measure the cytokine release from THP-1-derived M1 macrophages

To determine the role of THP-1-derived macrophages in regulating *C. concisus*-induced colonic epithelial barrier defects in co-culture conditions, the cytokines released from THP-1 cells were assessed using CBA kit 48 h p.i. The media were obtained from the basal compartment of control and infected monolayers maintained in co-culture conditions, which were subjected to cytokine analyses using capture bead technology of CBA according to the manufacturer's instruction. The cytokines IL-1β, IL-13, IL-4, IL-6, IL-10, IL-17A, IFN-γ and TNF-α were then measured using the flow cytometry technique with FACS Canto II. The data from FACS were analyzed and quantified by FACP Array software.

2.2.5. Evaluation of cell viability

The cell viability of HT-29/B6-GR/MR cells was determined at 48 h p.i., to ensure that the changes in functional ENaC activity or TJ expression resulting from *C. concisus* infection are independent of necrotic cell death.

2.2.5.1 Cytotoxicity of colonic epithelial cell monolayers used for functional ENaC activity measurements

The cytotoxicity of DBA-stimulated HT-29/B6-GR/MR monolayers was evaluated 48 h after *C. concisus* infection (Figure 1) by CCK-8 assay. In addition to the monolayers, HT-29/B6-GR/MR cells were also seeded into 96-well plates (10,000 cells per well) and grown in RPMI media for 7–10 days incubated at 37 °C in a humidified atmosphere (95% air/5% CO_2). The cells were then stimulated with DBA for four days and infected with *C. concisus* at a MOI of 400. The 96-well plates with the infected cells and controls after DBA stimulation were placed at 37 ^oC in the microaerobic atmosphere with H_2. The cells were washed with gentamycin-supplemented RPMI media at 48 h p.i and the viability was determined by CCK-8 assay. 10 µL of the enzyme solution WST-8 (2-(2-methoxy-4-nitrophenyl)-5-(2, 4-disulfophenyl)-2H-tetrazolium, monosodium salt) in the kit was added into 100 µL of the cell suspensions in 96-well plates. The 96-well plates were then placed in a humidified atmosphere (95% air/5% CO_2) at 37 ^oC for 1 h. WST-8 oxidizes cellular dehydrogenases to generate a water-soluble formazan dye, an orange-colored end product (Ishiyama et al., 1997; Tominaga et al., 1999). The absorbance of the formazan dye was measured using the TECAN spectrophotometer at 450 nm, with a reference wavelength of 600 nm. The absorbance values were directly proportional to the intensity of the formazan dye, which in turn represents the number of living cells.

2.2.5.2 Cell proliferation of colonic epithelial cell monolayers in monoculture and co-culture conditions

The cell viability of HT-29/B6-GR/MR monolayers was measured 48 h after *C. concisus* infection in both monoculture and co-culture conditions using the CCK-8 assay. In addition, the cell proliferation rate of HT-29/B6-GR/MR cells in 96-well plates was also determined. For this purpose, fresh HT-29/B6-GR/MR cells were seeded in 96-well plates with 10,000 cells per

well and incubated overnight at 37 ºC in a humidified atmosphere (95% air/5% CO_2). Then the cells were washed and incubated for about 24 h in antibiotic-free RPMI media supplemented with 10% heat-inactivated FCS. HT-29/B6-GR/MR cells in 96-well plates were then infected with *C. concisus* at MOI of 25, 50, 100, 200, 400, 500 and 1000. The infected cells along with the controls were placed in the microaerobic atmosphere with H_2 at 37 ºC. Forty-eight hours p.i., the cell proliferation rate was determined by CCK-8 assay.

In parallel to HT-29/B6-GR/MR cell monolayers, the THP-1 monocytes were seeded in 96-well plates with 1.8 x 10^5 cells per well. They were differentiated into M1 macrophages using 100 nM PMA. M1 macrophages in 96-well plates were washed and incubated overnight with antibiotic-free RPMI media supplemented with 10% heat-inactivated FCS. Then the cells in 96-well plates were infected with *C. concisus* at MOI of 25, 50, 100, 200, 400, 500 and 1000. After infection, the 96-well plates were placed in the microaerobic atmosphere with H_2. The cell proliferation rate was measured by the CCK-8 assay. Then the cell proliferation rate of the infected cells was normalized to controls and the percentage change in cell proliferation in infected cells was determined with respect to controls.

2.2.6 Statistics

In the results, data are expressed as mean value ± standard error of the mean (SEM). Statistical analyses were performed with GraphPad Prism version 5.0. An unpaired t-test was used to compare the mean values of two independent data sets. To compare two data sets with unequal variances, an unpaired t-test with Welch's correction was used. More than two data sets in a single comparison were analyzed using one-way ANOVA with Bonferroni–Holm adjustment. To compare data sets that were not normally distributed, the Mann–Whitney *U*-Test was used. $P < 0.05$ was considered statistically significant.

2.2.7 Ethics statement

Animal experiments were carried out in the animal facility at the Forschungseinrichtung für Experimentelle Medizin (Charité-Universitätsmedizin Berlin) according to the German animal protection law (approval number G0172/16, LAGeSo Berlin).

3. Results

3.1. Functional ENaC actvity impairment by *Campylobacter concisus in vitro*

To investigate the pathological impact of *Campylobacter* spp. on the ion transport in epithelial cells, HT-29/B6-GR/MR monolayers were infected with *C. concisus* and *C. jejuni* at a MOI of 400 (Nattramilarasu et al., 2020). Forty-eight hours p.i., ENaC activity i.e. electrogenic Na^+ absorption via ENaC was measured in the Ussing chamber. The viability of the monolayers was tested by evaluating Cl^- secretion in the epithelial cells at the end of each experiment. In parallel to the functional evaluation of ENaC activity, the transcriptional regulation of α, β, and γ subunits of ENaC was also analyzed.

3.1.1 *Campylobacter concisus* impairs sodium absorption via ENaC in HT-29/B6-GR/MR cells

HT-29/B6-GR/MR cells induced an increase in ENaC activity (ΔI_{SC} in $\mu A/cm^2$ after 100 µM amiloride, which depicts ENaC-dependent Na^+ absorption) after DBA stimulation (Figure 1). A marked decrease in ENaC function was observed in both *C. concisus*- and *C. jejuni*-infected HT-29/B6-GR/MR monolayers compared to DBA-stimulated controls (Figure 1). However, a decrease in ENaC activity was more pronounced in *C. jejuni*-infected monolayers compared with *C. concisus*-infected monolayers (Figure 9).

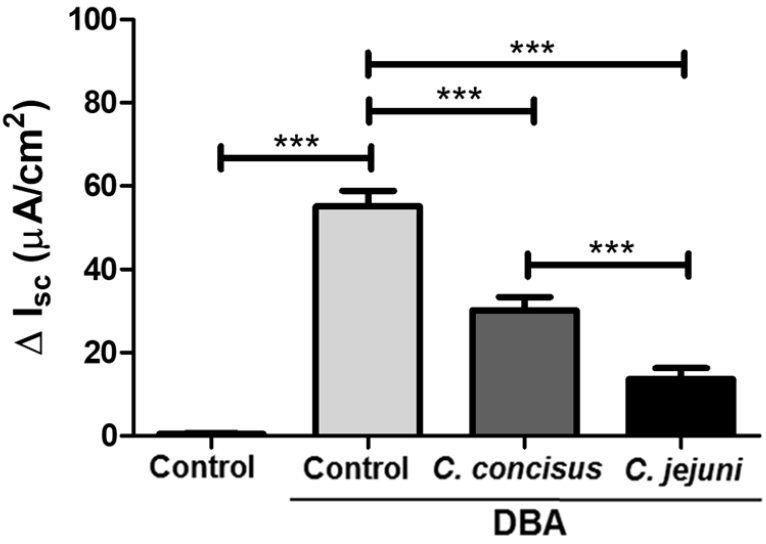

Figure 9. Functional measurement of ENaC activity in HT-29/B6-GR/MR cells 48 h after *Campylobacter concisus* and *Campylobacter jejuni* infection. ENaC-mediated Na^+ absorption was measured as change in short-circuit current (ΔI_{SC} in $\mu A/cm^2$) after 100 µM amiloride in the apical compartment of the Ussing chamber (n = 15, *** $P < 0.001$). HT-29/B6-GR/MR cells were stimulated with the glucocorticoid dexamethasone (D, 50 nM), sodium salt of butyrate (B, 2 mM) and mineralocorticoid aldosterone (A, 3 nM). ΔI_{SC} after 100 µM amiloride was also recorded in controls without DBA stimulation (modified from Nattramilarasu et al., 2020).

3.1.2 Functional viability tests of HT-29/B6-GR/MR monolayers 48 h post infection

As *C. concisus* impair ENaC activity at a MOI of 400, HT-29/B6-GR/MR monolayers were evaluated for their retention of functional transport capacity at 48 h p.i. For this purpose, the active Cl^- secretion in the infected cell monolayers and controls were measured in parallel to ENaC activity in Ussing chambers. Electrogenic Cl^- secretion was measured as the transient increase in short-circuit current (ΔI_{SC} in $\mu A/cm^2$) after the addition of PGE_2 and theophylline (both acting via cAMP stimulation) or cholinergic agonist carbachol (acting via Ca^{2+} as the second messenger) in the Ussing chambers. No significant differences in ΔI_{SC} were observed between DBA-stimulated controls and *C. concisus*-infected cell monolayers neither to PGE_2 and theophylline nor to carbachol treatments (Figure 10). This confirmed that HT-29/B6-GR/MR monolayers preserved their functional viability during infection. In addition, no differences in ΔI_{SC} were observed between DBA-stimulated controls and controls without DBA stimulation.

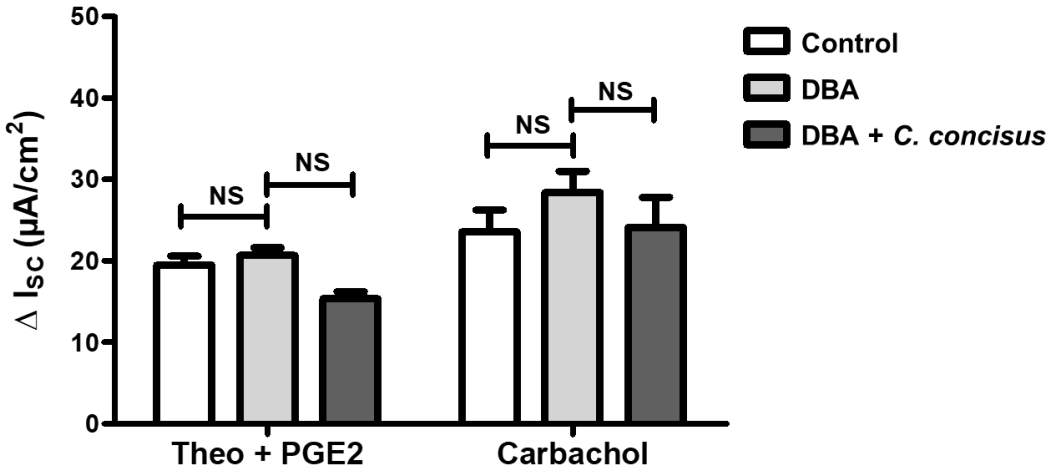

Figure 10. Preserved viability of HT-29/B6-GR/MR cell monolayers 48 h after *Campylobacter concisus* infection represented by unaltered chloride channel activation. Chloride secretion was determined as a transient increase in short circuit current (ΔI_{SC} in $\mu A/cm^2$) 2–3 min after addition of prostaglandin E_2 (PGE_2) (10 µM, basal side) and theophylline (10 mM, apical and basal side) to the Ussing chamber. In the same experiment, transient changes in I_{SC} (ΔI_{SC} in $\mu A/cm^2$) were also measured 2–3 min after the addition of carbachol (100 µM, basal side). *C. concisus*-infected cell monolayers were compared to DBA-stimulated controls (n = 4–5 each, NS = not significant). DBA = dexamethasone, butyrate and aldosterone (modified from Nattramilarasu et al., 2020).

3.1.3 Gene expression of α-, β- and γ-ENaC subunits

DBA stimulation induced an increase in mRNA levels of β- and γ-ENaC genes, *SCNN1B* and *SCNN1G* (Figure 11). The mRNA levels of the α-ENaC gene, *SCNN1A*, was not increased by DBA stimulation (Figure 11). Forty-eight hours p.i., *C. concisus* induced a marked decrease in the mRNA levels of *SCNN1B* and *SCNN1G*, while mRNA expression of *SCNN1A* was unchanged compared to DBA-stimulated controls (Figure 11). Thus, the downregulation in the mRNA expressions of *SCNN1B* and *SCNN1G* by *C. concisus* contributes to the impairment of ENaC-mediated Na^+ absorption.

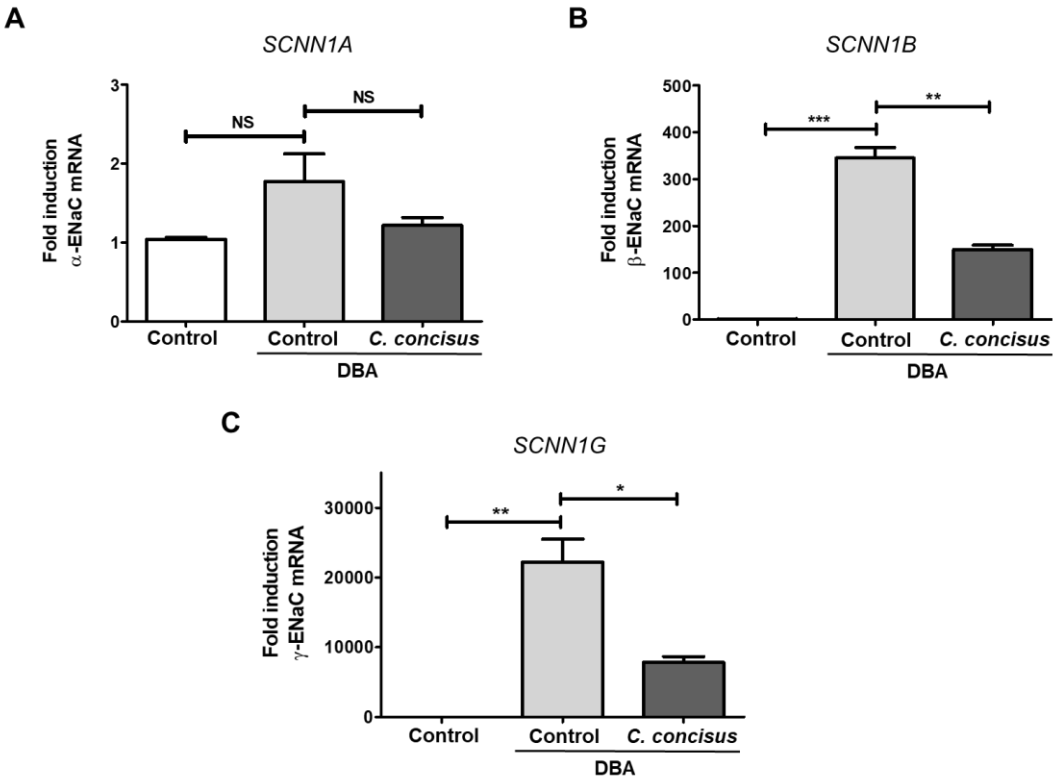

Figure 11. The mRNA expression of ENaC subunits (α, β and γ) 48 h post infection in HT-29/B6-GR/MR cells. RT-qPCR measurements showing **(A)** mRNA expression of α-ENaC gene (*SCNN1A*) in controls, DBA-stimulated monolayers and *C. concisus*-infected monolayers after DBA stimulation (n = 4, NS = not significant, P > 0.05). **(B)** mRNA expression of β-ENaC gene (*SCNN1B*) (n = 4, *** $P < 0.001$, ** $P < 0.01$). **(C)** mRNA expression of γ-ENaC gene (*SCNN1G*) (n = 4, ** $P < 0.01$, * $P < 0.05$). DBA = dexamethasone, butyrate and aldosterone (modified from Nattramilarasu et al., 2020).

3.2. *Campylobacter concisus* dysregulates ENaC function by activation of mitogen-activated protein kinase

Among different MAPK enzymes, ERK activation negatively regulates ENaC activity in colon mucosae of CD and lymphocytic colitis patients (Zeissig et al., 2008; Barmeyer et al., 2016). Moreover, ERK activation was also discerned as an intracellular cell signaling pathway in negatively regulating ENaC function from the bioinformatics predictions of RNA-Seq data from colon biopsies of *C. jejuni*-infected patients (personal communication R. Bücker, unpublished data). Therefore, the phosphorylation or activation of the ERK was assessed in HT-29/B6-GR/MR monolayers after *C. concisus* or *C. jejuni* infections in parallel to the functional measurements of ENaC activity.

3.2.1 Activation of extracellular signal-regulated kinase (ERK) by *Campylobacter concisus* and *Campylobacter jejuni*

Forty-eight hours p.i., western blotting was performed to assess the phosphorylation or activation of ERK 15 min after DBA stimulation in controls and *Campylobacter* spp.-infected cell monolayers. Phosphorylation of isoforms ERK1 (44 kDa band) and ERK2 (42 kDa band) were increased by both *C. concisus* and *C. jejuni* (Figure 12A). The phosphorylation of ERK1/2 in the infected cells was measured as a fold change compared with controls set at 1-fold. Densitometry results statistically confirmed that *C. concisus* and *C. jejuni* increased ERK phosphorylation after DBA stimulation (Figure 12B). It indicates that *C. concisus* and *C. jejuni* induced ERK activation parallel to ENaC dysfunction in HT-29/B6-GR/MR cells. Furthermore, no significant differences were observed in the fold change of ERK phosphorylation between *C. concisus* and *C. jejuni* infections in HT-29/B6-GR/MR cells.

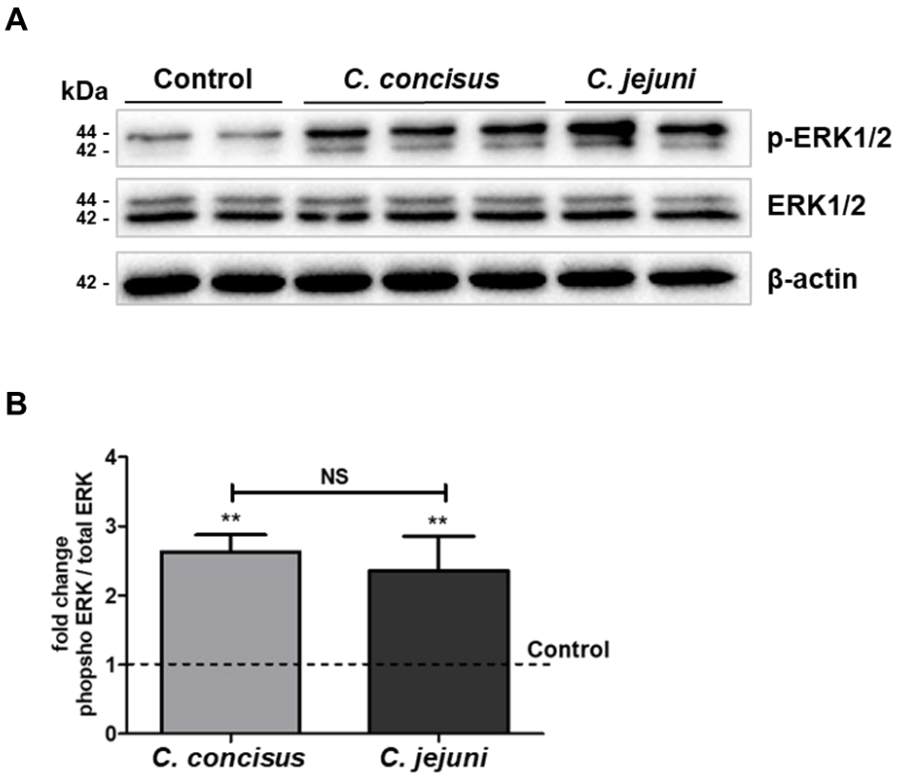

Figure 12. Activation of extracellular signal-regulated kinase (ERK) in HT-29/B6-GR/MR cell monolayers by *Campylobacter concisus* and *Campylobacter jejuni* 48 h post infection. (**A**) Western blots of the phosphorylated ERK (p-ERK1/2) and total ERK (ERK1/2) 15 min after DBA stimulation and *C. concisus* or *C. jejuni* infection. (**B**) ERK activation by *C. concisus* and *C. jejuni* infections represented as fold-change in the bar graphs depicting band intensity ratio of p-ERK1/2 to ERK1/2 (normalized to β-actin). DBA-stimulated controls

set at one fold indicated by dotted line (n = 4–6, NS = not significant, ** $P < 0.01$). DBA = dexamethasone, butyrate and aldosterone (modified from Nattramilarasu et al., 2020).

3.2.2 Functional inhibition of extracellular signal-regulated kinase (ERK) attenuates *Campylobacter concisus*-induced ENaC dysfunction

To determine if ERK activation induced by *C. concisus* was responsible for the impairment of ENaC activity, ERK activation was functionally blocked by upstream inhibition of MEK by U0126. ENaC activity was tested in *C. concisus*-infected monolayers after inhibition of ERK activation by U0126. Based on measurements of the amiloride-sensitive increase in I_{SC} 48 h p.i., U0126 promoted a partial but significant rescue of the ENaC activity impaired by *C. concisus*-induced (Figure 13), suggesting that ERK blockade ameliorates the ENaC dysfunction induced by *C. concisus*. Furthermore, this confirmed that ERK activation by *C. concisus* is an important intracellular cell signaling mechanism in mediating ENaC dysfunction.

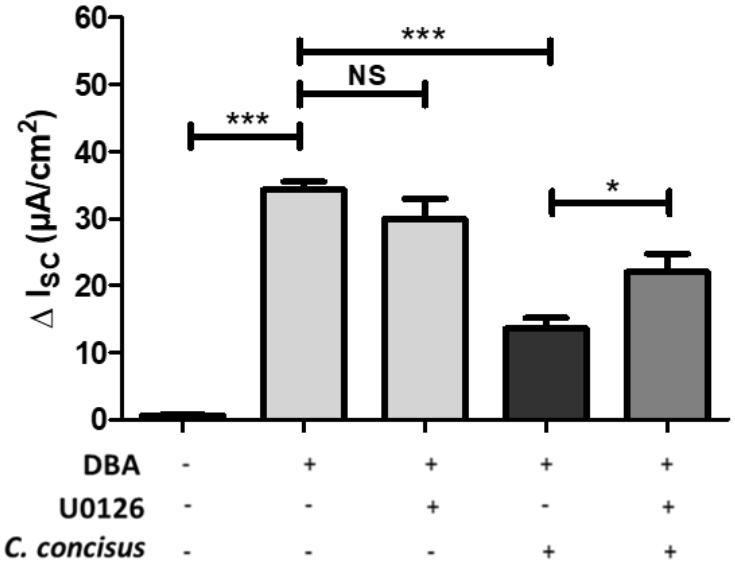

Figure 13. Inhibition of extracellular signal-regulated kinase (ERK) attenuates *Campylobacter concisus*-induced ENaC impairment on the functional level. The specific ERK inhibitor U0126 (10 µM) was applied to HT-29/B6-GR/MR cell monolayers 2 h before *C. concisus* infection. In parallel, control cell monolayers were stimulated by DBA without infection. ENaC activity was measured as a decrease in short-circuit current (ΔI_{SC} in $\mu A/cm^2$) 15 min after addition of amiloride (100 µM) to the apical side of the Ussing chambers (n = 6–8, * $P < 0.05$, *** $P < 0.001$, NS = not significant). DBA = dexamethasone, butyrate and aldosterone (modified from Nattramilarasu et al., 2020).

3.2.3 Gene expression analyses and bioinformatics predictions from RNA-Seq data

RNA-Seq was performed to evaluate the genes, which are differentially expressed after *C. concisus* infection in DBA-stimulated HT-29/B6-GR/MR cells. At 48 h p.i., the total RNA from HT-29/B6-GR/MR monolayers was subjected to reverse transcription to synthesize cDNA, which was then subjected to RNA-Seq. From the gene expression studies of RNA-Seq data through Bioconductor package DESeq2 (Love et al., 2014), 1667 genes were differentially expressed (P>0.05) by *C. concisus* infection. The Fastq files containing the unprocessed raw reads from sequencing and a raw counts matrix table were deposited in a publicly available database Gene Expression Omnibus (GEO) archive of the National Centre for Biotechnology Information (NCBI). This can be viewed online with GEO accession ID GSE141217 (https://www.ncbi.nlm.nih.gov/gds/?term=GSE141217) under the topic "*Campylobacter concisus* impairs sodium absorption via ENaC dysfunction and claudin-8 disruption" (Nattramilarasu et al., 2020).

Furthermore, the gene expression changes from RNA-Seq data were also evaluated by Bioconductor package edge R (Robinson et al., 2010), and represented as counts per million (CPM) values, in which 66 genes were upregulated and 120 genes were downregulated (Nattramilarasu et al., 2020). Interestingly, IL-32 was found to be the only proinflammatory cytokine, whose mRNA expression was upregulated after *C. concisus* infection (Figure 14).

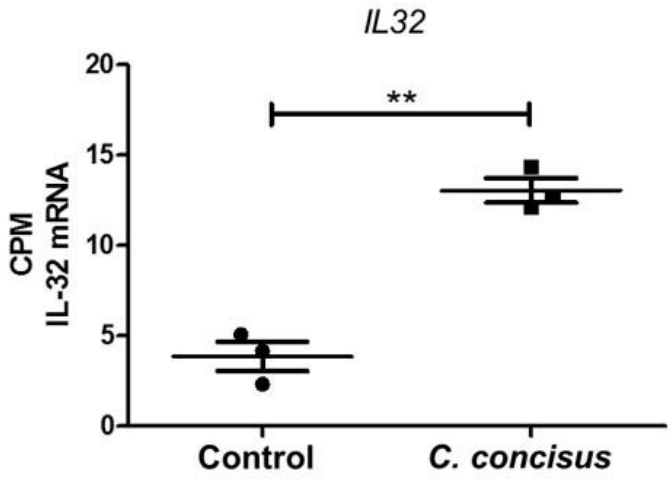

Figure 14. Interleukin-32 (IL-32) mRNA expression in HT-29/B6-GR/MR cell monolayers 48 h after *Campylobacter concisus* infection. The mRNA expression of IL-32 (gene name: *IL32*) in controls and *C. concisus*-infected cell monolayers after DBA stimulation. Data are expressed in counts per million (CPM) calculated by differential gene expression analyses of RNA-Seq data (n = 3, ** $P < 0.01$). DBA = dexamethasone, butyrate and aldosterone (modified from Nattramilarasu et al., 2020).

RNA-Seq data was also used for the bioinformatics predictions through IPA, from which the Upstream regulator analysis was performed to determine the transcriptional regulators, which targets IL-32 and ERK. The upstream regulators can be a transcription factor, microRNA, kinase, compound or drug, which targets a gene. Interestingly, IPA analyses revealed that IL-32 is an upstream regulator, which targets ERK, which in turn leads to ENaC dysfunction. Furthermore, IFN-γ, IL-1β, LPS, nuclear factor 'kappa-light-chain-enhancer' of activated B-cells (NF-κB) complex and dexamethasone were identified as upstream regulators, which target IL-32 (Supplemental Table S1). All the upstream regulators which target IL-32 showed an overlap *P*-value < 0.01, which indicates a significant overlap between the data set genes from the existing literature and genes targeted by upstream regulators. In addition to overlap *P*-value, *Z*-score was another statistical measure computed by IPA, which indicates if an upstream regulator has more activated ($Z > 0$) or inhibited ($Z < 0$) predictions. The upstream regulators which target IL-32 are predicted to be in an activated state, and IL-5 was ascertained as another cytokine that was activated although it doesn't target IL-32 (Supplemental Table S1).

The Na^+ transport via ENaC is also influenced by the expression and function of other ion transporters in the colonic epithelium, for instance CFTR, NKCC1, NHE3, Na^+/K^+-ATPase, Ca^{2+}-activated Cl^- channel (CaCC) and DRA. Hence, the gene expression of the aforementioned

ion transporters was analyzed 48 h after *C. concisus* infection from RNA-Seq data. The mRNA expression was depicted as gene counts from the Bioconductor package DESeq2 (Love et al., 2014), and the statistical significance was estimated by *P*-values adjusted by the Benjamin-Hochberg procedure. The mRNA expressions of CFTR and NKCC1 channels were downregulated by *C. concisus* infection, while the expressions of other transporters were unaltered (Supplemental Table S2).

3.3. *Campylobacter concisus* impairs paracellular barrier function in parallel to the ENaC dysfunction through claudin-8 disruption

In addition to the assessment of ERK activation, gene expression changes and bio-informatics pathway predictions following the measurements of functional ENaC activity in HT-29/B6-GR/MR monolayers, the paracellular barrier function and the cell viability of the monolayers were also assessed in response to *C. concisus* infection.

3.3.1 Impairment of paracellular barrier function and downregulation of claudin-8 expression by *Campylobacter concisus*

To investigate the paracellular barrier function of cell monolayers 48 h after *C. concisus* infection in DBA-stimulated HT-29/B6-GR/MR monolayers, TER was measured 20 min after amiloride addition in DBA-stimulated cell monolayers. Under these conditions, TER reflected paracellular sealing by TJ proteins. In *C. concisus*-infected cell monolayers at 48 h p.i., TER was decreased compared to control values (Figure 15A). It gives direct evidence of *C. concisus*-induced impairment of paracellular barrier function in HT-29/B6-GR/MR cells under glucocorticoid and mineralocorticoid stimulation. Then, the changes in TJ integrity were examined at the molecular level using RT-qPCR. It turned out that claudin-8 (*CLDN8*) mRNA expression was decreased 48 h post-*C. concisus* infection (Figure 15B). In addition, the expression of different TJ proteins by Western blotting and the corresponding densitometric analysis indicated that *C. concisus* induced a decrease in claudin-8 expression when compared to controls (Figure 15C). The expression of the other TJ proteins (claudin-1, -2, -4, and -5) was not affected by *C. concisus* infection when compared to DBA-stimulated controls.

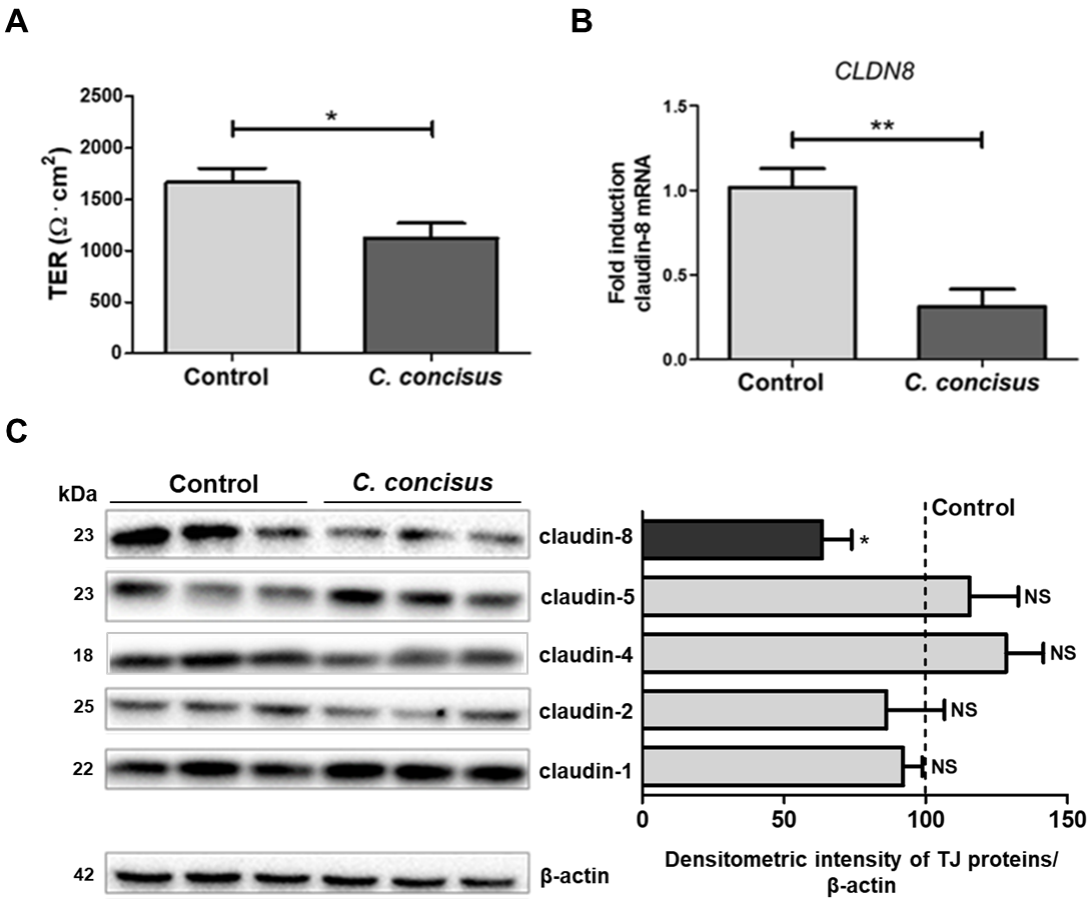

Figure 15. Changes in transepithelial electrical resistance and tight junction protein expression in HT-29/B6-GR/MR cell monolayers 48 h after *Campylobacter concisus* infection. (A) Transepithelial electrical resistance (TER) was recorded 20 min after the addition of amiloride (100 µM). TER of *C. concisus*-infected cell monolayers were compared to DBA-stimulated controls (n = 7–8, * $P < 0.05$). **(B)** The mRNA expression changes of claudin-8 (*CLDN8*) in *C. concisus*-infected cell monolayers were measured with qPCR and compared to DBA-stimulated controls (n = 4, ** $P < 0.01$). **(C)** Western blots of tight junction proteins and the corresponding densitometry showing changes in the expression of tight junctions in *C. concisus*-infected cell monolayers. DBA-stimulated controls were set at 100, indicated by dotted line (n = 3–5, * $P < 0.05$, NS = not significant). DBA = dexamethasone, butyrate and aldosterone (modified from Nattramilarasu et al., 2020).

3.3.2 Delocalization of claudin-8 from the epithelial tight junction by *Campylobacter concisus*

As we found a reduction in claudin-8 expression 48 h after *C. concisus* infection, structural microscopic analysis was carried out by investigation of claudin-8 localization in TJ by CLSM. We observed a redistribution of claudin-8 off the TJ domain of the epithelial cells. Z-stack analyses of CLSM images revealed that claudin-8 was accumulated as intracellular aggregates

in *C. concisus*-infected cell monolayers, whereas a clear co-localization of claudin-8 with ZO-1 was observed in TJs in control cell monolayers (Figure 16).

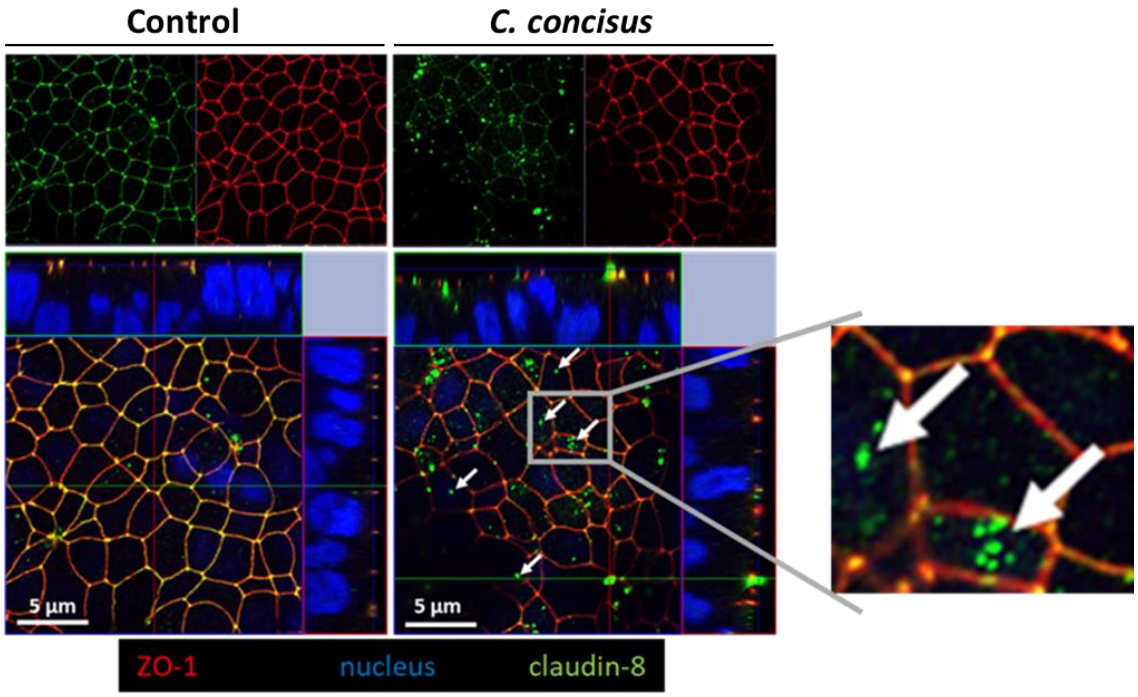

Figure 16. Subcellular distribution of claudin-8 in HT-29/B6-GR/MR cell monolayers 48 h after *Campylobacter concisus* infection. Claudin-8 (green) was intact in the intercellular tight junction and co-localized with zonula occludens protein-1 (ZO-1) (red) in DBA-stimulated control cell monolayers. Nuclei (blue) were stained by 4′-6-diamidino-2-phenylindole dihydrochloride (DAPI). In *C. concisus*-infected cell monolayers, claudin-8 was redistributed off the tight junction into intracellular compartments, indicated by white arrows. DBA = dexamethasone, butyrate and aldosterone (modified from Nattramilarasu et al., 2020).

3.3.3 Cell viability of HT-29/B6-GR/MR cells 48 hours post infection

To confirm the cell viability 48 h after *C. concisus* infection, cell proliferation rate and cytotoxicity of the cells were tested using the CCK-8 assay. No significant differences were detected in cell viability after *C. concisus* infection compared to controls after DBA stimulation (Figure 17), indicating that *C. concisus*-induced paracellular barrier defects were independent of necrotic cell death.

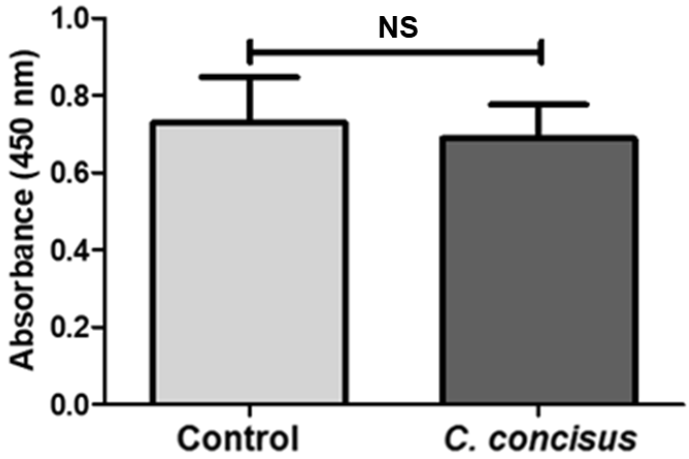

Figure 17. Cell viability of HT-29/B6-GR/MR cells 48 h after *Campylobacter concisus* infection. Colorimetric assay Cell Counting Kit-8 (CCK-8) was used for the determination of cell viability in cytotoxicity testing. Absorbance values were recorded at 450 nm with a reference wavelength of 600 nm in DBA-stimulated controls and *C. concisus*-infected cells, which reflected cellular activity 1 h after addition of water-soluble tetrazolium salt (WST-8 in the CCK8 assay; n = 8, $P > 0.05$, NS = not significant). DBA = dexamethasone, butyrate and aldosterone (modified from Nattramilarasu et al., 2020).

3.4 Functional ENaC activity impairment by *Campylobacter concisus in vivo*

The secondary abiotic IL-$10^{-/-}$ mouse is a sophisticated *in vivo* model to study the functionality of the inflamed intestine in *C. jejuni* infection (Haag et al., 2012; Heimesaat et al., 2014). Hence, this mouse model was employed to determine the *in vivo* effects of *C. concisus* in colonic epithelium, especially Na^+ absorption via ENaC in the distal colon. *Campylobacter concisus* infection induced a decrease in the amiloride-sensitive I_{SC} (ΔI_{SC} in $\mu A/cm^2$) in colonic tissues of distal colon mounted in Ussing chambers, which reflects ENaC dysfunction (Figure 18). Furthermore, a pronounced decrease in ENaC activity of distal colon was observed in *C. jejuni*-infected IL-$10^{-/-}$ mice compared to *C. concisus*-infected IL-$10^{-/-}$ mice (Figure 18). This corresponds to our *in vitro* results of ENaC dysfunction induced by *C. concisus* and *C. jejuni* (Figure 18).

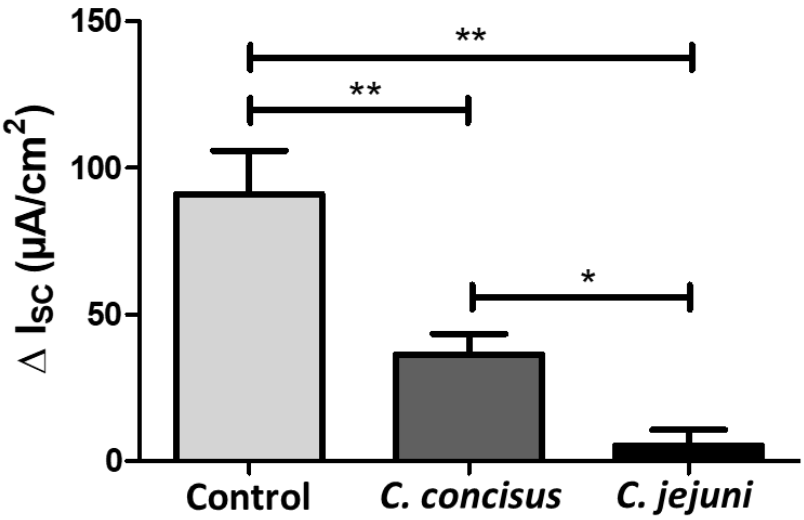

Figure 18. Functional impairment of ENaC in the distal colon of abiotic IL-10$^{-/-}$ mice 6 days following *Campylobacter concisus* and *Campylobacter jejuni* infections. Colon specimens from the distal colon of infected mice and controls were stimulated for 6 h with the mineralocorticoid aldosterone (3 nM) in Ussing chambers. The colon samples of IL-10$^{-/-}$ mice mono-associated with commensal *E. coli* were used as controls. The decrease in short circuit current (ΔI_{SC}; µA/cm^2) 20 min after addition of amiloride (100 µM) was measured and represented as ENaC-dependent Na^+ absorption (n = 4–9, ** $P < 0.01$, * $P < 0.05$) (modified from Nattramilarasu et al., 2020).

To ensure the viability of colonic tissues after ENaC activity measurement in the Ussing chambers, the activity of electrogenic Cl^- secretion was tested by stimulation with PGE_2 and theophylline. In addition, the inhibition of Cl^- secretion was tested with bumetanide. The transient changes in I_{SC} in response to Cl^- secretion and its inhibition were recorded. Cl^- secretion and its inhibition were evident in colonic mucosae of IL-10$^{-/-}$ mice 6 hours after aldosterone stimulation (Table 1). No significant differences were observed between controls and *C. concisus*-infected IL-10$^{-/-}$ mice, reflecting an active and viable mucosa (Table 1). In addition, no difference in the epithelial (R^{epi}) and subepithelial resistance (R^{sub}) of the colon specimens were observed between controls and *C. concisus*-infected IL-10$^{-/-}$ mice (Table 1). This implies that ENaC dysfunction induced by *C. concisus* was independent of epithelial barrier changes by leaks or tissue destruction in the colonic epithelium of IL-10$^{-/-}$ mice.

IL-10$^{-/-}$ mice	ΔI_{SC} (µA/cm^2) after PGE_2 + theophylline	ΔI_{SC} (µA/cm^2) after bumetanide	Resistance		
			R^{epi}	R^{sub}	R^{t}
Control (n = 4–8)	27 ± 8.0	−15 ± 4.1	28 ± 3.6	25 ± 2.2	52 ± 3.6
C. concisus-infection (n = 5–8)	25 ± 8.1	−16 ± 5.6	33± 3.1	29 ± 2.6	62 ± 3.9
Significance	NS	NS	NS	NS	NS

Table 1. Evaluation of colonic integrity in *Campylobacter concisus*-infected mice. Data represent the mean ± SEM ($P > 0.05$, ns). No significant difference was observed in correction factors (R^{total}/R^{epi}) for active transport rates, i.e. I_{SC} changes after PGE_2 + theophylline or bumetanide between *C. concisus*-infected IL-10$^{-/-}$ mice and controls (controls = 1.99 ± 0.18 and *C. concisus* = 1.91 ± 0.10, n = 8, $P > 0.05$, NS) (modified from Nattramilarasu et al., 2020). Controls are commensal *E. coli* mono-associated IL-10$^{-/-}$ mice. NS - not significant, PGE_2 - prostaglandin E_2, R^t - total transmural resistance, R^{sub} - subepithelial resistance, R^{epi} - epithelial resistance.

3.5. *Campylobacter concisus* aggravates epithelial barrier dysfunction in the colonic epithelila cells in co-culture with immune cells

In order to investigate the influence of subepithelial immune activation on the epithelial barrier dysfunction induced by *C. concisus*, we used an *in vitro* co-culture model of colonic epithelial cell monolayers with THP-1-derived macrophages (Nattramilarasu et al., 2021).

3.5.1 Pronounced transepithelial electrical resistance decrease in colonic epithelial cell monolayers in co-culture with THP-1-derived macrophages

The TER of the cell monolayers were recorded in the monoculture and co-culture conditions (with THP-1-derived macrophages on the basal side of HT-29/B6-GR/MR cell monolayers). We observed a marked decrease in the TER of the cell monolayers 24 h and 48 h after *C. concisus* infection compared to controls in monoculture and co-culture conditions (Figure 19). At 24 h p.i., the TER of the infected cell monolayers in the monoculture condition was comparable to the TER of the infected cell monolayers in the co-culture condition with no significant differences (Figure 19). Interestingly, at 48 h p.i. a profound decrease was detected in the TER of the infected cell monolayers in the co-culture compared to the monoculture condition (Figure 19).

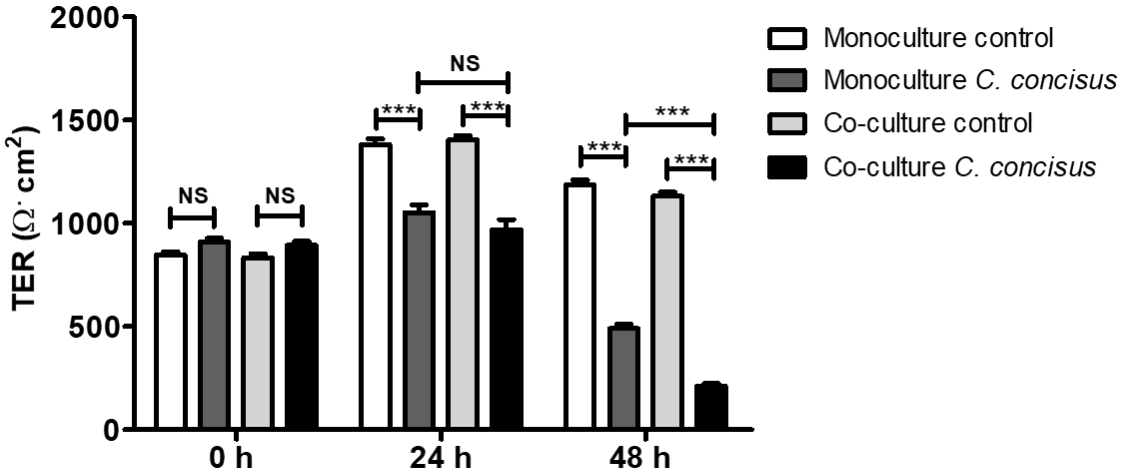

Figure 19. Transepithelial electrical resistance changes in HT-29/B6-GR/MR cell monolayers maintained in monoculture and co-culture (with THP-1-derived macrophages on the basal side) conditions 48 h after *C. concisus* infection. Transepithelial electrical resistance (TER) of control cell monolayers (white/bright grey bars) in monoculture and co-culture conditions were recorded and compared with infected monolayers (dark grey/black bars) at 0 h (before infection), 24 and 48 h post-*C. concisus* infection. The cell monolayers were infected with a multiplicity of infection (MOI) of 200 (n = 23 in three independent experiments, NS = not significant, *** $P <$ 0.001) (modified from Nattramilarasu et al., 2021).

3.5.2 Tight junction changes in colonic epithelial cell monolayers in monoculture and co-culture conditions

Comprehensive analyses of the TJ protein expression were performed in *C. concisus*-infected HT-29/B6-GR/MR cell monolayers in monoculture and co-culture conditions. Forty-eight hours p.i., the expression of claudin-1, -2, -4, -5, -7, -8, occludin and tricellulin were assessed in *C. concisus*-infected monolayers and controls. Among barrier-forming claudins, we observed a marked decrease in claudin-5 expression 48 h after *C. concisus* infection in both monoculture and co-culture conditions. In contrast, the expression of claudin-1 was increased in both monoculture and co-culture conditions at 48 h p.i. (Figure 20). Although a strong tendency of increase in claudin-4 was observed in both monoculture and co-culture conditions after *C. concisus* infection, the expression changes were insignificant compared to controls (Figure 20). We also observed no significant differences in the expression of claudin-7 and -8 in the infected monolayers in monoculture and co-culture conditions (Figure 20). In addition, the expression of the pore-forming claudin-2 was also unchanged post-*C. concisus* infection in both monoculture and co-culture conditions (Figure 20). Interestingly, the expressions of occludin

and tricellulin were downregulated by *C. concisus* infection in co-culture monolayers compared to controls, whereas the expression of both occludin and tricellulin were unchanged in monoculture monolayers after *C. concisus* infection (Figure 20).

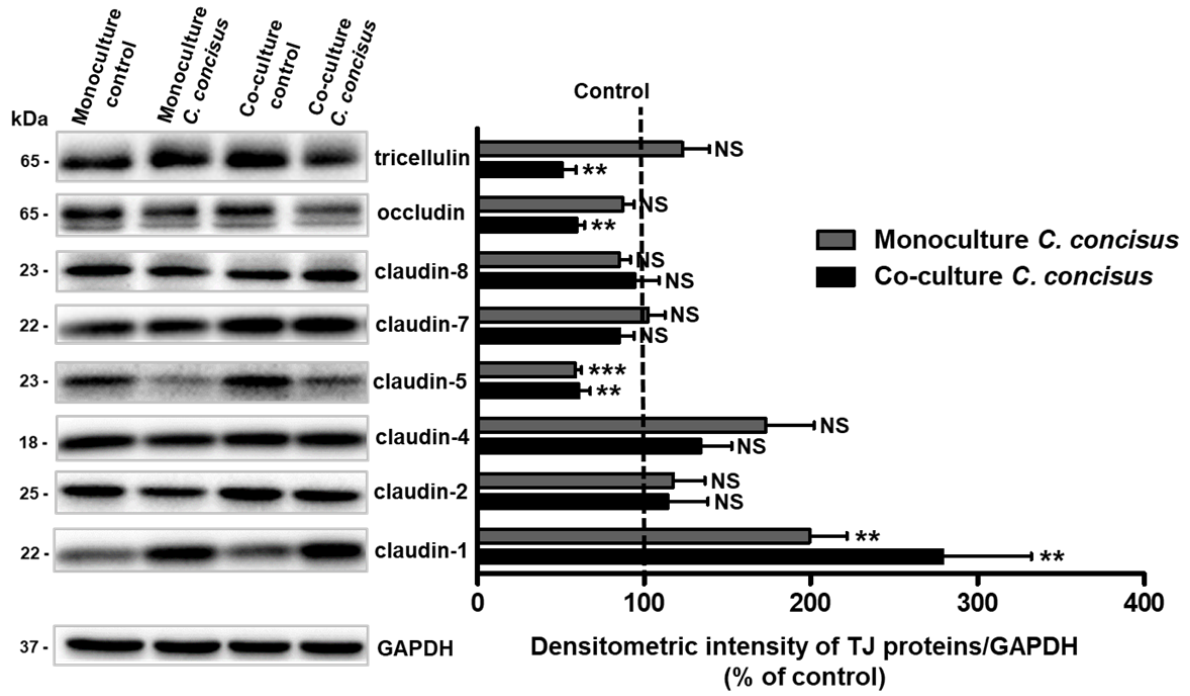

Figure 20. Tight junction protein expression changes in *Campylobacter concisus*-infected HT-29/B6-GR/MR cell monolayers in monoculture or co-culture condition (with THP-1-derived macrophages on the basal side). Western blots of different tight junction (TJ) proteins (claudin-1, -2, -4, -5, -7, -8, occludin and tricellulin) and their corresponding densitometry 48 h after *C. concisus* infection (n = 6-9 in two to three independent experiments, NS = not significant, ** $P < 0.01$, *** $P < 0.001$). TJ changes were represented as increase or decrease in the protein expressions with respect to controls set at 100, indicated by the dotted line (modified from Nattramilarasu et al., 2021).

3.5.3 Occludin and tricellulin delocalization in colonic epithelial cells

To investigate if the reduction in occludin and tricellulin expression in HT-29/B6-GR/MR monolayers 48 h after *C. concisus* infection is also accompanied by structural changes, the localization of tricellulin and occludin in intercellular junctions was analyzed in Z-stacks of XY-scans in CLSM. A strong redistribution of occludin from bTJ to the subcellular spaces was observed in HT-29/B6-GR/MR monolayers infected by *C. concisus* maintained in co-culture conditions, whereas ZO-1 remained intact in the bTJ (Figure 21A). In monoculture and co-culture controls, a strong intercellular co-localization of ZO-1 and occludin in bTJ was observed

(Figure 21A). A redistribution of occludin from bTJ into intracellular regions after *C. concisus* infection was also found in monoculture conditions (Figure 21A). However, this redistribution was either confined only to very few regions or almost absent. As supportive evidence, a marked decrease of Pearson correlation coefficient for co-localization of occludin and ZO-1 was detected in infected monolayers in co-culture, but not in monoculture conditions (Figure 21B).

In control cell monolayers in both monoculture and co-culture conditions, tricellulin remained intact in the tTJ and co-localized with ZO-1. *Campylobacter concisus* infection induced a strong redistribution of tricellulin from tTJ into the subapical intracellular regions in co-culture conditions (Figure 22A). In contrast, the redistribution of tricellulin off the tTJ was rare or almost absent in monoculture cell monolayers 48 h after *C. concisus* infection (Figure 13A). This was confirmed by a marked decrease in Pearson correlation coefficient values for co-localization of tricellulin and ZO-1 in infected cell monolayers in co-culture compared to monoculture conditions (Figure 22B).

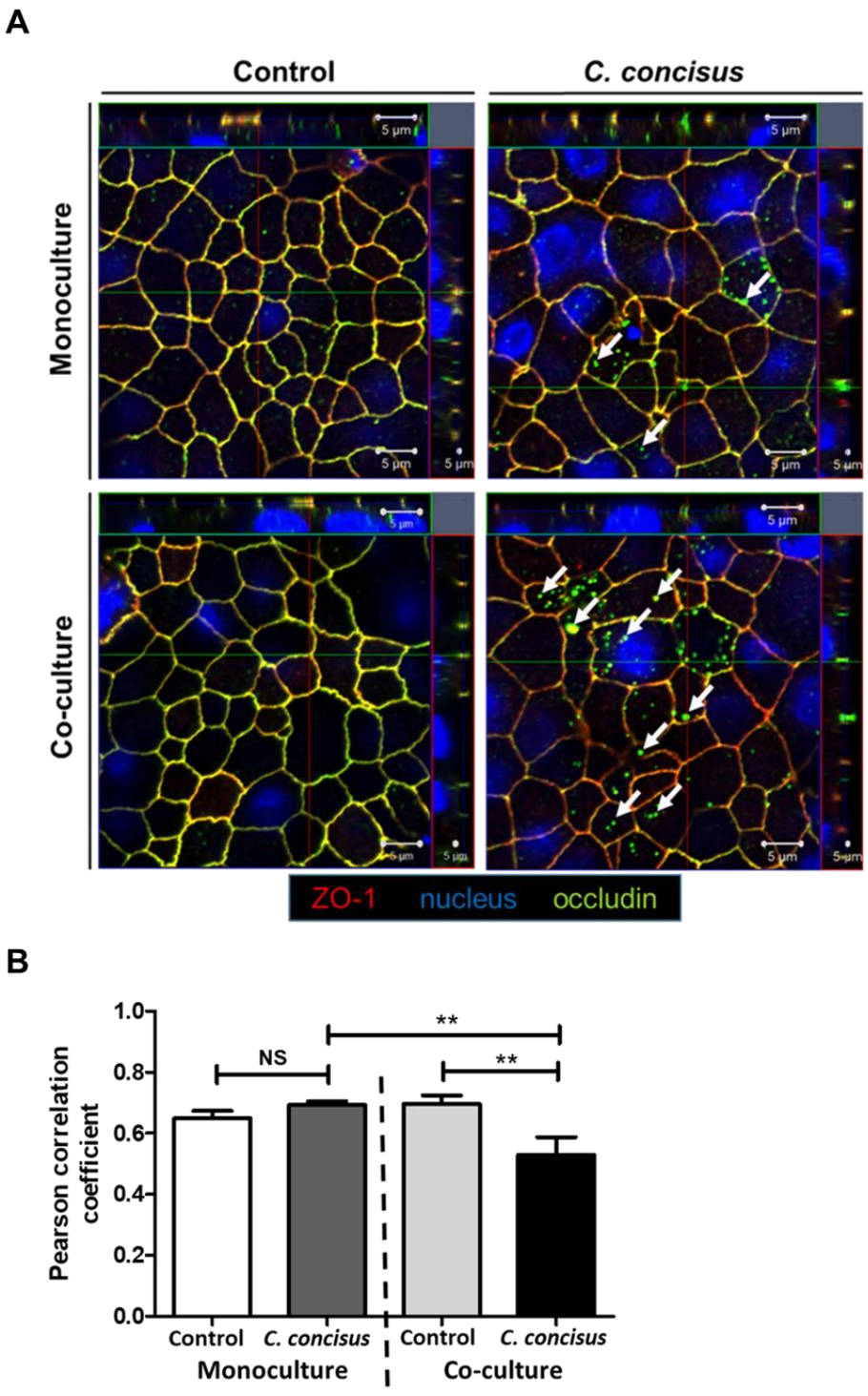

Figure 21. Localization of occludin in controls and *Campylobacter concisus*-infected HT-29/B6-GR/MR cell monolayers 48 h post infection. (A) Occludin (green) and ZO-1 (red) are co-localized in the bicellular tight junction (bTJ) of controls in both monoculture and co-culture conditions (with THP-1-derived macrophages on the basal side). Nuclei were stained blue with DAPI. The white arrows indicate a redistribution of occludin from bTJ into intracellular compartments (modified from Nattramilarasu et al., 2021). **(B)** Co-localization of ZO-1 and occludin were determined from Pearson correlation coefficient **(**n = 2-3, three to six randomly picked regions, NS = not significant, ** $P < 0.01$).

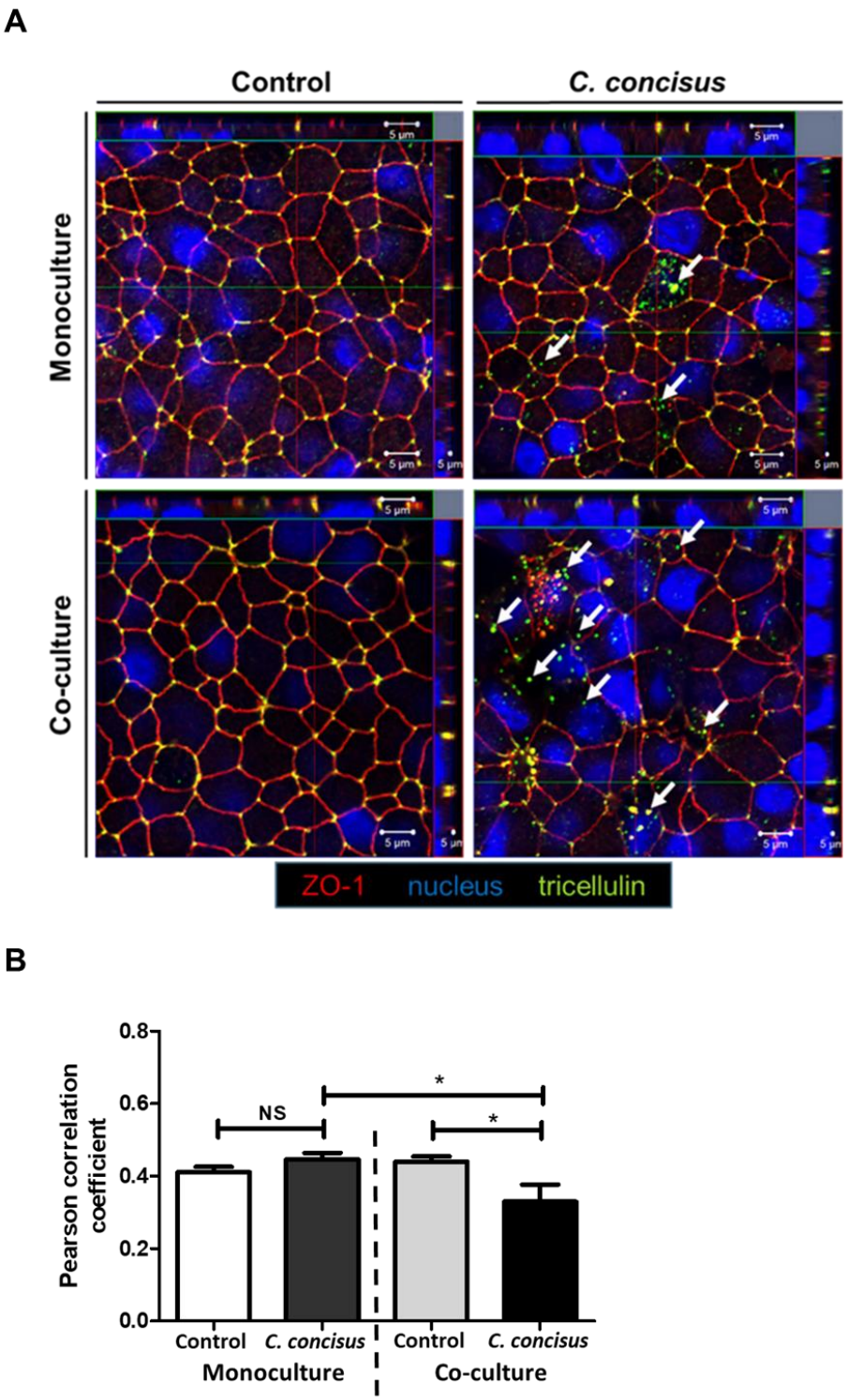

Figure 22. Localization of tricellulin in controls and *Campylobacter concisus*-infected HT-29/B6-GR/MR cell monolayers 48 h post infection. (A) Tricellulin (green) was localized in the tricellular tight junction (tTJ) along with ZO-1 (red) in controls of both, monoculture and co-culture conditions (with THP-1-derived macrophages on the basal side). Nuclei (blue) were stained by DAPI. The white arrows indicate a redistribution of tricellulin from the tTJs into intracellular compartments (modified from Nattramilarasu et al., 2021). **(B)** Co-localization of ZO-1 and tricellulin were determined from Pearson correlation coefficient (n = 2-3, three to six randomly picked regions, NS = not significant, * $P < 0.05$).

3.5.4 Epithelial apoptosis in colonic epithelial cells

Campylobacter concisus induced epithelial apoptosis in HT-29/B6-GR/MR monolayers in monoculture and co-culture conditions 48 h p.i. (Figure 23A). To determine the extent of epithelial apoptosis in the cell monolayers maintained in monoculture and co-culture conditions, the ratio of apoptotic to the total number of cells was quantified. The ratio of apoptotic cells to the total cells was higher in *C. concisus*-infected cell monolayers compared to controls (Figure 23B). Interestingly, no significant differences were observed in the apoptotic rate between the *C. concisus*-infected cell monolayers maintained in monoculture and co-culture conditions (Figure 23B). This confirmed that epithelial apoptosis is a major contributor to the *C. concisus*-induced epithelial barrier defects as shown in a previous study (Nielsen et al., 2011). However, the aggravation of epithelial barrier dysfunction induced by *C. concisus* in presence of THP-1-derived macrophages does not result from increased epithelial apoptosis.

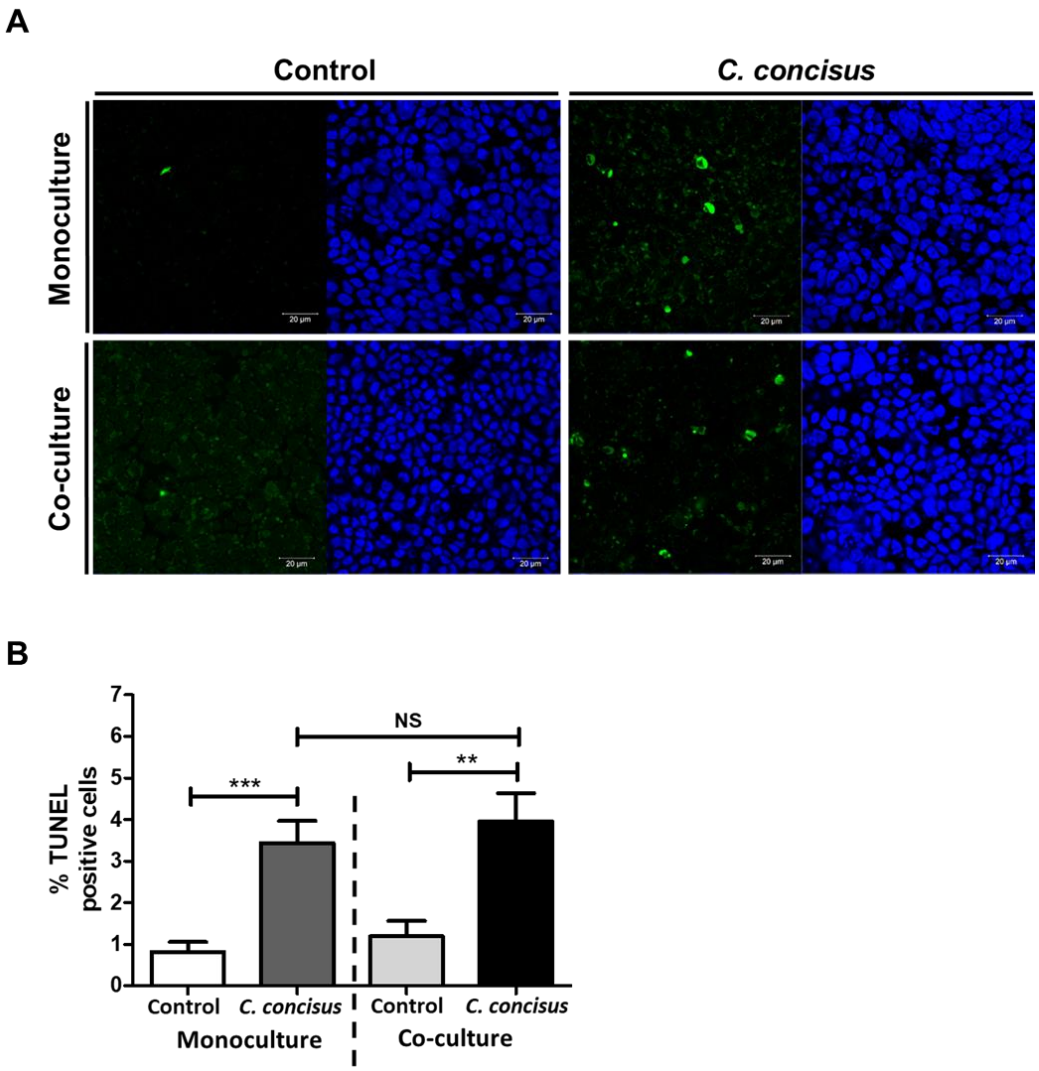

Figure 23. Epithelial apoptosis in colonic epithelial cell monolayers in monoculture or co-culture condition (with THP-1-derived macrophages on the basal side) 48 h after *Campylobacter concisus* infection. (A) In HT-29/B6-GR/MR monolayers, the apoptotic cells were stained green by TUNEL assay and the nuclei were stained blue by DAPI. **(B)** Percentage of apoptotic or TUNEL-positive cells quantified in 5 to 8 different regions of the cell monolayers (n = 3 in independent experiments, NS = not significant, ** $P < 0.01$, *** $P < 0.001$) (modified from Nattramilarasu et al., 2021).

3.6 *Campylobacter concisus*-induced epithelial permeability changes in colonic epithelial cells

A marked decrease in TER was observed in HT-29/B6-GR/MR cell monolayers 48 h after *C. concisus* infection in co-culture compared to monoculture condition (Figure 19), which represents ion permeability changes. Therefore, the epithelial permeability of HT-29/B6-GR/MR cell monolayers was measured in monoculture and co-culture conditions with fluorescent tracers of different molecular weights, namely fluorescein (332 Da) and FITC-

dextran (4 kDa). The permeability to fluorescein was increased in *C. concisus*-infected cell monolayers compared to controls in both monoculture and co-culture conditions (Figure 24A). However, a marked increase was detected in the permeability to fluorescein after *C. concisus* infection in co-culture compared to monoculture condition (Figure 24A).

Surprisingly, a profound increase was observed in the permeability to FITC-dextran 4 kDa in *C. concisus*-infected cell monolayers compared with controls in co-culture conditions, which was in contrast to infected monlayers in monoculture conditions (Figure 24B). The differences in the permeability to molecules of different molecular weights after *C. concisus* infection could be a consequence of structural changes in the cells. In monoculture conditions, *C. concisus*-infected cell monolayers were permeable to fluorescein, but not FITC-dextran 4 kDa. This points to redistribution of occludin from the bTJ. In contrast, a remarkable increase in the permeability to FITC-dextran 4 kDa and fluorescein after *C. concisus* infection in co-culture condition points to the loss of tTJ integrity through delocalization of tricellulin from tTJ, since increased macromolecule permeability has been shown to be associated with a loss of tricellulin from tTJ (Krug et al., 2009).

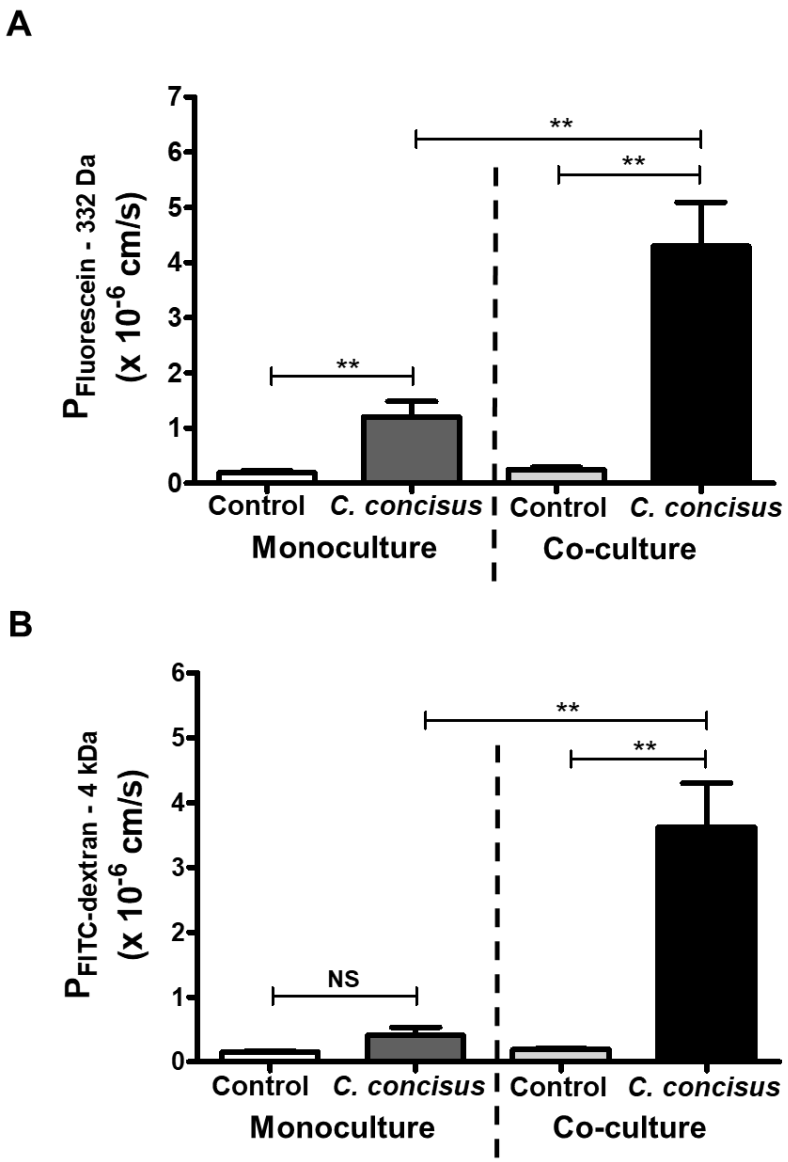

Figure 24. Epithelial permeability of HT-29/B6-GR/MR cell monolayers to fluorescein and FITC-dextran 4 kDa under monoculture or co-culture conditions after *Campylobacter concisus* infection. (A) Permeability to fluorescein (332 Da) in controls and *C. concisus*-infected cell monolayers under monoculture and co-culture conditions (with THP-1-derived macrophages on the basal side) 48 h p.i. (n = 6-8 in three independent experiments, ns = not significant, ** $P < 0.01$). **(B)** Permeability to FITC-dextran (4 kDa) in controls and *C. concisus*-infected cell monolayers under monoculture and co-culture conditions 48 h p.i. (n = 6-8 in three independent experiments, NS = not significant, ** $P < 0.01$) (modified from Nattramilarasu et al., 2021).

3.7 Inflammatory response of macrophages by *Campylobacter concisus* infection

To ascertain if the inflammatory response of THP-1-derived macrophages aggravates *C. concisus*-induced epithelial barrier dysfunction in HT-29/B6-GR/MR monolayers, the cytokines released from macrophages were measured 48 h p.i. by CBA assay. A marked

increase was detected in the release of proinflammatory cytokines TNF-α, IL-1β and IL-6 from differentiated THP-1 cells after *C. concisus* infection compared to controls (Figure 25). In addition, the levels of the proinflammatory cytokines IFN-γ, IL-13, IL-2 and IL-17A were unaltered after infection (Figure 25). In addition, *C. concisus* infection elicited an anti-inflammatory response with an increase in the levels of IL-10 released by THP-1 cells (Figure 25).

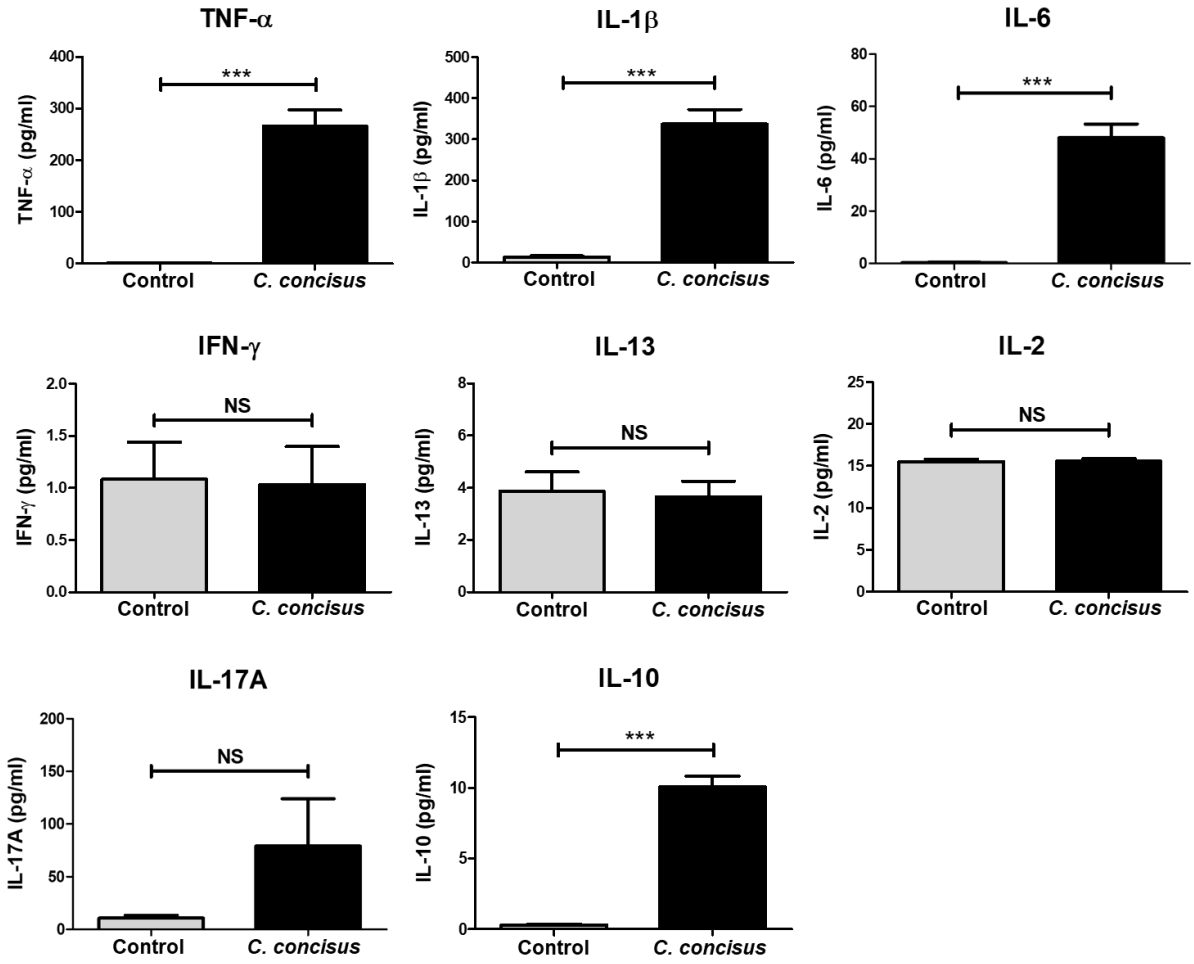

Figure 25. Cytokines released from differentiated THP-1 cells in controls and 48 h after *Campylobacter concisus* infection. The cytokines released from THP-1-derived marophages were quantified in co-culture conditions (HT-29/B6-GR/MR cell monolayers with THP-1-derived macrophages on the basal side). The cell monolayers were infected with *C. concisus* at a MOI of 200 on both the apical and basal sides. The cytokines (TNF-α, IL-1β, IL-6, IFN-γ, IL-13, IL-2, IL-17A and IL-10) released from the infected cells (black bars) were compared to cytokines released from uninfected controls (bright grey bars) (n = 6 in two independent experiments, NS = not significant, *** $P < 0.001$) (modified from Nattramilarasu et al., 2021).

3.8 Cell viability of HT-29/B6-GR/MR cell monolayers in monoculture and co-culture conditions

The viability of polarized epithelium in HT-29/B6-GR/MR cell monolayers was evaluated using the CCK-8 assay 48 h after *C. concisus* infection in both monoculture and co-culture conditions. Concerning the cell viability, HT-29/B6-GR/MR cell monolayers were unaffected after *C. concisus* infection at an MOI of 200, as the absorbance values recorded at 450 nm were comparable to controls without any significant differences in both monoculture and co-culture conditions (Figure 26).

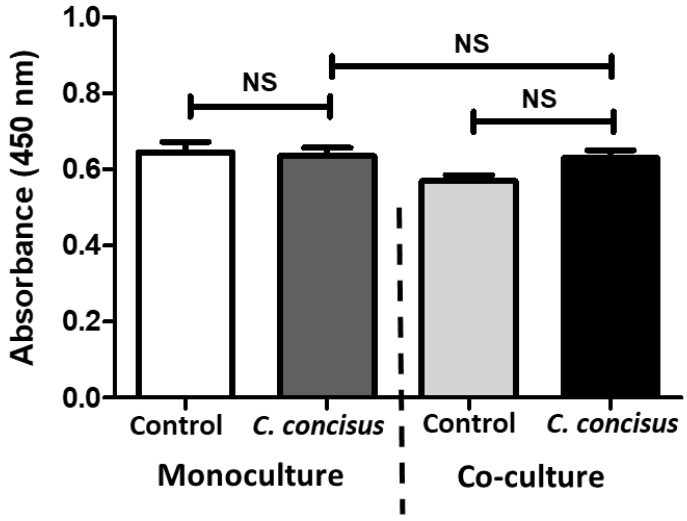

Figure 26. Cell viability of HT-29/B6-GR/MR cell monolayers 48 h after *Campylobacter concisus* infection. The cell monolayers maintained in monoculture and co-culture conditions (with THP-1-derived macrophages on the basal side) were infected with *C. concisus* at a MOI of 200 on both apical and basal side. Forty-eight hours p.i., the absorbance values were recorded at 450 nm with a reference wavelength of 600 nm (WST-8 in CCK-8 assay) in controls and infected cell monolayers (n = 6 in two independent experiments, NS = not significant) (modified from Nattramilarasu et al., 2021).

To optimize the right dosage (MOI) of *C. concisus* for HT-29/B6-GR/MR cells to investigate ENaC function and TJ changes, the cell proliferation rate of HT-29/B6-GR/MR cells were determined at 48 h p.i. with different MOI ranging from 25 to 1000. The cell proliferation rate of infected-HT-29/B6-GR/MR cells was comparable to controls and no significant changes were detected at MOI of 25, 50, 100, 200 and 400 (Figure 27A). However, cell proliferation rate declined at MOI above 500 (Figure 27A), which confirmed that the bacterial dosage at MOI above 500 is not an optimum for functional and molecular assays performed in HT-29/B6-

GR/MR cells. In addition, the cell proliferation rate of differentiated THP-1 cells also declined at MOI of 500 and 1000, although no significant differences were observed at a MOI of 400 (Figure 27B) 48 h after *C. concisus* infection. Interestingly, a marked increase in the cell proliferation rate of THP-1 cells was recorded at MOI of 25, 50, 100 and 200 (Figure 27B). This indicates a proliferation stimulus induced by *C. concisus* at MOI of 200 and below.

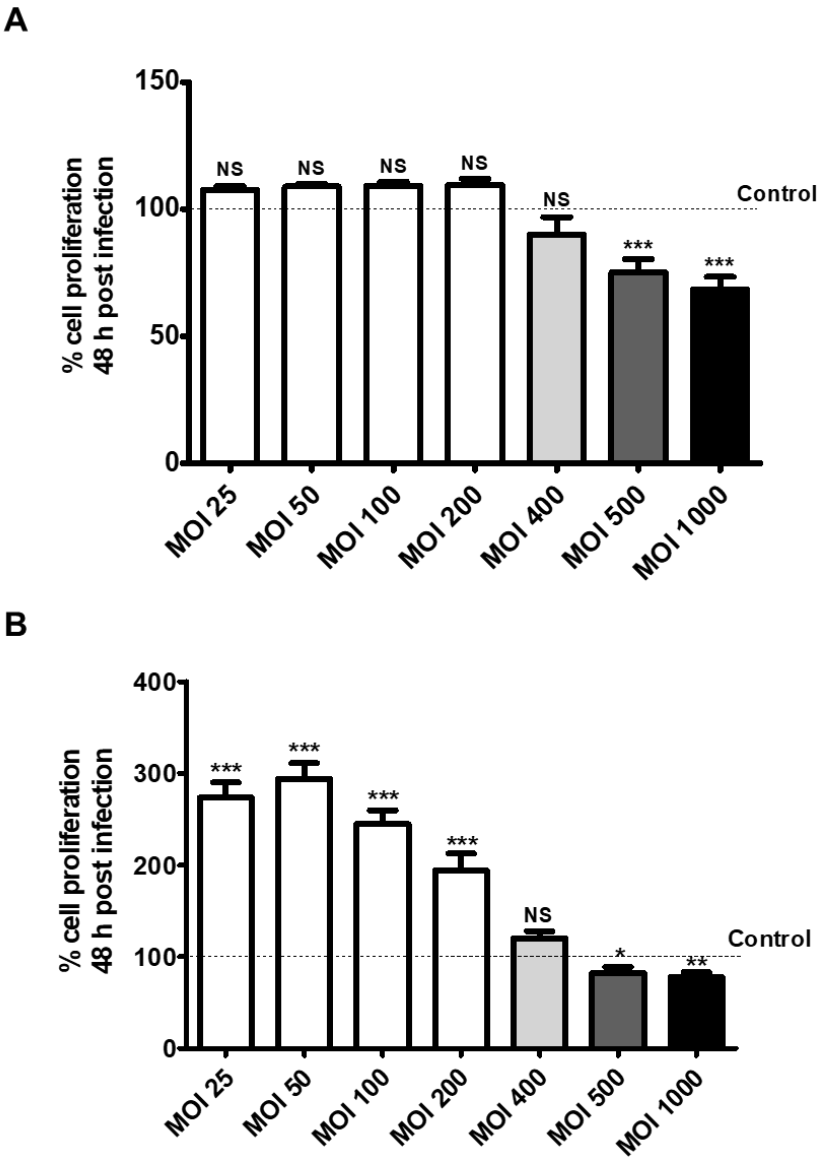

Figure 27. Cell viability of HT-29/B6-GR/MR and THP-1-derived macrophages 48 h after *Campylobacter concisus* infection. Absorbance values were recorded at 450 nm with a reference wavelength of 600 nm in controls and *C. concisus*-infected cells at different MOI from 25 to 1000. Percentage of increase or decrease in cell proliferation in infected cells were compared to controls set at 100, indicated by the dotted line **(A)** HT-29/B6-GR/MR cells. **(B)** THP-1-derived macrophages (WST-8 in the CCK8 assay; n = 4-17 in two to three independent experiments, NS = not significant, *** $P < 0.001$, ** $P < 0.01$, * $P < 0.05$) (modified from Nattramilarasu et al., 2021).

3.9 *Campylobacter concisus*-induced tight junction changes in colonic epithelium *in vivo*

The proteins isolated from colon mucosae of IL-10$^{-/-}$ mice were used to analyze *C. concisus*-induced TJ changes. No significant differences were observed in R^t and the R^{epi} between the colonic tissues of controls (commensal *E.coli* mono-associated mice) and *C. concisus*-infected IL-10$^{-/-}$ mice 6 days p.i. (Table 1). However, the expression of different TJ proteins was analyzed in the colon mucosae of IL-10$^{-/-}$ mice 6 days post-*C. concisus* infection (Figure 28A).

A significant reduction in the expression of claudin-7 and claudin-8 was observed in colon mucosae of *C. concisus*-infected IL-10$^{-/-}$ mice (Figure 28B). An increase in tricellulin with no change in occludin expression was also observed in colonic mucosae of *C. concisus*-infected IL-10$^{-/-}$ mice (Figure 28B). Furthermore, a decrease in claudin-1 expression was observed in *C. concisus*-infected IL-10$^{-/-}$ mice (Figure 28B).

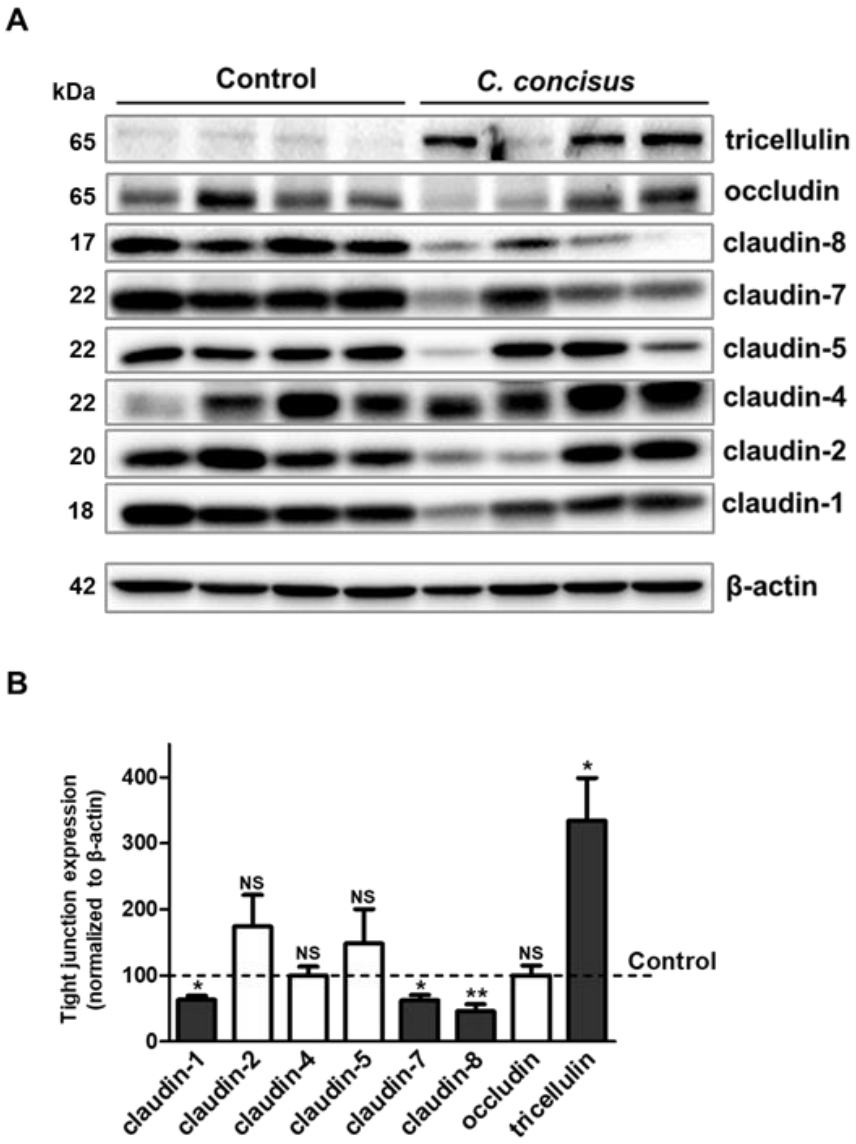

Figure 28. Changes in tight junction protein expression in the colonic tissues of IL-10$^{-/-}$ mice 6 days after *Campylobacter concisus* infection. (A) Western blots of tight junction (TJ) proteins (claudin-1, -2, -4, -5, -7, -8, occludin and tricellulin) in the colonic mucosae of IL-10$^{-/-}$ mice, mono-associated with *C. concisus* (6 days .p.i.) or with commensal *E. coli* as controls (n = 6-8 in two independent experiments, NS = not significant, * $P < 0.05$, ** $P < 0.01$). **(B)** Densitometry of the TJ blots (normalized to β-actin) in *C. concisus*-infected IL-10$^{-/-}$ mice represented as change in expression with respect to controls set at 100, indicated by a dotted line. β-actin was used as loading control.

4. Discussion

Campylobacter concisus is a human-hosted Gram-negative microbe, first detected in the oral cavity of periodontitis patients with advanced stage of gingival inflammation (Tanner et al., 1981; Tanner et al., 1985). Over time, the concrete research evidence established *C. concisus* as an enteropathogen in the context of intestinal inflammation and diarrhea (Kaakoush et al., 2011; Ismail et al., 2012). More importantly, *C. concisus* induces intestinal epithelial barrier dysfunction via moderate TJ changes and epithelial apoptosis (Man et al., 2010a; Nielsen et al., 2011). However, the regulatory mechanisms of the epithelial transport function in the intestine by *C. concisus* was not explored. Therefore, we investigated the influence of *C. concisus* on intestinal ion transport function with a special focus on Na^+ transport via ENaC in the distal colon (Nattramilarasu et al., 2020), and the corresponding results are discussed in section 4.1. Furthermore, the influence of mucosal immune components in regulating the intestinal epithelial barrier dysfunction induced by *C. concisus* was investigated using a co-culture model of colonic epithelial cell monolayers and THP-1-derived macrophages (Nattramilarasu et al., 2021), and the results are discussed in section 4.2.

4.1. *Campylobacter concisus* impairs sodium absorption in the distal colon by ENaC dysfunction and claudin-8 disruption

In the context of infectious diarrhea, the loss of ENaC function through transcriptional downregulation of β-ENaC in the colon has been first ascertained in *Salmonella enterica* infection in BALB/c mice (Marchelletta et al., 2013). Later, in the human colon with acute *C. jejuni* infection, a defective ENaC-mediated electrogenic Na^+ absorption was reported (Bücker et al., 2018), in which the loss of ENaC function in the distal colon is characterized as one diarrheal pathomechanism in human campylobacteriosis. Since *C. concisus* is the frequently detected non-zoonotic *Campylobacter* spp. in the stools of diarrheal patients, we determined if it induces loss of ENaC activity and Na^+ malabsorption in the distal colon.

4.1.1 Colonic ENaC dysfunction *in vitro* and *in vivo*

The principal experiment to determine *in vitro* ENaC function following *C. concicus* infection in HT-29/B6-GR/MR cell model revealed that *C. concisus* impairs ENaC-mediated Na^+ absorption, as amiloride-sensitive I_{SC} was decreased after *C. concisus* infection. This was

accompanied by transcriptional downregulation of β- and γ-ENaC genes (Nattramilarasu et al., 2020). *Campylobacter concisus* inhibits ENaC activity *in vitro* through a mechanism similar to *C. jejuni*, which also promote a transcriptional downregulation of regulatory ENaC subunits in colon biopsies of patients with acute *C. jejuni* infection (Bücker et al., 2018). During diarrheal states, ENaC-mediated electrogenic Na^+ absorption is activated in the distal colon by glucocorticoids and mineralocorticoids to minimize the loss of Na^+ (Schultheis et al., 1998). As *C. concisus* induces functional ENaC impairment in the *in vitro* cell model (Nattramilarasu et al., 2020), it could lead to a loss of net Na^+ absorption in the colon, which in turn can result in the loss of water into the lumen. This correlates to the clinical epidemiology study, which has shown that *C. concisus*-infected patients presented a chronic diarrhea (>2 weeks) with watery stools in contrast to bloody and mucoid diarrhea in *C. jejuni*/*C. coli*-infected patients (Nielsen et al., 2012). Furthermore, the same study also identified that 12% of the *C. concisus*-infected patients developed microscopic colitis in a six-month follow-up period. Concomitantly, in lymphocytic colitis (a subtype of microscopic colitis), watery diarrhea was accompanied by Na^+ malabsorption in sigmoid colon as a result of functional ENaC impairment (Barmeyer et al., 2016). Recent clinical studies have also reported a high risk for microscopic colitis in diarrheal patients infected with *C. concisus* (Nielsen et al., 2020; Yde Aagaard et al., 2020).

To study and characterize the *in vivo* effects of *C. concisus* in the intestine, BALB/c mice were used after immune suppression with cyclophosphamide and vancomycin (Aabenhus et al., 2008). However, this study reported poor colonization of *C. concisus* in different intestinal segments without any substantial inflammation seven days after infection, and proposed an improved mouse model to determine the inflammatory outcome in the intestine at early stages of *C. concisus* infection about 3 days p.i. Moreover, in the intestine, mice display strong resistance to physiological colonization due to mouse-specific gut microbiota, which could protect from enteropathogenic infections like *C. jejuni* (Bereswill et al., 2011; Masanta et al., 2013). The effective colonization and pathogenesis of *C. jejuni* was first identified in the intestinal segments of secondary abiotic IL-$10^{-/-}$ mice with C57BL/6 strain background, which was created by depletion of gut microbiota by broad-spectrum antibiotic treatment (Haag et al., 2012). The secondary abiotic IL-$10^{-/-}$ mouse model was employed in our study to determine the *in vivo* effects of *C. concisus* on ENaC function in the distal colon. A successful colonization in the intestinal segments and fecal detection was observed in secondary abiotic IL-$10^{-/-}$ mice six days after *C. concisus* infection by oral gavage. More importantly, *C. concisus* impaired electrogenic Na^+ absorption via ENaC in the distal colon of infected-IL-$10^{-/-}$ mice compared to

control IL-10$^{-/-}$ mice mono-associated with commensal *E. coli* (Nattramilarasu et al., 2020). This corresponds to the *in vitro* experimental results and gives concrete *in vivo* evidence for *C. concisus*-induced ENaC dysfunction in the distal colon.

In tracheal epithelium, *Pseudomonas aeruginosa* induces flagellin-mediated impairment of Na^+ absorption via ENaC to promote mucociliary clearance, a mechanism that is attenuated in cystic fibrosis (Kunzelmann et al., 2006). Interestingly, electron microscopic analysis revealed that flagellum of *Campylobacter* spp. could evade the immune responses from host cell TLR-5 unlike *Salmonella* Typhimurium due to the absence of residues 89 to 96 in the D1 domain of the flagellum (Galkin et al., 2008). The flagella of clinical isolates of *C. concisus* aids the bacterium to attach to the microvilli expressed in Caco-2 cells (Man et al., 2010a), while the flagellin-B of *C. concisus* was ascertained as a major immune reactive protein in sera of pediatric CD patients tested positive for *C. concisus* (Kovach et al., 2011). Concerning *C. jejuni*, an *in vivo* study with abiotic IL-10$^{-/-}$ mice revealed that both flagellin-A and -B subunits of flagellin are essential to induce intestinal and systemic immune responses in murine campylobacteriosis (Schmidt et al., 2019). Therefore, future studies should determine if the flagellin of the *Campylobacter* spp. regulates ENaC function in the colonic epithelium in a mechanism similar to flagellin of *Pseudomonas aeruginosa* in tracheal epithelium. Moreover, the ability of *C. concisus* to form biofilms and its varying motility in viscous liquids *in vitro* indicate that *C. concisus* can evade the immune response and survive in the inner mucus layer of the intestine (Laverncic et al., 2012). This will in turn facilitate *C. concisus* to attach the intestinal epithelium via flagellum and thereby mediate ENaC dysfunction by flagellin, as *C. concisus* do not enhance surface expression TLR5 in epithleial cells (Ismail et al., 2013).

With regard to barrier function in colonic epithelium, no significant difference was observed in subepithelial (R^{sub}) resistance in the colon mucosae of *C. concisus*-infected IL-10$^{-/-}$ mice compared to controls (Nattramilarasu et al., 2020). This indicates that *C. concisus* induces ENaC dysfunction in the colonic epithelium of IL-10$^{-/-}$ mice without substantial inflammation, and corresponds to the effects of *C. jejuni*, as it did not induce subepithelial inflammation in the colon of infected patients (Bücker et al., 2018). The epithelial barrier function was impaired by differential regulation of TJ proteins in *C. jejuni*-infected human colon in parallel to ENaC dysfunction (Bücker et al., 2018). *Campylobacter concisus*-induced ENaC dysfunction was also

accompanied by paracellular barrier defects and defined TJ changes in the *in vitro* cell model (Nattramilarasu et al., 2020).

4.1.2 Claudin-8 disruption and paracellular back-leakage of sodium into the lumen

Claudin-8 was ascertained to form a non-specific cation barrier in the renal tubules of distal nephron and thin ascending limb impermeable to Na^+ and other cations (Yu et al., 2003; Li et al., 2004). Furthermore, claudin-8 was also shown to form a paracellular barrier and prevent a passive leak of ammonium NH_4^+ and HCO_3^- in Madin-Darby Canine Kidney (MDCK) II cells, implying its permissive role in urinary net acid secretion (Angelow et al., 2006). In the human sigmoid colon stimulated by aldosterone, an increase in protein expression of claudin-8 was detected with a significant reduction in serosal to mucosal Na^+ flux (Amasheh et al., 2009a). Furthermore, in HT-29/B6-GR monolayers, the synthetic glucocorticoid dexamethasone induced upregulation of claudin-8 accompanied by an increase in paracellular resistance (Amasheh et al., 2009a). This indicates that colonic epithelial cells stimulated by mineralocorticoids and glucocorticoids not only induce Na^+ absorption via ENaC but also prevent paracellular back-leakage of Na^+ into the lumen by enhancing claudin-8 expression. In the present study, HT-29/B6-GR/MR monolayers stimulated by DBA, transcriptional downregulation of claudin-8 was induced by *C. concisus* infection (Nattramilarasu et al., 2020). More importantly, *C. concisus* induces a significant TER drop in HT-29/B6-GR/MR monolayers after ENaC blockade by amiloride, which reflects paracellular barrier defects induced by *C. concisus* (Nattramilarasu et al., 2020). This was accompanied by a reduction in protein expression of claudin-8, while the expression of other TJ proteins was unaltered. Furthermore, as a structural correlate, claudin-8 was redistributed off the TJ domain in HT-29/B6-GR/MR monolayers (Nattramilarasu et al., 2020). In summary, *C. concisus* impairs Na^+ absorption in colonocytes by ENaC dysfunction and induces claudin-8 disruption, which leads to back-leakage of Na^+ into the lumen via the paracellular route (scheme, Figure 20). This correlates to the pathomechanism of lymphocytic colitis, in which claudin-8 disruption and ENaC dysfunction synergistically promote watery diarrhea (Barmeyer et al., 2016; Barmeyer et al., 2017).

In the secondary abiotic IL-10$^{-/-}$ mouse model, the barrier function and epithelial resistance of the colon mucosae were unaffected by *C. concisus* infection, although ENaC function was impaired 6 days p.i. (Nattramilarasu et al., 2020). However, the claudin-8 protein expression was significantly reduced in the colon mucosae of *C. concisus*-infected IL-10$^{-/-}$ mice (Figure 18). A recent study reported that claudin-8 is co-regulated with γ-ENaC in the epithelium of renal collecting ducts, and the coupled function of claudin-8 and γ-ENaC is responsible to prevent the back-leakage of Na^+ into the lumen via the paracellular route (Sassi et al., 2020). In *C. concisus*-induced ENaC dysfunction, transcriptional downregulation of both claudin-8 and γ-ENaC was observed in HT-29/B6-GR/MR monolayers (Nattramilarasu et al., 2020). The *in vivo* results from the secondary abiotic IL-10$^{-/-}$ mice also demonstrate that ENaC dysfunction induced by *C. concisus* 6 days p.i., was accompanied by claudin-8 downregulation. Therefore, we could speculate that the dysfunction of claudin-8 and paracellular back-leakage of Na^+ into the intestinal lumen by *C. concisus* infection could be a consequence of the transcriptional downregulation of the γ-ENaC. In addition to claudin-8, claudin-7 also plays a pivotal role in regulating the paracellular Na^+ flux, as it increased the paracellular conductance to Na^+ ions in LLC-PK1, a porcine epithelial-like kidney cell line (Alexandre et al., 2005). Furthermore, in homozygous claudin-7 knockout (CLDN7$^{-/-}$) in collecting duct cells of the kidney, the net Na^+ flux from serosal to mucosal side was decreased, which was accompanied by an increase in mRNA and protein expression of α-, β- and γ-ENaC subunits (Fan et al., 2019). Therefore, in contrast to claudin-8, claudin-7 negatively regulates the expression of ENaC subunits and promote paracellular loss of Na^+ ions into the lumen of the kidney. In our study, claudin-7 protein expression was decreased in the colon mucosae of *C. concisus*-infected IL-10$^{-/-}$ mice (Figure 18), which might prevent the paracellular back-leakage of Na^+ into the lumen resulting from claudin-8 downregulation. However, this should be confirmed in the future by changes in serosal to mucosal Na^+ flux measurements and claudin-7 protein expression data after *C. concisus* infection in parallel to ENaC dysfunction. Surprisingly, we also found an increase in tricellulin and a decrease in claudin-1 protein expression in the colon mucosae of IL-10$^{-/-}$ mice. The changes in claudin-1 and tricellulin expressions cannot be correlated to the impaired ENaC function or unchanged barrier function in colon mucosae of *C. concisus*-infected IL-10$^{-/-}$ mice when compared with controls. Hence, we can only speculate this as a compensatory regulation to maintain the epithelial barrier function in the colon of *C. concisus*-infected IL-10$^{-/-}$ mice.

4.1.3 ENaC dysfunction via activation of ERK pathway

In the intracellular cell signaling pathways regulating ENaC function, MAPK signaling cascades ensure the cell surface localization and expression of ENaC, and subsequent electrogenic Na^+ absorption. Among different MAPK enzymes, ERK plays a crucial role in ENaC function as it negatively regulates ENaC-mediated Na^+ absorption by interaction with neuronally expressed developmentally downregulated (NEDD)-4/2 protein, an E3 ubiquitin ligase enzyme responsible for ubiquitination and delocalization of ENaC from the apical membrane (Soundararajan et al., 2009). Hence, the investigation of ERK activation in regulating *C. concisus*-induced ENaC dysfunction became indispensable. Bioinformatics predictions through IPA from RNA-Seq data of colon biopsies from *C. jejuni*-infected patients revealed that ERK activation could negatively regulate ENaC function of distal colon in human campylobacteriosis (personal communication R. Bücker, unpublished data). Therefore, we investigated if ERK activation is accompanied by *C. jejuni*- and *C. concisus*-induced ENaC dysfunction.

The *in vitro* results indicated that both *C. jejuni* and *C. concisus* induce ERK1/2 activation in HT-29/B6-GR/MR monolayers parallel to ENaC dysfunction (Nattramilarasu et al., 2020). It has been reported in a previous study that *P. aeruginosa*-induced ENaC dysfunction in mouse tracheal epithelium was rescued by functional blockade of ERK1/2 (Kunzelmann et al., 2006). In our study, the functional blockade of ERK1/2 resulted in a partial rescue of colonic ENaC dysfunction by *C. concisus* infection (Nattramilarasu et al., 2020). This confirmed that the activation of the ERK signaling pathway resulted in *C. concisus*-induced ENaC dysfunction in colonic epithelium, which correlates to the pathophysiology of intestinal ENaC dysfunction in CD and lymphocytic colitis (Zeissig et al., 2008; Barmeyer et al., 2016). TNF-α and IL-1β were identified as the proinflammatory cytokines, which induce ENaC dysfunction by transcriptional downregulation of regulatory ENaC subunits (Amasheh et al., 2004; Barmeyer et al., 2004). Since *C. concisus* elevated TNF-α release from the supernatants of HT-29/B6 cells (Man et al., 2010a), it was presumed that TNFα-mediated ERK activation might contribute to ENaC dysfunction in *C. concisus* infection. However, RNA-Seq data from HT-29/B6-GR/MR cells demonstrated that *C. concisus* infection significantly upregulated mRNA expression of the proinflammatory cytokine IL-32. IL-32 has been reported to induce ERK activation in fibroblast-like synoviocytes in rheumatoid arthritis (Kim et al., 2010) and human calcified

aortic valves (Tsai et al., 2018). Bioinformatics predictions by IPA from RNA-Seq data of HT-29/B6-GR/MR cells (Nattramilarasu et al., 2020) indicated that *C. concisus* could induce ERK activation via transcriptional upregulation of IL-32 (scheme, Figure 29).

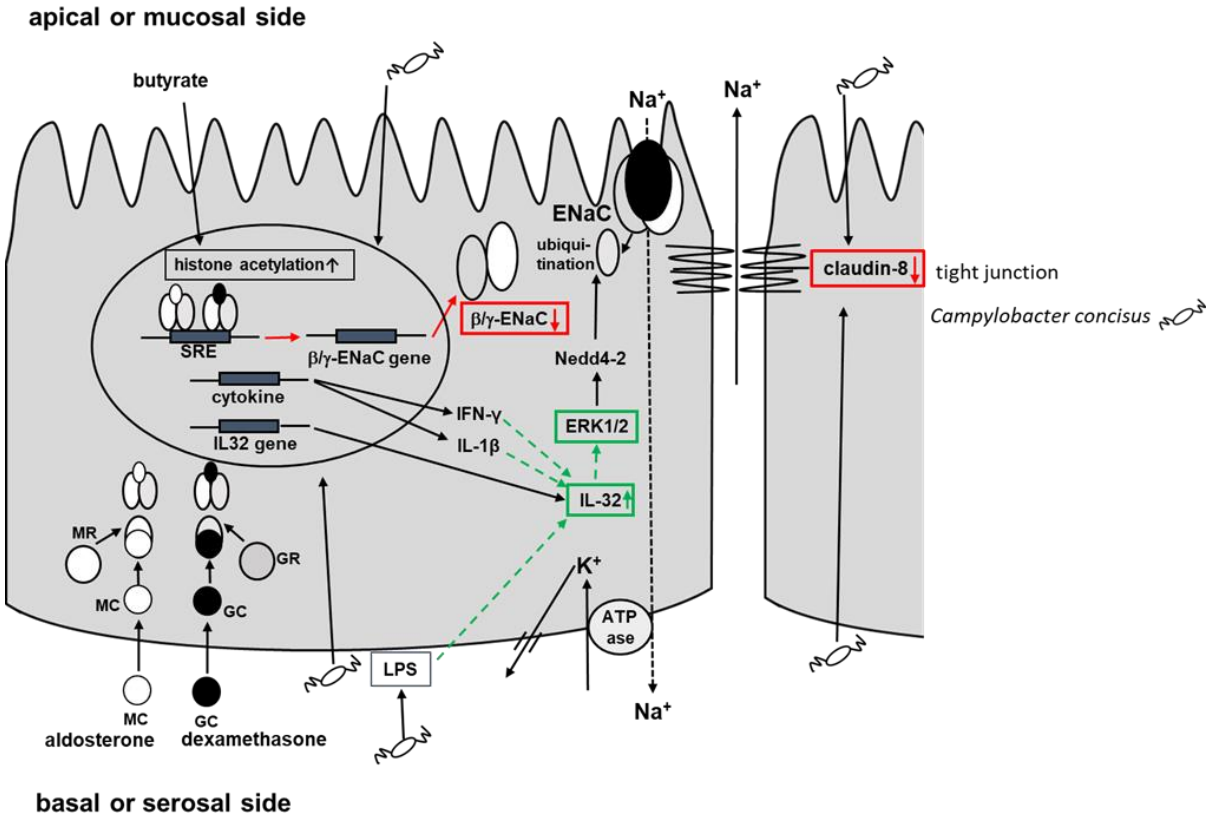

Figure 29. Scheme of *Campylobacter concisus*-induced impairment of sodium absorption via epithelial sodium channel (ENaC) and paracellular back-leakage of sodium in colonic epithelial cells. The genes or proteins, which were upregulated or activated, are highlighted by green boxes, while those that were downregulated are highlighted by red boxes. *Campylobacter concisus* infection promotes a transcriptional upregulation of interleukin (IL)-32, which might increase its protein expression (indicated by upward green arrow). The dotted green arrrows represent the predicted activation of IL-32 by upstream regulators interferon (IFN)-γ, IL-1β, and bacterial lipopolysaccharides (LPS) after *C. concisus* infection, which could in turn activate ERK1/2 leading to ENaC dysfunction (bioinformatics prediction from RNA-Seq data by Ingenuity Pathway Analysis (IPA) software). The reduction in claudin-8 protein expression by *C. concisus* is indicated by red color. The reduction in claudin-8 expression (indicated by downward red arrow) and its redistribution off the tight junction domain could result in back-leakage of Na^+ into the lumen via the paracellular route, contributing to the net loss of Na^+ (modified from Nattramilarasu et al., 2020).

The data available from the literature and our novel findings of the regulative cell signaling pathways of ENaC after *C. concisus* infection (Nattramilarasu et al., 2020) is depicted in the

schematic representation (Figure 29). In diarrheal state, GR and MR are activated by glucocorticoids (GC) like cortisol and mineralocorticoids (MC) like aldosterone, respectively (Shultheis et al., 1998). In Figure 29, dexamethasone was shown instead of cortisol as GC, as dexamethasone is the synthetic glucorticoid used in our *in vitro* experiments. GC and MC bind to the intracellular receptors GR and MR, respectively, and forms a heterodimer to bind to their respective promoter regions in steroid-responsive element (SRE). This in turn induces the transcription of β- and γ-ENaC genes, and subsequently increases the protein synthesis and electrogenic Na^+ absorption (Will et al., 1980; Fromm et al., 1993; Epple et al., 2000). The heterodimeric activation by GC and MC enhances the electrogenic Na^+ absorption (Grotjohann et al., 1999). Butyrate, a fermentative by-product of colonic bacteria from the lumen induces inhibition of histone deacetylases, and thereby promotes histone acetylation in the nucleus (Bultman, 2013). Histone acetylation in turn stimulates ENaC function by inhibition of ubiquitination and degradation of the ENaC subunits by NEDD4-2 (Butler et al., 2015). Neural precursor cell expressed developmentally down-regulated protein 4 (NEDD4)-like protein NEDD4-2 is an E3-ubiquitin protein ligase, which binds to all the three subunits of ENaC in PY-rich motifs and regulates ENaC function via ubiquitination and degradation of ENaC (Harvey et al., 2001; Fotia et al., 2003). In addition to NEDD4-2, ERK activation plays a pivotal role in Na^+ absorption via ENaC. Although it was initially presumed that ERK inhibits the opening of ENaC pores via NEDD4-2 to limit Na^+ absorption via ENaC (Michlig et al., 2005), it turned out that ERK activation directly phosphorylates ENaC, which in turn activates NEDD4-2 to cause the subsequent ubiquitination and internalization of ENaC (Eaton et al., 2014). Butyrate also promotes transcriptional upregulation of β- and γ-ENaC with transcription factor Sp3 binding to the promoter of γ-ENaC to induce the gene expression, and thereby enhancing Na^+ absorption via ENaC (Zeissig et al., 2007a). Furthermore, ENaC-mediated Na^+ absorption was substantially enhanced by butyrate in the presence of corticosteroid hormones in rat colon and HT-29/B6-GR cells (Zeissig et al., 2007a). *C. concisus* induces an increase in IL-32 protein expression via transcriptional upregulation of IL-32, and leads to activation of ENaC via ERK, which can in turn cause ubiquitination and internalization of ENaC via NEDD4-2, and thereby impairs electrogenic Na^+ absorption (Nattramilarasu et al., 2020). Furthermore, IPA predictions from RNA-Seq data identified LPS, IFN-γ and IL-1β as upstream regulators that target IL-32 (Nattramilarasu et al., 2020), which in turn induces ERK activation and subsequent internalization of ENaC by NEDD4-2 the impairment of Na^+ absorption. Hence, it is reasonable to assume that cytokines IFN-γ and IL-1β released from the sub-epithelial

immune compartment in response to *C. concisus* infection could possibly induce ENaC dysfunction.

Apart from IFN-γ and IL-1β, NF-κB complex (proinflammatory pathway) and dexamethasone (anti-inflammatory pathway) were the other cytokines activated by *C. concisus* infection to target IL-32 (Supplemental Table S1). NF-κB complex has previously been described as one of the key proinflammatory cytokines activated by *C. concisus* in THP-1-derived macrophages (Kaakoush et al., 2015). The cytokine pathway of IL-5 (Th2 cytokine) was also activated by *C. concisus* infection in HT-29/B6-GR/MR cells, although it does not target IL-32 (Supplemetal Table S1). This correlates to a previous study, in which RNA-Seq data indicated that *C. concisus* strain BAA-1457 upregulated IL-5 signaling in Caco-2 cells (Deshpande et al., 2016). However, IL-5 activation in the subepithelium of the human colon has not been reported by bacterial infections to date, although one study identified IL-5 activation by *Entamoeba histolytica* in the cecum of CBA/J mice (Guo et al., 2008). IPA analyses revealed that IL-5 targets the genes involved in cell cycle control and carcinogenesis after *C. concisus* infection (Supplemental Table S1). Moreover, *C. concisus* was ascertained as an etiological agent associated with the progression of pre-malignant Barrett's oesopheagus to oesophageal adenocarcinoma (Namin et al., 2015; Namin and Dallal, 2018). Metagenomic analyses of the tongue microbiome in IBD patients discerned *C. concisus* as the abundant microbe associated with the gastric pre-cancerous cascade (Cui et al., 2019). However, it still remains elusive whether *C. concisus* infection induces the progression of IBD to gastric or colorectal cancer, which should be elucidated in future studies. Interestingly, ENaC activity was also regulated by the tumour suppressor gene, adenomatous polyposis coli (APC), as colonic Na^+ absorption and the expression of γ-ENaC gene in mice were enhanced by heterozygous deletion of APC gene (Ousingsawat et al., 2008). In this context, we could interpret that inhibition of ENaC activity by *C. concisus* can in turn enhance the expression of the tumour suppressor genes to subvert the carcinogenesis induced by *C. concisus*.

4.1.4 Gene expression of ion transporters in concerted activity with the ENaC

The transcriptional regulation of different ion transporters that function in concert with ENaC in the colonic epithelium was analyzed from RNA-Seq data of DBA-stimulated HT-29/B6-GR/MR cells 48 h after *C. concisus* infection. The mRNA expression of electroneutral

transporters, NHE3 and DRA, was not downregulated by *C. concisus* infection (Supplemental Table S2). This was in contrast to acute *C. jejuni* infection in the human colon, in which a transcriptional downregulation of DRA was observed, suggesting a disturbance also in electroneutral NaCl absorption (Bücker et al., 2018). Another *in vivo* study reported that *Brachyspira*, a spirochete bacterium, induces diarrhea in pigs by loss of electroneutral Na^+ absorption and transcriptional downregulation of NHE3 in proximal, apex, and distal segments of the colon (Enns et al., 2020). Interestingly in the spirochete-induced Na^+ malabsorptive diarrhea in pigs, no changes were observed in electrogenic Na^+ absorption via ENaC in the distal colon (Enns et al., 2020). Na^+/K^+-ATPase creates a lumen negative potential difference for electrogenic Na^+ absorption via ENaC in the apical membrane of the colonic epithelium by energy-driven Na^+ transport across the basolateral side (Sandle, 1998). Therefore, the gene expression of Na^+/K^+-ATPase was analyzed in HT-29/B6-GR/MR cells, which was unaltered after *C. concisus* infection (Supplemental Table S2). From this, we could presume that inhibition of ENaC-mediated electrogenic Na^+ transport by *C. concisus* is independent of Na^+/K^+-ATPase activity. However, this should be confirmed in the future by measurements of Na^+/K^+-ATPase activity after *C. concisus* infection.

The mRNA expression of the secretory and absorptive Cl^- channels, CaCC and NKCC1, localized in apical and basolateral membranes in colonic epithelia, were not differentially regulated after *C. concisus* infection *in vitro*, which explains the retention of cholinergic Cl^- secretion (ΔI_{SC} after carbachol, Figure 2). Surprisingly, mRNA expression of CFTR was downregulated following *C. concisus* infection in HT-29/B6-GR/MR cells, which was also observed in the colon mucosae of *C. jejuni*-infected patients (Bücker et al., 2018). However, no functional loss of cAMP-dependent Cl^- secretion (ΔI_{SC} after PGE_2 and theophylline, Figure 2) was observed after *C. concisus* infection *in vitro*, in contrast to impaired Cl^- secretion via CFTR by *C. jejuni* infection in the human colon (Bücker et al., 2018).

To briefly sum up the research findings discussed in section 4.1, *C. concisus* impairs ENaC-dependent electrogenic Na^+ absorption in colonocytes via transcriptional downregulation of β- and γ-ENaC. At the same time, the viability of colonocytes was retained with active Cl^- secretion accompanied by the absence of lesions or cytotoxic destruction after *C. concisus* infection. *Campylobacter concisus*-induced ENaC dysfunction results from activation of the ERK pathway. Furthermore, the transcriptional upregulation of proinflammatory cytokine IL-

32 by *C. concisus* infection might induce ERK activation and promote ENaC dysfunction. In parallel to ENaC dysfunction, *C. concisus* disrupts claudin-8, which acts as a paracellular barrier to prevent back-leakage of Na^+ into the lumen. Taken together, *C. concisus* induces ENaC dysfunction via ERK activation and subverts claudin-8-dependent paracellular barrier function, both of which contribute to Na^+ malabsorption and diarrhea (Nattramilarasu et al., 2020).

4.2. Immune-mediated aggravation of *Campylobacter concisus*-induced epithelial barrier dysfunction

Besides the ENaC dysfunction, *C. concisus* also induces epithelial barrier dysfunction in HT-29/B6-GR/MR monolayers (not stimulated by DBA) with a significant decrease in TER at 24 and 48 h p.i. (Nattramilarasu et al., 2021). Interestingly, it has also been reported that different *C. concisus* strains obtained from IBD patients induce immune activation *in vitro* with the release of proinflammatory cytokines TNF-α, IL-1β and IL-12, and the chemokine IL-8 from macrophages and colonocytes (Man et al., 2010a; Kaakoush et al., 2011). Furthermore, regardless of their isolation sites, *C. concisus* strains obtained from healthy and diarrheal patients induced barrier defects in HT-29 cells by epithelial apoptosis and TJ perturbance (Nielsen et al., 2011). An *in vitro* co-culture model of HT-29/B6-GR/MR monolayers with THP-1-derived macrophages on the basal side was employed to investigate the causal link between the immune activation and epithelial barrier dysfunction induced by *C. concisus* (Nattramilarasu et al., 2021). The results obtained from this investigation are discussed in this section 4.2.

4.2.1 Macrophage activation by *Campylobacter concisus* potentiate the barrier damage

Campylobacter concisus induced a profound TER drop in HT-29/B6-GR/MR monolayers in co-culture condition (with THP-1-derived macrophages on the basal side) compared to monoculture condition at 48 h p.i. (Nattramilarasu et al., 2021). It was accompanied by a marked increase in the release of proinflammatory cytokines, TNF-α, IL-1β and IL-6 from THP-1-derived macrophages after *C. concisus* infection in co-culture conditions. In addition, the cell proliferation rate of THP-1-derived macrophages was also elevated 48 h after *C. concisus* infection at MOI of 200 and below. The *in vitro* results of macrophage activation by

C. concisus correlate to the *in vivo* results, as an ultra-structural analyses revealed macrophage activation in the rectal mucosae of *Campylobacter* colitis patients (Polimood et al., 2008). Furthermore, macrophages and monocytes were elevated in colon mucosae of *C. coli*-infected IL-10$^{-/-}$ mice challenged with human fecal microbiota, which was accompanied by severe mucosal inflammation (Heimesaat et al., 2020). This finding supports the view of mucosal immune activation being a central mechanism of the barrier and other functional defects induced by *Campylobacter* infection in the colon. However, the mucosal inflammation is not restricted only to bacterial infections, as the epithelial barrier dysfunction induced by HIV was also accompanied by macrophage activation with an increase in the release of proinflammatory cytokines TNF-α, IL-1β, IFN-γ and IFN-α (Stockmann et al., 2000). The proinflammatory cytokine TNF-α induces barrier loss in epithelial cells via occludin internalization and delocalization from TJ via interactions mediated by the C-terminal coiled-coil occludin/ELL domain (OCEL) (Buschmann et al., 2013), whereas IL-1β induces a progressive downregulation of occludin accompanied by an increase in claudin-1 expression in Caco-2 monolayers (Al-Sadi and Ma, 2007). Moreover, the immune regulation by cytokines in IBD patients can cause intestinal epithelial barrier dysfunction not only by TJ disruption but also through epithelial apoptosis (Schulzke et al., 2009).

The inflammatory responses induced by enteropathogenic *E. coli* (EPEC) and *C. jejuni* in colon mucosae through cytokine responses from the epithelium and immune cells hamper the epithelial barrier function (Schifflet et al., 2005; Bücker et al., 2018). In *V. cholera*-, *S. enterica*- and *C. jejuni*-induced diarrhea, TNF-α was ascertained as a key proinflammatory cytokine in modulating the detrimental effects of inflammatory responses on intestinal epithelial barrier function (Bücker et al., 2018; Ou et al., 2009; Nickerson et al., 2001). TNF-α, either alone or in combination with IFN-γ and IL-13, regulates the epithelial barrier function in active IBD patients (Prasad et al., 2005; Mankertz et al., 2009; Zeissig et al., 2007b). IL-1β plays a dual role as it induces a host-inflammatory response to combat the infection, and at the same time facilitates the influx of luminal content into the subepithelial compartment of the mucosa to exacerbate the inflammation (Siegmund et al., 2001). *Campylobacter jejuni* elicited a proinflammatory response by release of IL-1β from THP-1 monocytes and macrophages *in vitro* (Jones et al., 2003; Lobo de Sá et al., 2019), and in the colon mucosae of IL-10$^{-/-}$ mice *in vivo* (Sun et al., 2012). In addition to TNF-α and IL-1β, IL-6 was also ascertained as another proinflammatory cytokine released by macrophages after *C. jejuni* infection (Lobo de Sá et al., 2019). Similar to *C. jejuni*, *C. concisus* induced a proinflammatory response by a marked

increase in the proinflammatory cytokines TNF-α, IL-1β and IL-6 released by THP-1-derived macrophages (Nattramilarasu et al., 2021). Hence, the activation of THP-1-derived macrophages by *C. concisus* and subsequent release of proinflammatory cytokines could be ascertained as underlying phenomena behind the pronounced epithelial barrier dysfunction induced by *C. concisus* infection in our *in vitro* co-culture model of epithelial cells and macrophages (Nattramilarasu et al., 2021). More importantly, the pronounced drop in TER or barrier damage induced by *C. concisus* in our *in vitro* co-culture model does not result from a direct interaction of macrophages and epithelial cells but happens through the proinflammatory cytokines released by macrophages. The macrophages and epithelial cells were well separated in the basal and apical sides of the cell culture filters in the *in vitro* co-culture setting.

Besides the proinflammatory response elicited by *C. concisus*, it also induces an anti-inflammatory response in THP-1-derived macrophages by a marked increase in the release of anti-inflammatory cytokine IL-10 in infected cells compared to controls (Nattramilarasu et al., 2021). The anti-inflammatory response could be induced by the cAMP responsive element binding protein 1 (CREB1), as it has been reported from RNA-Seq analyses that CREB1 promotes transcriptional upregulation of IL-10 in THP-1 macrophages induced by *C. concisus* (Kaakoush et al., 2015). Moreover, IL-10 is an anti-inflammatory cytokine constitutively produced by macrophages and plays a pivotal role in modulating the uncontrolled mucosal immune responses induced by acute bacterial infections (Krause et al., 2015). However, a clinical epidemiology study proposed that the local inflammatory responses in the intestinal segments of IBD patients could augment the colonization of *C. concisus* in the intestinal mucosa (Ismail et al., 2012), which might in turn potentiate the epithelial barrier damage. TJ modifications and/or apoptosis induction, which are the possible molecular correlates of the epithelial barrier damage, can in turn enhance the luminal antigen influx and cytokine secretion by immune activation to exacerbate the barrier dysfunction. This leads to a vicious circle of mucosal inflammation and epithelial barrier dysfunction (Lobo de Sá et al., 2021a). Therefore, TJ modifications and epithelial apoptosis induced by *C. concisus* infection were investigated in HT-29/B6-GR/MR monolayers maintained in co-culture condition and compared with the infected monolayers in monoculture condition without macrophages on the basal side.

4.2.2. Tight junction modifications in colonic epithelial cells by *Campylobacter concisus*

Even though the earlier studies reported that *C. concisus* induces moderate TJ changes in the colonocytes to promote epithelial barrier dysfunction (Man et al., 2010a; Nielsen et al., 2011), a comprehensive analysis of TJ protein expression and localization changes induced by *C. concisus* was still lacking. *Camplyobacter concisus* induces a proinflammatory response in colonic epithelial cells and macrophages (Man et al., 2010a; Kaakoush et al., 2015). However, the influence of mucosal immune activation on the regulation of TJ expression and the epithelial barrier function remained unexplored. Hence, TJ protein expression changes induced by *C. concisus* was analyzed in HT-29/B6-GR/MR colonic epithelial cell monolayers in co-culture with THP-1-derived macrophages (Nattramilarasu et al., 2021).

4.2.2.1 Downregulation and redistribution of occludin from the bicellular tight junction

The protein expression of occludin was unaltered in *C. concisus*-infected HT-29/B6-GR/MR monolayers in monoculture conditions. However, the protein expression of occludin was downregulated in infected monolayers in co-culture conditions (Nattramilarasu et al., 2021). Although a previous study observed downregulation of protein expression of occludin in membrane fractions of Caco-2 cells after *C. concisus* infection, the protein expression was unchanged in the whole-cell lysates (Man et al., 2010a). In contrast, we delineated a reduction in protein expression of occludin by *C. concisus* in the whole-cell lysates of HT-29/B6-GR/MR monolayers maintained in co-culture condition (Nattramilarasu et al., 2021). This was accompanied by an intense redistribution of occludin from bTJ. The loss of occludin from bTJ and its reduction in protein expression following *C. concisus* infection could result from the inflammatory response of THP-1-derived macrophages, as macrophage-derived IL-6 and IL-1β were described in previous studies to induce downregulation and redistribution of occludin in intestinal epithelial cells (Kim et al., 2018; Guo et al., 2017; Ogawa et al., 2018).

Apart from IL-6 and IL-1β, TNF-α also induces downregulation of occludin expression in the epithelium of the rat colon, which in turn compromise the epithelial barrier function (Amasheh et al., 2009b). Furthermore, it has also been identified that TNF-α is the predominant proinflammatory cytokine in DSS-induced colitis mouse, which induces the colonic epithelial barrier dysfunction (Hernández-Chirlaque et al., 2016). Occludin knockdown in MDCK monolayers increases the paracellular flux of macromolecules up to a size of 40 KDa or a

diameter of up to 125 Å (Buschmann et al., 2013). Therefore, *C. concisus* might induce an increase in paracellular permeability of HT-29/B6-GR/MR monolayers to fluorescein (332 Da) and FITC-dextran (4 kDa) by loss of occludin from bTJ in co-culture conditions. However, a recent study on paracellular leak pathway (for solutes < 100 Å) by transwell assay revealed that leakage of macromolecules was localized to the cells in the outer edges of the transwells in occludin knock-down CacoBBe cells (Richter et al., 2019). This raises the possibility that the enhanced permeability to FITC-dextran 4 kDa by *C. concisus* infection in HT-29/B6-GR/MR monolayers under co-culture condition is independent of the loss of occludin in bTJ.

4.2.2.2 Downregulation and redistribution of tricellulin from the tricellular tight junction

The TJs of the tricellular contact sides in the intestinal epithelium are called tricellular tight junctions (tTJS). The corners of tricellular contacts, where two vertical strands associate laterally with the plasma mebranes of the neighboring cells, form a hollow central tube, which is supposed to be a weak point of the epithelial barrier (Ikenouchi et al., 2005). Tricellulin is an integral component of intestinal epithelial tight junctions in the tricellular contact points, which seals the central tube and thereby regulates the paracellular barrier function in tTJ (Krug et al., 2009). In HT-29/B6-GR/MR monolayers maintained in co-culture condition, *C. concisus* induces downregulation of tricellulin expression and promotes the redistribution of tricelllulin from the tTJ (Nattramilarasu et al., 2021). Tricellulin was ascertained as a receptor for bacterial invasion in epithelial tTJ, as the knockdown of tricellulin in MDCK monolayers prevented the intercellular movement and shedding of *Shigella* spp. (Fukumatsu et al., 2012). Furthermore, in EPEC-induced barrier damage in Caco-2 monolayers, a redistribution of tricellulin from tTJ was observed along with a significant downregulation in protein expression at 4 h p.i. (Morampudi et al., 2017). In a mechanism similar to EPEC infection, *C. concisus* induced a significant downregulation of tricellulin expression and redistribution off tTJ in HT-29/B6-GR/MR monolayers, however, only in co-culture condition. The downregulation of tricellulin and its delocalization from tTJ in co-culture monolayers could also occur via downregualation of occludin by *C. concisus*, as occludin supports the tricellular localization of tricelluin (Ikenouchi et al., 2008). Interestingly, the tricellulin protein expression was unaltered after *C. jejuni* infection in HT-29/B6-GR/MR monolayers in co-culture condition at 22 h p.i. (Butkevych et al., 2020). At 48 h p.i., *C. jejuni* might present a different outcome of the expression and localization of tricellulin in HT-29/B6-GR/MR monolayers. Furthermore, a direct interaction of *C. jejuni* or *C. concisus* with tricellulin is also possible like interaction of

Shigella spp with tricellulin (Fukumatsu et al., 2012). However, this should be addressed through ultrastructural investigations in the future.

The downregulation of tricellulin expression and the delocalization of tricellulin from tTJ by *C. concisus* was paralleled by a profound increase in epithelial permeability to FITC-dextran 4 kDa and fluorescein in HT-29/B6-GR/MR monolayers maintained in co-culture condition (Nattramilarasu et al., 2021). This mimics the intestinal leak flux pathomechanism of diarrhea in IBD patients, as tricellulin downregulation was accompanied by an increase in paracellular permeability to FITC-dextran 4 kDa in the colon mucosae of UC patients and ileal biopsies of CD monozygotic twins, (Krug et al., 2018; Keita et al., 2018). More importantly, *C. concisus* infection dissociates tricellulin from tTJ under the influence of mucosal immune activation. This can create large channels in the central tubes of the epithelial tricellular contacts, which might in turn enhance the influx of even larger macromolecules and/or bacterial antigens from the lumen into the intestinal mucosa, and potentiates the inflammatory processes.

IL-13 was identified as the proinflammatory cytokine that induces tricellulin downregulation and redistribution off the tTJ in colon mucosae of UC patients (Krug et al., 2018). In contrast, *C. concisus* infection did not elicit an IL-13 response from THP1-derived macrophages, but increased TNF-α released from macrophages (Nattramilarasu et al., 2021). This brings us to a presumption that *C. concisus* induces IL-13-independent tricellulin disruption from tTJ, in a mechanism similar to *Tropheryma whipplei*, which downregulates tricellulin via macrophage-derived TNF-α and impair epithelial barrier function in duodenal mucosae of Whipple's Disease patients (Epple et al., 2017). However, IL-13-independent regulation of tricellulin expression and localization changes by *C. concisus* should be confirmed in the future either with *in vivo* or other *in vitro* macrophage models like peripheral blood mononuclear cells (PBMCs), which induce a strong IL-13 response.

4.2.2.3 Functional role of claudins in *Campylobacter concisus*-induced epithelial barrier dysfunction

Among the different claudin variants that seal the paracellular barrier of the intestinal epithelium, the mRNA and protein expression of claudin-5 was downregulated by oral and fecal isolates of *C. concisus*. This was also accompanied by an increase in paracellular flux of small molecule fluorescein 332 Da (Nielsen et al., 2011). In the present study, the protein expression

of claudin-5 was also downregulated by *C. concisus* in HT-29/B6-GR/MR monolayers in both monoculture and co-culture conditions (Nattramilarasu et al., 2021). In lymphocytic colitis patients, the barrier impairment in colon mucosae was accompanied by downregulation of claudin-5 expression and transcriptional upregulation of TNF-α (Barmeyer et al., 2017). In HT-29/B6 cells, a marked increase of TNF-α was detected in cell culture supernatants 48 h post-*C. concisus* infection (Man et al., 2010a). Hence, it can be presumed that downregulation of claudin-5 protein expression by *C. concisus* infection results from enhanced TNF-α response in the subepithelial regions of colonic epithelium. In HT-29/B6-GR/MR monolayers, in both monoculture and co-culture conditions, claudin-5 downregulation was accompanied by an increase in epithelial permeability to fluorescein (332 Da). Therefore, the claudin-5 downregulation by *C. concisus* could influence the increase in epithelial permeability to the small molecule fluorescein (332 Da) in epithelial cell monolayers in the absence of inflammatory response from macrophages (Nielsen et al., 2011; Nattramilarasu et al., 2021).

RNA-Seq studies reported that a weak epithelial response was induced by *C. concisus* infection in Caco-2 cells, while a strong immune response was observed by *C. concisus* infection in THP-1-derived macrophages (Deshpande et al., 2016; Kaakoush et al., 2015). However, the gene expression of claudin-1 and claudin-2 appeared to be differentially regulated in Caco-2 cells after infection with an invasive *C. concisus* strain (Deshpande et al., 2016). In HT-29/B6-GR/MR monolayers, no changes were detected in claudin-2 protein expression 48 h after *C. concisus* infection (Nattramilarasu et al., 2021). However, claudin-1 expression was upregulated in the infected monolayers in both monoculture and co-culture conditions (Nattramilarasu et al., 2021). This correlates to the increase in claudin-1 expression in colonic epithelial cell monolayers after *Campylobacter fetus*, *C. coli* and *C. jejuni* infections (Bücker et al., 2017; Bücker et al., 2018; Butkevych et al., 2020). The upregulation in the protein expression of the barrier-forming claudin-1 could also result from a marked increase in TNF-α released by macrophages, as TNF-α induces upregulation of claudin-1 expression via the NF-κB pathway (Amasheh et al., 2010). The phenomenon of an increase in the protein expression of the barrier-forming claudin-1 in HT-29/B6-GR/MR monolayers by *C. concisus*, despite a marked decrease in the TER, is called caludin-1 paradox. This implies that although the claudin-1 expression is increased in epithelial cells by infection with *Campylobacter* spp., it does not rescue the impaired barrier function due to redistribution of claudin-1 off the TJ domain (Bücker et al., 2018; Butkevych et al., 2020). In addition, claudin-1 expression was increased in the colon mucosae of IBD patients and inflammation-induced colon tumorigenesis (Weber et al.,

2008; Pope et al., 2014). However, it still remains elusive if claudin-1 possesses self-regulatory properties or is subjected to expression changes in response to epithelial barrier damage resulting from inflammation.

Campylobacter concisus did not induce downregulation of claudin-8 in HT-29/B6-GR/MR monolayers in both monoculture and co-culture conditions at 48 h p.i. in spite of the impaired epithelial barrier function (Nattramilarasu et al., 2021). This was in contrast to the monoculture monolayers stimulated by DBA, in which the *C. concisus*-induced ENaC dysfunction was accompanied by paracellular barrier defects and downregulation in mRNA and protein expression of claudin-8 (Nattramilarasu et al., 2020). Therefore, claudin-8 downregulation by *C. concisus* should result from impaired ENaC function and downregulation of γ-ENaC in colonic epithelial cells, as claudin-8 expression was coupled with γ-ENaC expression in renal collecting ducts (Sassi et al., 2020).

4.2.3 Epithelial apoptosis in *Campylobacter concisus*-induced intestinal epithelial barrier dysfunction

Apart from TJ disruptions in the paracellular barrier of the epithelium, epithelial cell apoptosis is directly barrier-relevant and can modulate epithelial leaks in cytokine-induced inflammation (Gitter et al., 2000; Schulzke et al., 2006; Heller et al., 2008). Epithelial apoptosis in the intestine was discerned as a major contributor in leak flux diarrhea induced by the protozoan parasite *Giardia lamblia* and *C. jejuni* (Troeger et al., 2007b; Bücker et al., 2018). *Camplylobacter concisus* infection in HT-29 cells also induced barrier dysfunction mainly by epithelial apoptosis, although a moderate perturbation in TJs was evident (Nielsen et al., 2011). In *C. jejuni*, blockade of epithelial apoptosis completely restored the barrier dysfunction induced in HT-29/B6-GR/MR monolayers in co-culture conditions (Butkevych et al., 2020).

Epithelial apoptosis induced by *C. jejuni* in HT-29/B6-GR/MR monolayers under co-culture condition increased the paracellular flux to 4 kDa macromolecule FITC-dextran (Butkevych et al., 2020). *Campylobacter concisus* infection also facilitates the flux of the macromolecule FITC-dextran (4 kDa) in HT-29/B6-GR/MR monolayers in co-culture condition, but not in monoculture condition. Epithelial apoptosis was also ascertained after *C. concisus* infection in HT-29/B6-GR/MR monolayers in both monoculture and co-culture conditions. However, no significant differences exist in the number of apoptotic cells between the infected monolayers

in monoculture and co-culture conditions (Nattramilarasu et al., 2021). This suggests that in co-culture conditions, the increase in the paracellular flux of the macromolecule FITC-dextran (4 kDa) does not result from apoptotic leaks induced by *C. concisus* in HT-29/B6-GR/MR monolayers. The epithelial apoptosis could result from the putative cytotoxins, for instance, CDT-like toxin, which induces apoptosis in monocytes and cell cycle arrest in epithelial cells to mediate intracellular survival of *C. jejuni* (Jain et al., 2009; Hickey et al., 2005). However, *C. concisus* infection increases the flux of fluorescein (332 Da) in HT-29/B6-GR/MR monolayers in both monoculture and co-culture conditions. Therefore, in the absence of macrophage immune response, the increase in the flux of fluorescein could result from epithelial apoptosis in synergy with the loss of occludin and claudin-5 from the bTJ. More importantly, the necrotic cell death mechanisms do not influence the barrier dysfunction from *C. concisus* infection in HT-29/B6-GR/MR cell monolayers, as no significant differences were observed between control and infected monolayers at an MOI of 200 (Nattramilarasu et al., 2021).

To briefly sum up section 4.2, *C. concisus* facilitates the flux of smaller molecules (< 4 kDa) and induces barrier dysfunction in colonic epithelium by epithelial apoptosis and functional loss of occludin. However, with the mucosal immune activation and inflammatory response of THP-1-derived macrophages, which resembles the *in vivo* situation of the inflamed colon in human campylobacteriosis and IBD, the epithelial barrier dysfunction aggravates with the loss of tricellulin from tTJs. The delocalization of tricellulin from tTJ induced by *C. concisus* disrupts the integrity of central sealing elements in epithelial tricellular contacts. This can create a channel in the central tube (pore diameter of 10 nm) of the tricellular contacts, and promote the influx of bacterial antigens or macromolecules < 100 Å by leak pathway. The influx of macromolecules could in turn exacerbate the mucosal immune response and barrier damage leading to bloody or watery diarrhea (Nattramilarasu et al., 2021).

4.3 Future perspectives

Our present studies indicate that *C. concisus* induces ENaC dysfunction and pronounced epithelial barrier damage as a consequence of elevated immune response of M1 macrophages (Nattramilarasu et al., 2020; Nattramilarasu et al., 2021). The effects of *C. concisus* on ENaC activity and epithelial barrier function were investigated only with respect to a single strain AAuH 37 UCo-a (Kirk et al., 2018), an oral isolate from a male Danish UC patient who

underwent IPAA. However, *C. concisus* is a genetically heterogeneous *Campylobacter* spp. (Kaakoush and Mitchell, 2012), and the bioinformatics analyses predicted that it possess either a single or multiple virulence factors irrespective of whether it is isolated from healthy controls or from microscopic colitis, gastroenteritis and IBD patients (Kirk et al., 2018; Gemmell et al., 2018; Yde Aagaard et al., 2020). Among the different virulence factors exhibited by diverse *C. concisus* strains, exotoxin-9 and ZOT genes were highly detected in *C. concisus* strains from IBD patients (Kaakoush et al., 2014b; Mahendran et al., 2013; Underwood et al 2016). A recent clinical epidemiology study with a large cohort of diarrheal patients reported an increased risk of microscopic colitis in *C. concisus*-positive stool cultures compared with culture-negative stool cultures (Nielsen et al., 2020). To get a clear picture on the pathogenesis of *C. concisus* in microscopic colitis, it becomes indispensable to investigate the effects on intestinal transport and barrier function in *C. concisus*-positive intestinal biopsies from microscopic colitis patients.

ZOT is an enterotoxin first identified in *V. cholerae* which induces disruption of ZO-1 from TJ (Fasano et al., 1991), and was later found to enhance the intestinal permeability and TJ modifications by reversible and transient changes in TER of the intestinal epithelial cells (Schmidt et al., 2007). *Campylobacter concisus* also expresses ZOT, although the proteomic analysis revealed that *C. concisus* ZOT had only four conserved domains when compared to *V. cholerae* ZOT (Kaakoush et al., 2010). In contrast to transient epithelial barrier defects induced by *V. cholerae* ZOT, *C. concisus* ZOT induced an irreversible and prolonged epithelial barrier dysfunction with apoptosis induction and release of proinflammatory cytokines as IL-8 and TNF-α from the intestinal epithelial cells *in vitro* (Mahendran et al., 2016). In parallel, a transcriptomic analysis on the intestinal epithelial responses to *C. concisus* ZOT in Caco-2 cells revealed that *C. concisus* ZOT can target the intestinal cellular junctions through upregulation of Protease-activated receptor-2 (PAR-2) in a mechanism similar to *V. cholerae* ZOT (Deshpande et al., 2016). Nevertheless, whether *C. concisus* ZOT induces intestinal epithelial barrier dysfunction only by apoptosis or it also involves TJ modifications still remains elusive. Therefore, a detailed investigation of the effects of *C. concisus* ZOT on the epithelial TJ modification in intestine and the regulative host-cell signalling pathways is essential to compare its functionality with *V. cholerae* ZOT. A recent study identified an increase in the expression of ZOT genes in the *C. concisus* strains obtained from intestinal mucosae of lymphocytic colitis patients (Aaagaard et al., 2020). Lymphocytic colitis patients present watery diarrhea with impairment of colonic ENaC function (Barmeyer et al., 2017). Of note, the oral *C. concisus* strain from a UC patient used in our study, which impairs ENaC function, also possesses the

ZOT gene (Kirk et al., 2018). Therefore, future studies should target the investigation of *C. concisus* ZOT in regulating the colonic ENaC function.

Campylobacter concisus also plays a pivotal role in modulating the innate immune response of intestinal epithelia as the clinical *C. concisus* isolates from IBD patients enhanced the surface expression of TLR-4, which can in turn induce the epithelial inflammatory responses to LPS from commensals or other bacterial pathogens (Ismail et al., 2013). It was also demonstrated that LOS of *C. concisus* elicited a TNF-α-mediated immune response in differentiated THP-1 cells, even though the TNF-α secretion was significantly lower when compared with *C. jejuni* LOS (Brunner et al., 2018). A recent finding with human gastric intestinal organoids has shown that gastric epithelium senses TNF-α and bacterial LPS from the basolateral side to enhance the epithelial immune response by an increase in IL-8 transcription (Kayisoglu et al., 2021). In our study, we found that *C. concisus* induced a pronounced epithelial barrier dysfunction in the co-culture model of the epithelial cell monolayers with THP-1-derived macrophages on the basolateral side (Nattramilarasu et al., 2021). Since the *C. concisus* infection was carried out with MOI of 200 on both apical and basolateral sides, it raises the possibility that *C. concisus* LOS might induce TNF-α secretion in THP-1-derived macrophages to potentiate the epithelial barrier dysfunction. More importantly, *C. concisus* LOS could directly interact with the basolateral receptors of epithelial cells to intensify the epithelial barrier damage via enhanced transcription of IL-8 in epithelial cells. This should be further investigated in the future studies by two-dimensional (2D) organoids of human gastric epithelium grown in extracellular matrix.

Besides ZOT and LOS, recent studies also identified other virulence factors, for instance, genes encoding the extra-chromosomal plasmids pICON and pSMA1 in *C. concisus* strains associated with CD and UC patients, respectively (Liu et al., 2018; Liu et al., 2020). Therefore, it also becomes indispensable to investigate if the aforementioned virulence factors are involved in the exacerbation of epithelial barrier dysfunction induced by *C. concisus* in the context of intestinal inflammation in IBD patients. Furthermore, the pathogenic properties of other putative cytotoxins of *C. concisus*, for instance CDT, which can induce cell cycle arrest and apotosis, should be elucidated by future investigations.

5. Summary

Campylobacter concisus impaired colonic epithelial sodium channel (ENaC) function with the transcriptional downregulation of regulatory ENaC subunits (-β and -γ). The activation of intracellular mitogen-activated protein kinase (MAPK) enzyme extracellular signal-regulated kinase (ERK) by *C. concisus* is ascertained as an intracellular cell signaling pathway in inducing ENaC dysfunction. The transcriptional upregulation of interleukin (IL)-32 plays a pivotal role in *C. concisus*-induced ENaC dysfunction as the bioinformatics prediction from ingenuity pathway analysis (IPA) identified IL-32 as a potential activator of the ERK signaling pathway. The increase in expression of tight junction (TJ) protein claudin-8 following steroid stimulation prevents paracellular back-leakage of sodium (Na^+) ions absorbed by ENaC in colonic epithelium. Claudin-8 protein expression was decreased along with the subcellular redistribution off the tight junction (TJ) domain by *C. concisus* infection in the colonic epithelial cells stimulated by steroids. Therefore, claudin-8 disruption in the colonic epithelium is another cellular pathomechanism of *C. concisus* in the context of Na^+-malabsorptive diarrhea.

The epithelial barrier dysfunction induced by *C. concisus* was more pronounced under the influence of immune response in the co-culture model of colonic epithelial cells and macrophages. The macrophage activation by *C. concisus* in the co-culture setup was accompanied by an increase in the release of proinflammatory cytokines, tumor necrosis factor (TNF)-α, IL-1β and IL-6. Concomitantly, the expression of TJ proteins occludin and tricellulin was decreased along with the subcellular redistribution of these proteins from the TJ domains. Moreover, *C. concisus* infection increased the flux of fluorescein (332 Da) in the monoculture and co-culture cell monolayers. In contrast, the flux of the macromolecule fluorescein isothiocyanate (FITC)-dextran (4 kDa) was increased only in the co-culture monolayers after infection. Furthermore, *C. concisus* induced epithelial apoptosis in the co-culture monolayers. However, the quantification data implied no significant difference in the apoptotic cell numbers between the infected monolayers in monoculture and co-culture conditions. Therefore, the epithelial apoptotic leaks and the functional loss of occludin by *C. concisus* infection contribute to the increase in the flux of small molecules as fluorescein (332 Da). However, under the regulatory influence of macrophage immune response, *C. concisus* additionally enhances the flux of macromolecules as dextran 4 kDa by the opening of the leak pathway through tricellulin disruption in the tTJ.

6. Zusammenfassung

Campylobacter concisus beeinträchtigte die Funktion des epithelialen Natriumkanals (ENaC) im Colon durch die transkriptionelle Herabregulation der regulatorischen ENaC-Untereinheiten (-β und -γ). Die Aktivierung der intrazellulären mitogen-aktivierten Proteinkinase (MAPK) in Form des Enzyms Extracellular Signal-regulated Kinase (ERK) durch *C. concisus* wurde als intrazellulärer Zellsignalweg bei der Induktion der ENaC-Dysfunktion festgestellt. Die transkriptionelle Hochregulierung von Interleukin (IL)-32 spielt eine zentrale Rolle bei der *C. concisus*-induzierten ENaC-Dysfunktion, da die bioinformatische Vorhersage aus der Ingenuity Pathway Analysis (IPA) IL-32 als potenziellen Aktivator des ERK-Signalwegs identifizierte. Die Zunahme der Expression des Tight Junction (TJ)-Proteins Claudin-8 nach Steroidstimulation verhindert den parazellulären Rückstrom von Natrium Na^+-Ionen, die vom ENaC im Kolonepithel resorbiert werden. Die Claudin-8-Proteinexpression wurde zusammen mit der subzellulären Umverteilung von Claudin-8 aus der Tight Junction (TJ)-Domäne der Epithelzelle heraus durch die *C. concisus*-Infektion vermindert. Daher ist die Claudin-8-Umverteilung im Kolonepithel ein weiterer zellulärer Pathomechanismus von *C. concisus* im Kontext der durch die Na^+-Resorptionsstörung bedingten malabsorptiven Diarrhoe.

Die durch *C. concisus* induzierte epitheliale Barrieredysfunktion war unter dem Einfluss der Immunantwort im Co-Kulturmodell von Kolonepithelzellen und Makrophagen stärker ausgeprägt. Die Makrophagenaktivierung durch *C. concisus* im Co-Kultur-Setup ging mit einer erhöhten Freisetzung der pro-inflammatorischen Zytokine Tumor-Nekrose-Faktor (TNF)-α, IL-1β und IL-6 einher. Gleichzeitig war die Expression der TJ-Proteine Occludin und Tricellulin vermindert, zusammen mit einer subzellulären Umverteilung dieser Proteine aus den TJ-Domänen heraus. Darüber hinaus erhöhte die *C. concisus*-Infektion die epitheliale Permeabilität für Fluorescein (332 Da) in den Zellmonolayern der Monokultur und der Co-Kultur. Im Gegensatz dazu war die epitheliale Permeabilität für das Makromolekül Fluorescein Isothiocyanat (FITC)-Dextran (4 kDa) nur in den Co-Kultur-Monolayern nach der Infektion erhöht. Darüber hinaus induzierte *C. concisus* in den Co-Kultur-Monolayern die epitheliale Apoptose. Die Quantifizierungsdaten ergaben jedoch keinen signifikanten Unterschied in der Anzahl der apoptotischen Zellen zwischen den infizierten Monolayern in Monokultur und Co-Kultur. Daher tragen die epithelialen apoptotischen Lecks und der Funktionsverlust von Occludin durch die *C. concisus*-Infektion zur Erhöhung der epithelialen Permeabilität für kleine Makromoleküle bei. Unter dem regulierenden Einfluss der Makrophagen-Immunantwort erhöht

C. concisus darüber hinaus jedoch die epitheliale Permeabilität für Makromoleküle wie Dextran 4 kDa durch Öffnung der tTJ (Leak pathway) infolge einer Störung der Tricellulin-Verteilung.

7. Bibliography

Aabenhus, R., On, S. L., Siemer, B. L., Permin, H., & Andersen, L. P. (2005). Delineation of Campylobacter concisus genomospecies by amplified fragment length polymorphism analysis and correlation of results with clinical data. *J Clin Microbiol*, *43*(10), 5091-5096.

Aabenhus, R., Permin, H., On, S. L., & Andersen, L. P. (2002). Prevalence of Campylobacter concisus in diarrhoea of immunocompromised patients. *Scand J Infect Dis*, *34*(4), 248-252.

Aabenhus, R., Stenram, U., Andersen, L. P., Permin, H., & Ljungh, A. (2008). First attempt to produce experimental Campylobacter concisus infection in mice. *World J Gastroenterol*, *14*(45), 6954-6959.

Al-Sadi, R., Khatib, K., Guo, S., Ye, D., Youssef, M., & Ma, T. (2011). Occludin regulates macromolecule flux across the intestinal epithelial tight junction barrier. *Am J Physiol Gastrointest Liver Physiol*, *300*(6), G1054-1064.

Al-Sadi, R. M., & Ma, T. Y. (2007). IL-1beta causes an increase in intestinal epithelial tight junction permeability. *J Immunol*, *178*(7), 4641-4649.

Alexandre, M. D., Jeansonne, B. G., Renegar, R. H., Tatum, R., & Chen, Y. H. (2007). The first extracellular domain of claudin-7 affects paracellular Cl- permeability. *Biochem Biophys Res Commun*, *357*(1), 87-91.

Alexandre, M. D., Lu, Q., & Chen, Y. H. (2005). Overexpression of claudin-7 decreases the paracellular Cl- conductance and increases the paracellular Na+ conductance in LLC-PK1 cells. *J Cell Sci*, *118*(Pt 12), 2683-2693.

Alutis, M. E., Grundmann, U., Fischer, A., Kuhl, A. A., Bereswill, S., & Heimesaat, M. M. (2014). Selective gelatinase inhibition reduces apoptosis and pro-inflammatory immune cell responses in Campylobacter jejuni-infected gnotobiotic IL-10 deficient mice. *Eur J Microbiol Immunol (Bp)*, *4*(4), 213-222.

Amasheh, S., Epple, H. J., Mankertz, J., Detjen, K., Goltz, M., Schulzke, J. D., & Fromm, M. (2000). Differential Regulation of ENaC by Aldosterone in Rat Early and Late Distal colon. *Ann N Y Acad Sci*, *915*, 92-4.

Amasheh, M., Fromm, A., Krug, S. M., Amasheh, S., Andres, S., Zeitz, M., Fromm, M., & Schulzke, J. D. (2010). TNFalpha-induced and berberine-antagonized tight junction barrier impairment via tyrosine kinase, Akt and NFkappaB signaling. *J Cell Sci*, *123*(Pt 23), 4145-4155.

Amasheh, M., Grotjohann, I., Amasheh, S., Fromm, A., Soderholm, J. D., Zeitz, M., Fromm, M., & Schulzke, J. D. (2009). Regulation of mucosal structure and barrier function in rat colon exposed to tumor necrosis factor alpha and interferon gamma in vitro: a novel model for studying the pathomechanisms of inflammatory bowel disease cytokines. *Scand J Gastroenterol*, *44*(10), 1226-1235.

Amasheh, S., Barmeyer, C., Koch, C. S., Tavalali, S., Mankertz, J., Epple, H. J., Gehring, M. M., Florian, P., Kroesen, A. J., Zeitz, M., Fromm, M., & Schulzke, J. D. (2004). Cytokine-dependent transcriptional down-regulation of epithelial sodium channel in ulcerative colitis. *Gastroenterology*, *126*(7), 1711-1720.

Amasheh, S., Meiri, N., Gitter, A. H., Schoneberg, T., Mankertz, J., Schulzke, J. D., & Fromm, M. (2002). Claudin-2 expression induces cation-selective channels in tight junctions of epithelial cells. *J Cell Sci*, *115*(Pt 24), 4969-4976.

Amasheh, S., Milatz, S., Krug, S. M., Bergs, M., Amasheh, M., Schulzke, J. D., & Fromm, M. (2009). Na+ absorption defends from paracellular back-leakage by claudin-8 upregulation. *Biochem Biophys Res Commun*, *378*(1), 45-50.

Angelow, S., Kim, K. J., & Yu, A. S. (2006). Claudin-8 modulates paracellular permeability to acidic and basic ions in MDCK II cells. *J Physiol*, *571*(Pt 1), 15-26.

Arango Duque, G., & Descoteaux, A. (2014). Macrophage cytokines: involvement in immunity and infectious diseases. *Front Immunol*, *5*, 491.

Bajnath, R. B., Dekker, K., Vaandrager, H. R., de Jonge, H. R., & Groot, J. A. (1992). Biphasic Increase of Apical Cl^- Conductance by Muscarinic Stimulation of HT-29cl.19A Human Colon Carcinoma Cell Line: Evidence for Activation of Different Cl^- Conductances by Carbachol and Forskolin. *J Mebrane Biol*, *127*(2), 81-94.

Balda, M. S., & Matter, K. (2009). Tight junctions and the regulation of gene expression. *Biochim Biophys Acta*, *1788*(4), 761-767.

Barmeyer, C., Amasheh, S., Tavalali, S., Mankertz, J., Zeitz, M., Fromm, M., & Schulzke, J. D. (2004). IL-1beta and TNFalpha regulate sodium absorption in rat distal colon. *Biochem Biophys Res Commun*, *317*(2), 500-507.

Barmeyer, C., Erko, I., Awad, K., Fromm, A., Bojarski, C., Meissner, S., Loddenkemper, C., Kerick, M., Siegmund, B., Fromm, M., Schweiger, M. R., & Schulzke, J. D. (2017). Epithelial barrier dysfunction in lymphocytic colitis through cytokine-dependent internalization of claudin-5 and -8. *J Gastroenterol*, *52*(10), 1090-1100.

Barmeyer, C., Erko, I., Fromm, A., Bojarski, C., Loddenkemper, C., Dames, P., Kerick, M., Siegmund, B., Fromm, M., Schweiger, M. R., & Schulzke, J. D. (2016). ENaC Dysregulation Through Activation of MEK1/2 Contributes to Impaired Na+ Absorption in Lymphocytic Colitis. *Inflamm Bowel Dis*, *22*(3), 539-547.

Barmeyer, C., Horak, I., Zeitz, M., Fromm, M., & Schulzke, J. D. (2002). The interleukin-2-deficient mouse model. *Pathobiology*, *70*(3), 139-142.

Benoit, S. L., Maier, R. J., Sawers, R. G., Greening, C. (2020). Molecular Hydrogen Metabolism: a Widespread Pathiogenic Bacteria and Protists. *Microbiol Mol Biol Rev*, *84*(1), e00091-19.

Benoit, S. L., & Maier, R. J. (2018). Site-directed mutagenesis of Campylobacter concisus respiratory genes provides insight into the pathogen's growth requirements. *Sci Rep*, *8*(1), 14203.

Benos, D. J., Awayda, M. S., Ismailov, I. I., & Johnson, J. P. (1995). Structure and Function of Amiloride-sensitive Na^+ Channels. *J Membrane Biol*, *143*, 1-18.

Benos, D. J. (1982). Amiloride: a molecular probe of sodium transport in tissues and cells. *Am J Physiol*, *142*, C131-C145.

Bereswill, S., Fischer, A., Plickert, R., Haag, L. M., Otto, B., Kuhl, A. A., Dasti, J. I., Zautner, A. E., Munoz, M., Loddenkemper, C., Gross, U., Gobel, U. B., & Heimesaat, M. M. (2011). Novel murine infection models provide deep insights into the "menage a trois" of Campylobacter jejuni, microbiota and host innate immunity. *PLoS ONE*, *6*(6), e20953.

Bereswill, S., Grundmann, U., Alutis, M. E., Fischer, A., Kuhl, A. A., & Heimesaat, M. M. (2017). Immune responses upon Campylobacter jejuni infection of secondary abiotic mice lacking nucleotide-oligomerization-domain-2. *Gut Pathog*, *9*, 33.

Bergann, T., Fromm, A., Borden, S. A., Fromm, M., & Schulzke, J. D. (2011). Glucocorticoid receptor is indispensable for physiological responses to aldosterone in epithelial Na+ channel induction via the mineralocorticoid receptor in a human colonic cell line. *Eur J Cell Biol*, *90*(5), 432-439.

Bergann, T., Ploger, S., Fromm, A., Zeissig, S., Borden, S. A., Fromm, M., & Schulzke, J. D. (2009a). A colonic mineralocorticoid receptor cell model expressing epithelial Na+ channels. *Biochem Biophys Res Commun*, *382*(2), 280-285.

Bergann, T., Zeissig, S., Fromm, A., Richter, J. F., Fromm, M., & Schulzke, J. D. (2009b). Glucocorticoids and tumor necrosis factor-alpha synergize to induce absorption by the epithelial sodium channel in the colon. *Gastroenterology*, *136*(3), 933-942.

Bookstein, C., DePaoli, A. M., Xie, Y., Niu, P., Musch, M. W., Rao, M. C., & Chang, E. B. (1994). Na^+/H^+ Exchangers, NHE-1 and NHE-3; Of Rat Interstine Expression and Localization. *J Clin Invest*, *93*(1), 106-13.

Bowcutt, R., Forman, R., Glymenaki, M., Carding, S. R., Else, K. J., & Cruickshank, S. M. (2014). Heterogeneity across the murine small and large intestine. *World J Gastroenterol*, *20*(41), 15216-15232.

Breuer, W., Kartner, N., Riordan, J. R., & Cabantchik, Z. I. (1992). Induction of expression of the cystic fibrosis transmembrane conductance regulator. *Journal of Biological Chemistry*, *267*(15), 10465-10469.

Brunner, K., John, C. M., Phillips, N. J., Alber, D. G., Gemmell, M. R., Hansen, R., Nielsen, H. L., Hold, G. L., Bajaj-Elliott, M., & Jarvis, G. A. (2018). Novel Campylobacter concisus lipooligosaccharide is a determinant of inflammatory potential and virulence. *J Lipid Res*, *59*(10), 1893-1905.

Bucker, R., Krug, S. M., Fromm, A., Nielsen, H. L., Fromm, M., Nielsen, H., & Schulzke, J. D. (2017). Campylobacter fetus impairs barrier function in HT-29/B6 cells through focal tight junction alterations and leaks. *Ann N Y Acad Sci*, *1405*(1), 189-201.

Bucker, R., Krug, S. M., Moos, V., Bojarski, C., Schweiger, M. R., Kerick, M., Fromm, A., Janssen, S., Fromm, M., Hering, N. A., Siegmund, B., Schneider, T., Barmeyer, C., & Schulzke, J. D. (2018). Campylobacter jejuni impairs sodium transport and epithelial barrier function via cytokine release in human colon. *Mucosal Immunol*, *11*(2), 474-485.

Bultman, S. J. (2014). Molecular pathways: gene-environment interactions regulating dietary fiber induction of proliferation and apoptosis via butyrate for cancer prevention. *Clin Cancer Res*, *20*(4), 799-803.

Buschmann, M. M., Shen, L., Rajapakse, H., Raleigh, D. R., Wang, Y., Wang, Y., Lingaraju, A., Zha, J., Abbott, E., McAuley, E. M., Breskin, L. A., Wu, L., Anderson, K., Turner, J. R., & Weber, C. R. (2013). Occludin OCEL-domain interactions are required for maintenance and regulation of the tight junction barrier to macromolecular flux. *Mol Biol Cell*, *24*(19), 3056-3068.

Butkevych, E., Lobo de Sa, F. D., Nattramilarasu, P. K., & Bucker, R. (2020). Contribution of Epithelial Apoptosis and Subepithelial Immune Responses in Campylobacter jejuni-Induced Barrier Disruption. *Front Microbiol*, *11*, 344.

Butler, P. L., Staruschenko, A., & Snyder, P. M. (2015). Acetylation stimulates the epithelial sodium channel by reducing its ubiquitination and degradation. *J Biol Chem*, *290*(20), 12497-12503.

Canessa, C. M., Schild, L., Buell, G., Thorens, B., Gautschi, I., Horisberger, J. D., & Rossier, B. C. (1994). Amiloride-sensitive epithelial Na^+ channel is made of three homologous subunits. *Nature*, *367*(6462), 463-7.

Castano-Rodriguez, N., Kaakoush, N. O., Lee, W. S., & Mitchell, H. M. (2017). Dual role of Helicobacter and Campylobacter species in IBD: a systematic review and meta-analysis. *Gut*, *66*(2), 235-249.

Chantret, I., Barbat, A., Dussaulux, E., Brattaijn, M. G., & Zwibaum, A. (1988). Epithelial Polarity, Villin Expression, and Enterocytic Differentiation of Cultured Human Colon Carcinoma Cells: A Survey of Twenty Cell Lines. *Cancer Res*, *48*(7), 1936-42.

Chiba, H., Osanai, M., Murata, M., Kojima, T., & Sawada, N. (2008). Transmembrane proteins of tight junctions. *Biochim Biophys Acta*, *1778*(3), 588-600.

Cooke, H. J. (1988). "Enteric Tears": Chloride Secretion and its Neural Regulation. *News Physiol Sci*, *13*, 269-274.

Cui, J., Cui, H., Yang, M., Du, S., Li, J., Li, Y., Liu, L., Zhang, X., & Li, S. (2019). Tongue coating microbiome as a potential biomarker for gastritis including precancerous cascade. *Protein Cell*, *10*(7), 496-509.

Dames, P., Bergann, T., Fromm, A., Bucker, R., Barmeyer, C., Krug, S. M., Fromm, M., & Schulzke, J. D. (2015). Interleukin-13 affects the epithelial sodium channel in the intestine by coordinated modulation of STAT6 and p38 MAPK activity. *J Physiol*, *593*(24), 5269-5282.

Debongnie, J. C., & Phillips, S. F. (1978). Capacity of the human colon to absorb fluid. *Gastroenterology*, *74*(4), 698-703.

Deshpande, N. P., Wilkins, M. R., Castaño-Rodríguez, N., Bainbridge, E., Sodhi, N., Riordan, S. M., Mitchell, H. M., & Kaakoush, N. O. (2016). Campylobacter concisus pathotypes induce distinct global responses in intestinal epithelial cells. *Scientific Reports*, *6*(1).

Dobin, A., Davis, C. A., Schlesinger, F., Drenkow, J., Zaleski, C., Jha, S., Batut, P., Chaisson, M., & Gingeras, T. R. (2013). STAR: ultrafast universal RNA-seq aligner. *Bioinformatics*, *29*(1), 15-21.

Dong, Y., Yang, Y., Liu, J., Awan, F., Lu, C., & Liu, Y. (2018). Inhibition of Aeromonas hydrophila-induced intestinal inflammation and mucosal barrier function damage in crucian carp by oral administration of Lactococcus lactis. *Fish Shellfish Immunol*, *83*, 359-367.

Dudeja, P. K., Rao, D. D., Syed, I., Joshi, V., Dahdal, R. Y., Gardner, C., Risk, M. C., Schmidt, L., Bavishi, D., Kim, K. E., Harig, M., Goldstein, J. L.; Layden, T. J., & Ramswamy, K. (1996). Intestinal distribution of human Na^+/H^+ exchanger isoforms NHE-1, NHE-2, and NHE-3 mRNA. *Am J Physiol*, *271*(3 Pt 1), G483-93.

Eaton, A. F., Yue, Q., Eaton, D. C., & Bao, H. F. (2014). ENaC activity and expression is decreased in the lungs of protein kinase C-alpha knockout mice. *Am J Physiol Lung Cell Mol Physiol*, *307*(5), L374-385.

Ekmekcioglu, C., Pomazal, K., Steffan, I., Schweiger, B., Marktl, W. (1999). Calcium transport across mineral waters across caco-2 cells. *J Agri Food Chem*, *47*(7), 2594-9.

Engberg, J., Bang, D. D., Aabenhus, R., Aarestrup, F. M., Fussing, V., & Gerner-Smidt, P. (2005). Campylobacter concisus: an evaluation of certain phenotypic and genotypic characteristics. *Clin Microbiol Infect*, *11*(4), 288-295.

Enns, C. B., Keith, B. A., Challa, N., Harding, J. C. S., & Loewen, M. E. (2020). Impairment of electroneutral Na(+) transport and associated downregulation of NHE3 contributes to the development of diarrhea following in vivo challenge with Brachyspira spp. *Am J Physiol Gastrointest Liver Physiol*, *318*(2), G288-G297.

Epple, H. J., Amasheh, S., Mankertz, J., Goltz, M., Schulzke, J. D., & Fromm, M. (2000). Early aldosterone effect in distal colon by transcriptional regulation of ENaC subunits. *Am J Physiol Gastrointest Liver Physiol*, *278*(5), G718-24.

Epple, H. J., Friebel, J., Moos, V., Troeger, H., Krug, S. M., Allers, K., Schinnerling, K., Fromm, A., Siegmund, B., Fromm, M., Schulzke, J. D., & Schneider, T. (2017). Architectural and functional alterations of the small intestinal mucosa in classical Whipple's disease. *Mucosal Immunol*, *10*(6), 1542-1552.

Epple, H. J., Mankertz, J., Ignatius, R., Liesenfeld, O., Fromm, M., Zeitz, M., Chakraborty, T., & Schulzke, J. D. (2004). Aeromonas hydrophila beta-hemolysin induces active chloride secretion in colon epithelial cells (HT-29/B6). *Infect Immun*, *72*(8), 4848-4858.

Falsen, E., Nehle, L., & Borjesson, A. (1987). Immunotyping campylobacters. *Taxonomic implications*, 56-59. IN b: Kaijser and E. Falsen (ed.), Campylobacter IV. University of Goteberg, Goteberg, Sweden.

Fan, J., Tatum, R., Hoggard, J., & Chen, Y. H. (2019). Claudin-7 Modulates Cl(-) and Na(+) Homeostasis and WNK4 Expression in Renal Collecting Duct Cells. *Int J Mol Sci*, *20*(15).

Farquhar, M. G., & Palde, G. E. (1963). Junctional complexes in various epithelia. *J Cell Biol*, *17*(2), 375-412.

Fasano, A., Baudry, B., Pumplin, D. W., Wasserman, S. S., Tall, B. D., Ketley, J. M., & Kaper, J. B. (1991). Vibrio cholerae produces a second enterotoxin, which affects intestinal tight junctions. *Proc Natl Acad Sci U S A*, *88*(12), 5242-6.

Field, L. H.; Underwood, J. L., Pope, L. M., & Berry, L. J. (1981). Intestinal colonization of neonatal animals by Campylobacter fetus subsp. jejuni. *Infect Immun, 33*(3), 884-92.

Field, M. (2003). Intestinal ion transport and the pathophysiology of diarrhea. *Journal of Clinical Investigation, 111*(7), 931-943.

Firsov, D., Gautschi, I., Merillatr, A. M., Rossier, B. C., & Schild, L. (1998). The heterotrimeric architecture of the epithelial sodium channel (ENaC). *EMBO J, 17*(2), 344-52.

Fossat, B., & Lahlou, B. (1982). Ion flux changes induced by voltage clamping or by amphotericin B in the isolated urinary bladder of the trout. *J Physiol, 325*, 111-23.

Fotia, A. B., Dinudom, A., Shearwin, K. E., Koch J-P., Korbmacher, C., Cook D. I., & Kumar, S. (2003). The role of individual Nedd4-2 (KIAA0439) WW domains in binding and regulating epithelial sodium channels. *FASEB J, 17*(1), 70-2.

Fox, G .J., Gorelick, P. L., Kullberg, M. C., Ge, Z., Dewhirst; F. E., & Ward, M. (1999). A Novel Urease-Negative *Helicobacter* Species Associates with Colitis and Typhlitis in IL-10-Deficient Mice. *Infect Immun, 67*(4), 1757-62.

Fromm, M., Schulzke, J. D.., & Hegel, U. (1985). Epithelial and subepithelial contributions to transmural electrical resistance of intact rat jejunum, in vitro. *Pflugers Arch, 405*(4), 400-2.

Fromm, M., Schulzke, J. D., & Hegel, U. (1993). Control of electrogenic Na^+ absorption in rat late distal colon by nanomolar aldosterone added in vitro. *Am J Physiol, 264*(1 Pt 1), E68-73.

Fujita, H., Sugimoto, K., Inatomi, S., Maeda, T., Osanai, M., Uchiyama, Y., Yamamoto, Y., Wada, T., Kojima, T., Yokozaki, H., Yamashita, T., Kato, S., Sawada, N., & Chiba, H. (2008). Tight junction proteins claudin-2 and -12 are critical for vitamin D-dependent Ca2+ absorption between enterocytes. *Mol Biol Cell, 19*(5), 1912-1921.

Fukumatsu, M., Ogawa, M., Arakawa, S., Suzuki, M., Nakayama, K., Shimizu, S., Kim, M., Mimuro, H., & Sasakawa, C. (2012). Shigella Targets Epithelial Tricellular Junctions and Uses a Noncanonical Clathrin-Dependent Endocytic Pathway to Spread Between Cells. *Cell Host & Microbe*, *11*(4), 325-336.

F**uller, P. J., Brennan, F. E., & Burgess, J. S. (2000).** Acute differential regulation by corticosteroids of epithelial sodium channel subunit and Nedd4 mRNA levels in the distal colon. *Pflugers Arch*, *441*(1), 94-101.

Furuse, M., Hirase, T., Itoh, M., Nagafuchi, A., Yonemura, S., Tsukita, S., & Tsukita, S. (1993). Occludin: a novel intergral membrane protein localizing at tight junctions. *J Cell Biol*, *123*(6 Pt 2), 1777-88.

Furuse, M., Fujita, K., Hiiragi, T., Fujimoto, K., & Tsukita, S. (1998). Claudin-1 and -2: novel integral membrane proteins localizing at tight junctions with no sequence similarity to occludin. *J Cell Biol*, *141*(7), 1539-50.

Galkin, V. E., Yu, X., Bielnicki, J., Heuser, J., Ewing, C. P., Guerry, & Egelman, H. (2008). Divergence of quaternary structures among bacterial falgellar filaments. *Science*, *320*(5874), 382-5.

Gemmell, M. R., Berry, S., Mukhopadhya, I., Hansen, R., Nielsen, H. L., Bajaj-Elliott, M., Nielsen, H., & Hold, G. L. (2018). Comparative genomics of Campylobacter concisus: Analysis of clinical strains reveals genome diversity and pathogenic potential. *Emerg Microbes Infect*, *7*(1), 116.

Gitter, A. H., Bendfeldt, K., Sculzke, J. D., & Fromm, M. (2000). Leaks in the epithelial barrer caused by spontaneous and TNF-α-induced single-cell apoptosis. *FASEB J*, *14*(12), 1749-53.

Gonzalez-Mariscal, L., Tapia, R., & Chamorro, D. (2008). Crosstalk of tight junction components with signaling pathways. *Biochim Biophys Acta*, *1778*(3), 729-756.

Grotjohann, I., Schulzke, J. D., & Fromm, M. (1999). Electrogenic Na^+ transport in rat late distal colon by natural and synthetic glucocorticosteroids. *Am J Physiol*, *276*(2), G491-8.

Gunzel, D. (2017). Claudins: vital partners in transcellular and paracellular transport coupling. *Pflugers Arch*, *469*(1), 35-44.

Gunzel, D., & Fromm, M. (2012). Claudins and other tight junction proteins. *Compr Physiol*, *2*(3), 1819-1852.

Gunzel, D., Stuiver, M., Kausalya, P. J., Haisch, L., Krug, S. M., Rosenthal, R., Meij, I. C., Hunziker, W., Fromm, M., & Muller, D. (2009). Claudin-10 exists in six alternatively spliced isoforms that exhibit distinct localization and function. *J Cell Sci*, *122*(Pt 10), 1507-1517.

Gunzel, D., & Yu, A. S. (2013). Claudins and the modulation of tight junction permeability. *Physiol Rev*, *93*(2), 525-569.

Guo, S., Gillingham, T., Guo, Y., Meng, D., Zhu, W., Walker, W. A., & Ganguli, K. (2017). Secretions of Bifidobacterium infantis and Lactobacillus acidophilus Protect Intestinal Epithelial Barrier Function. *J Pediatr Gastroenterol Nutr*, *64*(3), 404-412.

Guo, X., Stroup, S. E., & Houpt, E. R. (2008). Persistence of Entamoeba histolytica infection in CBA mice owes to intestinal IL-4 production and inhibition of protective IFN-gamma. *Mucosal Immunol*, *1*(2), 139-146.

Gurney, M. A., Laubitz, D., Ghishan, F. K., & Kiela, P. R. (2017). Pathophysiology of Intestinal Na(+)/H(+) exchange. *Cell Mol Gastroenterol Hepatol*, *3*(1), 27-40.

Haag, L. M., Fischer, A., Otto, B., Plickert, R., Kuhl, A. A., Gobel, U. B., Bereswill, S., & Heimesaat, M. M. (2012). Campylobacter jejuni induces acute enterocolitis in gnotobiotic IL-10-/- mice via Toll-like-receptor-2 and -4 signaling. *PLoS ONE*, *7*(7), e40761.

Hagemann, J. B., Haverkamp, S., Gruner, B., Kuchenbauer, F., & Essig, A. (2018). Pulmonary Campylobacter concisus infection in an immunocompromised patient with underlying mucormycosis. *Int J Infect Dis*, *76*, 45-47.

Harvey, K. F., Dinudom, A., Cook, D. I., & Kumar, S. (2001). The Nedd4-like protein KIAA0439 is a potential regulator of the epithelial sodium channel. *J Biol Chem*, *276*(11), 8597-8601.

Heimesaat, M. M., Bereswill, S., Fischer, A., Fuchs, D., Struck, D., Niebergall, J., Jahn, H. K., Dunay, I. R., Moter, A., Gescher, D. M., Schumann, R. R., Gobel, U. B., & Liesenfeld, O. (2006). Gram-negative bacteria aggravate murine small intestinal Th1-type immunopathology following oral infection with Toxoplasma gondii. *J Immunol*, *177*(12), 8785-8795.

Heimesaat, M. M., Genger, C., Klove, S., Weschka, D., Mousavi, S., & Bereswill, S. (2020). The Host-Specific Intestinal Microbiota Composition Impacts Campylobacter coli Infection in a Clinical Mouse Model of Campylobacteriosis. *Pathogens*, *9*(10).

Heimesaat, M. M., Grundmann, U., Alutis, M. E., Fischer, A., & Bereswill, S. (2017). Microbiota Composition and Immune Responses During Campylobacter Jejuni Infection in Conventionally Colonized IL-10(-/-) Mice Lacking Nucleotide Oligomerization Domain 2. *Eur J Microbiol Immunol (Bp)*, *7*(1), 1-14.

Heller, F., Fromm, A., Gitter, A. H., Mankertz, J., & Schulzke, J. D. (2008). Epithelial apoptosis is a prominent feature of the epithelial barrier disturbance in intestinal inflammation: effect of pro-inflammatory interleukin-13 on epithelial cell function. *Mucosal Immunol*, *1 Suppl 1*, S58-61.

Hering, N. A., Fromm, A., Kikhney, J., Lee, I. F., Moter, A., Schulzke, J. D., & Bucker, R. (2016). Yersinia enterocolitica Affects Intestinal Barrier Function in the Colon. *J Infect Dis*, *213*(7), 1157-1162.

Hering, N. A., Richter, J. F., Krug, S. M., Gunzel, D., Fromm, A., Bohn, E., Rosenthal, R., Bucker, R., Fromm, M., Troeger, H., & Schulzke, J. D. (2011). Yersinia enterocolitica induces epithelial barrier dysfunction through regional tight junction changes in colonic HT-29/B6 cell monolayers. *Lab Invest*, *91*(2), 310-324.

Hernandez-Chirlaque, C., Aranda, C. J., Ocon, B., Capitan-Canadas, F., Ortega-Gonzalez, M., Carrero, J. J., Suarez, M. D., Zarzuelo, A., Sanchez de Medina, F., & Martinez-Augustin, O. (2016). Germ-free and Antibiotic-treated Mice are Highly Susceptible to Epithelial Injury in DSS Colitis. *J Crohns Colitis*, *10*(11), 1324-1335.

Hickey, T. E., Majam, G., & Guerry, P. (2005). Intracellular survival of Campylobacter jejuni in human monocytic cells and induction of apoptotic death by cytholethal distending toxin. *Infect Immun*, *73*(8), 5194-5197.

Higashi, T., Tokuda, S., Kitajiri, S., Masuda, S., Nakamura, H., Oda, Y., & Furuse, M. (2013). Analysis of the 'angulin' proteins LSR, ILDR1 and ILDR2--tricellulin recruitment, epithelial barrier function and implication in deafness pathogenesis. *J Cell Sci*, *126*(Pt 4), 966-977.

Höglund, P., Halia, S., Socha, J., Tomaszewski, L., Saarialho-Kere, U., Karjalainen-Linsberg, M. L., Airlo, K., Holmberg, C., de la Chapelle, A., & Kere, J. (1996). Mutations of the Down-regulated in adenoma (DRA) gene cause congenital chloride diarrhea. *Nat Genet*, *14*(3), 316-9.

Huet, C., Sahuquillo-Merino, C., Coudrier, E., & Louvard, D. (1987). Absorptive and mucus-secreting subclones isolated from a multipotent intestinal cell line (HT-29) provide new models for cell polarity and terminal differentiation. *J Cell Biol*, *105*(1), 345-57.

Ikenouchi, J., Furuse, M., Furuse, K., Sasaki, H., Tsukita, S., & Tsukita, S. (2005). Tricellulin constitutes a novel barrier at tricellular contacts of epithelial cells. *J Cell Biol*, *171*(6), 939-945.

Ikenouchi, J., Sasaki, H., Tsukita, S., Furuse, M., & Tsukita, S. (2008). Loss of occludin affects tricellular localization of tricellulin. *Mol Biol Cell*, *19*(11), 4687-4693.

Ishiyama, M., Miyazono, Y., Sasamoto, K., Ohkura, Y., & Ueno K. (1997). A highly water-soluble disulfonated tetrazolium salt as a chromogenic indicator for NADH as well as cell viability. *Talanta*, *44*(7), 1299-305.

Ismail, Y., Lee, H., Riordan, S. M., Grimm, M. C., & Zhang, L. (2013). The effects of oral and enteric Campylobacter concisus strains on expression of TLR4, MD-2, TLR2, TLR5 and COX-2 in HT-29 cells. *PLoS ONE*, *8*(2), e56888.

Ismail, Y., Mahendran, V., Octavia, S., Day, A. S., Riordan, S. M., Grimm, M. C., Lan, R., Lemberg, D., Tran, T. A., & Zhang, L. (2012). Investigation of the enteric pathogenic potential of oral Campylobacter concisus strains isolated from patients with inflammatory bowel disease. *PLoS ONE*, *7*(5), e38217.

Istivan, T. S., Coloe, P. J., Fry, B. N., Ward, P., & Smith, S. C. (2004). Characterization of a haemolytic phospholipase A(2) activity in clinical isolates of Campylobacter concisus. *J Med Microbiol*, *53*(Pt 6), 483-493.

Istivan, T. S., Smith, S. C., Fry, B. N., & Coloe, P. J. (2008). Characterization of Campylobacter concisus hemolysins. *FEMS Immunol Med Microbiol*, *54*(2), 224-235.

Itoh, M., Furuse, M., Morita, K., Kubota, K., Saitou, M., & Tsukita, S. (1999). Direct binding of three tight junction-associated MAGUKs, ZO-1, ZO-2, and ZO-3, with the COOH termini of claudins. *J Cell Biol*, *147*(6), 1351-63.

Jain, D., Prasad, K. N., Sinha, S., & Vishwakarma, A. L. (2009). Cell cycle arrest & apoptosis of epithelial cell line by cytolethal distending toxin positive Campylobacter jejuni. *Indian J Med Res*, *129*(4), 418-23.

Janeway Jr, C. A. (2001). How the immune system protects the host from infection. *Microbes Infect*, *3*(13), 1167-71.

Johnson, C. C., & Finegold, S. M. (1987). Uncommonly encountered, motile, anearobic gram-negative bacilli associated with infection. *Rev Infect Dis, 9*(6), 1150-62.

Jones, M. A., Totemeyer, S., Maskell, D. J., Bryant, C. E., & Barrow, P. A. (2003). Induction of proinflammatory responses in the human monocytic cell line THP-1 by Campylobacter jejuni. *Infect Immun, 71*(5), 2626-2633.

Kaakoush, N. O., Castano-Rodriguez, N., Day, A. S., Lemberg, D. A., Leach, S. T., & Mitchell, H. M. (2014b). Campylobacter concisus and exotoxin 9 levels in paediatric patients with Crohn's disease and their association with the intestinal microbiota. *J Med Microbiol, 63*(Pt 1), 99-105.

Kaakoush, N. O., Deshpande, N. P., Man, S. M., Burgos-Portugal, J. A., Khattak, F. A., Raftery, M. J., Wilkins, M. R., & Mitchell, H. M. (2015). Transcriptomic and proteomic analyses reveal key innate immune signatures in the host response to the gastrointestinal pathogen Campylobacter concisus. *Infect Immun, 83*(2), 832-845.

Kaakoush, N. O., Deshpande, N. P., Wilkins, M. R., Tan, C. G., Burgos-Portugal, J. A., Raftery, M. J., Day, A. S., Lemberg, D. A., & Mitchell, H. (2011). The pathogenic potential of Campylobacter concisus strains associated with chronic intestinal diseases. *PLoS ONE, 6*(12), e29045.

Kaakoush, N. O., Man, S. M., Lamb, S., Raftery, M. J., Wilkins, M. R., Kovach, Z., & Mitchell, H. (2010). The secretome of Campylobacter concisus. *FEBS J, 277*(7), 1606-1617.

Kaakoush, N. O., & Mitchell, H. M. (2012). Campylobacter concisus - A new player in intestinal disease. *Front Cell Infect Microbiol, 2*, 4.

Kaakoush, N. O., Mitchell, H. M., & Man, S. M. (2014a). Role of emerging Campylobacter species in inflammatory bowel diseases. *Inflamm Bowel Dis, 20*(11), 2189-2197.

Kalischuk, L. D., & Inglis, G. D. (2011). Comparative genotypic and pathogenic examination of Campylobacter concisus isolates from diarrheic and non-diarrheic humans. *BMC Microbiol*, *11*, 53.

Kanwar, R. K., Ganguly, N. K., Kanwar, J. R., Kumar, L., & Walia, B. N. (1994). Impairment of Na^+,K^+-ATPase activity following enterotoxigenuc Campylobacer jejuni infection: changes in Na^+, Cl^- and 3-O-methyl-D-glucose transport in vitro, in rat ileum. *FEMS Microbiol Lett*, *124*(3), 381-5.

Kayisoglu, O., Weiss, F., Niklas, C., Pierotti, I., Pompaiah, M., Wallaschek, N., Germer, C. T., Wiegering, A., & Bartfeld, S. (2021). Location-specific cell identity rather than exposure to GI microbiota defines many innate immune signalling cascades in the gut epithelium. *Gut*, *70*(4), 687-697.

Keita, A. V., Lindqvist, C. M., Ost, A., Magana, C. D. L., Schoultz, I., & Halfvarson, J. (2018). Gut Barrier Dysfunction-A Primary Defect in Twins with Crohn's Disease Predominantly Caused by Genetic Predisposition. *J Crohns Colitis*, *12*(10), 1200-1209.

Kieber-Emmons, T., Lin, C., Foster, M. H., & Kleyman, T. R. (1999). Antiidiotypic antibody recognizes an amiloride binding domain within the alpha subunit of the epithelial Na^+ channel. *J Biol Chem*, *274*(14), 9648-55.

Kim, K. Y., Oh, T. W., Do, H. J., Yang, J. H., Yang, I. J., Jeon, Y. H., Go, Y. H., Ahn, S. C., Ma, J. Y., & Park, K. I. (2018). Acer palmatum thumb. Ethanol Extract Alleviates Interleukin-6-Induced Barrier Dysfunction and Dextran Sodium Sulfate-Induced Colitis by Improving Intestinal Barrier Function and Reducing Inflammation. *J Immunol Res*, *2018*, 5718396.

Kim, Y. G., Lee, C. K., Kim, S. H., Cho, W. S., Mun, S. H., & Yoo, B. (2010). Interleukin-32gamma enhances the production of IL-6 and IL-8 in fibroblast-like synoviocytes via Erk1/2 activation. *J Clin Immunol*, *30*(2), 260-267.

Kirk, K. F., Meric, G., Nielsen, H. L., Pascoe, B., Sheppard, S. K., Thorlacius-Ussing, O., & Nielsen, H. (2018). Molecular epidemiology and comparative genomics of Campylobacter concisus strains from saliva, faeces and gut mucosal biopsies in inflammatory bowel disease. *Sci Rep*, *8*(1), 1902.

Kosari, F., Sheng, S., Li, J., Mak, D. O., Foskett, J. K., & Kleyman, T. R. (1998). Subunit stoichiometry of the epithelial sodium channel. *J Biol Chem*, *273*(22), 13469-13474.

Kovach, Z., Kaakoush, N. O., Lamb, S., Zhang, L., Raftery, M. J., & Mitchell, H. (2011). Immunoreactive proteins of Campylobacter concisus, an emergent intestinal pathogen. *FEMS Immunol Med Microbiol*, *63*(3), 387-396.

Krause, G., Winkler, L., Mueller, S. L., Haseloff, R. F., Piontek, J., & Blasig, I. E. (2008). Structure and function of claudins. *Biochim Biophys Acta*, *1778*(3), 631-645.

Krause, P., Morris, V., Greenbaum, J. A., Park, Y., Bjoerheden, U., Mikulski, Z., Muffley, T., Shui, J. W., Kim, G., Cheroutre, H., Liu, Y. C., Peters, B., Kronenberg, M., & Murai, M. (2015). IL-10-producing intestinal macrophages prevent excessive antibacterial innate immunity by limiting IL-23 synthesis. *Nat Commun*, *6*, 7055.

Kreusel, K. M., Fromm, M., Schulzkle, J. D., & Hegel, U. (1991). Cl^- secretion in epithelial monolayers of mucus-forming human colon cells (HT-29/B6). *Am J Physiol*, *261*(4 Pt 1), C574-82.

Krug, S. M., Amasheh, S., Richter, J. F., Milatz, S., Gunzel, D., Westphal, J. K., Huber, O., Schulzke, J. D., & Fromm, M. (2009). Tricellulin forms a barrier to macromolecules in tricellular tight junctions without affecting ion permeability. *Mol Biol Cell*, *20*(16), 3713-3724.

Krug, S. M., Bojarski, C., Fromm, A., Lee, I. M., Dames, P., Richter, J. F., Turner, J. R., Fromm, M., & Schulzke, J. D. (2018). Tricellulin is regulated via interleukin-13-receptor alpha2, affects macromolecule uptake, and is decreased in ulcerative colitis. *Mucosal Immunol*, *11*(2), 345-356.

Krug, S. M., Gunzel, D., Conrad, M. P., Lee, I. F., Amasheh, S., Fromm, M., & Yu, A. S. (2012). Charge-selective claudin channels. *Ann N Y Acad Sci*, *1257*, 20-28.

Kunzelmann, K., Scheidt, K., Scharf, B., Ousingsawat, J., Schreiber, R., Wainwright, B., & McMorran, B. (2006). Flagellin of Pseudomonas aeruginosa inhibits Na^+ transport in airway epithelia. *FASEB J*, *20*(3), 545-6.

Laverncic, P., Kaakoush, N. O., Huinao, K. D., Kain, N., & Mitchell, H. M. (2012). Investigation of motility and biofilm formation by intestinal *Campylobacter concisus* strains. *Gut Pathog*, *4*(1), 22.

Lee, H., Ma, R., Grimm, M. C., Riordan, S. M., Lan, R., Zhong, L., Raftery, M., & Zhang, L. (2014). Examination of the Anaerobic Growth of Campylobacter concisus Strains. *Int J Microbiol*, *2014*, 476047.

Levitan, R., Fordtran, J. S., Burrows, B. A., & Ingelfinger, F. J. (1962). Water and salt absorption in the human colon. *J Clin Invest*, *41*, 1754-1759.

Li, W. Y., Heuy, C. L., & Yu, A. S. (2004). Expression of claudin-7 and -8 along the mouse nephron. *Am J Physiol Renal Physiol*, *286*(6), F1063-71.

Liao, Y., Smyth, G. K., & Shi, W. (2019). The R package Rsubread is easier, faster, cheaper and better for alignment and quantification of RNA sequencing reads. *Nucleic Acids Res*, *47*(8), e47.

Lindblom, G. B., Sjogren, E., Hansson-Westerberg, J., & Kaijser, B. (1995). Campylobacter upsaliensis, C. sputorum sputorum and C. concisus as common causes of diarrhoea in Swedish children. *Scand J Infect Dis*, *27*(2), 187-188.

Linley, J., Loganathan, A., Kopanati, S., Sandle, G. I., & Hunter, M. (2014). Evidence that two distinct crypt cell types secrete chloride and potassium in human colon. *Gut*, *63*(3), 472-479.

Lissner, D., Schumann, M., Batra, A., Kredel, L. I., Kuhl, A. A., Erben, U., May, C., Schulzke, J. D., & Siegmund, B. (2015). Monocyte and M1 Macrophage-induced Barrier Defect Contributes to Chronic Intestinal Inflammation in IBD. *Inflamm Bowel Dis*, *21*(6), 1297-1305.

Liu, F., Chen, S., Luu, L. D. W., Lee, S. A., Tay, A. C. Y., Wu, R., Riordan, S. M., Lan, R., Liu, L., & Zhang, L. (2020). Analysis of complete Campylobacter concisus genomes identifies genomospecies features, secretion systems and novel plasmids and their association with severe ulcerative colitis. *Microb Genom*, *6*(11).

Liu, F., Ma, R., Tay, C. Y. A., Octavia, S., Lan, R., Chung, H. K. L., Riordan, S. M., Grimm, M. C., Leong, R. W., Tanaka, M. M., Connor, S., & Zhang, L. (2018). Genomic analysis of oral Campylobacter concisus strains identified a potential bacterial molecular marker associated with active Crohn's disease. *Emerg Microbes Infect*, *7*(1), 64.

Livak, K. J., & Schmittgen, T. D. (2001). Analysis of relative gene expression data using real-time quantitative PCR and the 2(-Delta Delta C(T)) Method. *Methods*, *25*(4), 402-408.

Lobo de Sá, F. D., Schulzke, J. D., & Bücker, R. (2021a). Diarrheal Mechanisms and the Role of Intestinal Barrier Dysfunction in Campyloabcter Infections. *Curr Top Microbiol Immunol*, *431*, 203-231.

Lobo de Sa, F. D., Butkevych, E., Nattramilarasu, P. K., Fromm, A., Mousavi, S., Moos, V., Golz, J. C., Stingl, K., Kittler, S., Seinige, D., Kehrenberg, C., Heimesaat, M. M., Bereswill, S., Schulzke, J. D., & Bucker, R. (2019). Curcumin Mitigates Immune-Induced Epithelial Barrier Dysfunction by Campylobacter jejuni. *Int J Mol Sci*, *20*(19).

Lobo de Sa, F. D., Heimesaat, M. M., Bereswill, S., Nattramilarasu, P. K., Schulzke, J. D., & Bucker, R. (2021b). Resveratrol Prevents Campylobacter jejuni-Induced Leaky gut by Restoring Occludin and Claudin-5 in the Paracellular Leak Pathway. *Front Pharmacol*, *12*, 640572.

Love, M. I., Huber, W., & Anders, S. (2014). Moderated estimation of fold change and dispersion for RNA-seq data with DESeq2. *Genome Biol*, *15*(12), 550.

Luettig, J., Rosenthal, R., Barmeyer, C., & Schulzke, J. D. (2015). Claudin-2 as a mediator of leaky gut barrier during intestinal inflammation. *Tissue Barriers*, *3*(1-2), e977176.

MacCallum, A., Hardy, S. P., & Everest, P. H. (2005). Campylobacter jejuni inhibits the absorptive transport functions of Caco-2 cells and disrupts cellular tight junctions. *Microbiology (Reading)*, *151*(Pt 7), 2451-2458.

Mahendran, V., Liu, F., Riordan, S. M., Grimm, M. C., Tanaka, M. M., & Zhang, L. (2016). Examination of the effects of Campylobacter concisus zonula occludens toxin on intestinal epithelial cells and macrophages. *Gut Pathogens*, *8*(1).

Mahendran, V., Riordan, S. M., Grimm, M. C., Tran, T. A., Major, J., Kaakoush, N. O., Mitchell, H., & Zhang, L. (2011). Prevalence of Campylobacter species in adult Crohn's disease and the preferential colonization sites of Campylobacter species in the human intestine. *PLoS ONE*, *6*(9), e25417.

Mahendran, V., Tan, Y. S., Riordan, S. M., Grimm, M. C., Day, A. S., Lemberg, D. A., Octavia, S., Lan, R., & Zhang, L. (2013). The prevalence and polymorphisms of zonula occluden toxin gene in multiple Campylobacter concisus strains isolated from saliva of patients with inflammatory bowel disease and controls. *PLoS ONE*, *8*(9), e75525.

Maher, M., Finnegan, C., Collins, E., Ward, B., Carroll, C., & Cormican, M. (2003). Evaluation of culture methods and a DNA probe-based PCR assay for detection of Campylobacter species in clinical specimens of feces. *J Clin Microbiol*, *41*(7), 2980-2986.

Man, S. M., Kaakoush, N. O., Leach, S. T., Nahidi, L., Lu, H. K., Norman, J., Day, A. S., Zhang, L., & Mitchell, H. M. (2010a). Host attachment, invasion, and stimulation of proinflammatory cytokines by Campylobacter concisus and other non-Campylobacter jejuni Campylobacter species. *J Infect Dis*, *202*(12), 1855-1865.

Man, S. M., Zhang, L., Day, A. S., Leach, S. T., Lemberg, D. A., & Mitchell, H. (2010b). Campylobacter concisus and other Campylobacter species in children with newly diagnosed Crohn's disease. *Inflamm Bowel Dis*, *16*(6), 1008-1016.

Mandel, L. J., Bacallao, R., & Zampighi, G. (1993). Uncoupling of the molecular 'fence' and paracellualr 'gate' functions in epithelial tight junctions. *Nature*, *361*(6412), 552-5.

Mankertz, J., Amasheh, M., Krug, S. M., Fromm, A., Amasheh, S., Hillenbrand, B., Tavalali, S., Fromm, M., & Schulzke, J. D. (2009). TNFalpha up-regulates claudin-2 expression in epithelial HT-29/B6 cells via phosphatidylinositol-3-kinase signaling. *Cell Tissue Res*, *336*(1), 67-77.

Mansfield, L. S., Bell, J. A., Wilson, D. L., Murphy, A. J., Elsheikha, H. M., Rathinam, V. A., Fierro, B. R., Linz, J. E., & Young, V. B. (2007). C57BL/6 and congenic interleukin-10-deficient mice can serve as models of Campylobacter jejuni colonization and enteritis. *Infect Immun*, *75*(3), 1099-1115.

Marchelletta, R. R., Gareau, M. G., McCole, D. F., Okamoto, S., Roel, E., Klinkenberg, R., Guiney, D. G., Fierer, J., & Barrett, K. E. (2013). Altered expression and localization of ion transporters contribute to diarrhea in mice with Salmonella-induced enteritis. *Gastroenterology*, *145*(6), 1358-1368 e1351-1354.

Masanta, W. O., Heimesaat, M. M., Bereswill, S., Tareen, A. M., Lugert, R., Gross, U., & Zautner, A. E. (2013). Modification of intestinal microbiota and its consequences for innate immune response in the pathogenesis of campylobacteriosis. *Clin Dev Immunol*, *2013*, 526860.

Masuda, S., Oda, Y., Sasaki, H., Ikenouchi, J., Higashi, T., Akashi, M., Nishi, E., & Furuse, M. (2011). LSR defines cell corners for tricellular tight junction formation in epithelial cells. *J Cell Sci*, *124*(Pt 4), 548-555.

McCardell, B., Madden, J. M., & Lee, E. C. (1984). Campylobacter jejuni and Campylobacter coli Production of a Cytotoxic Toxin Immunologically similar to Cholera Toxin *J Food Prot*, *47*(12), 943-949..

McGhee, J. R., & Fujihashi, K. (2012). Inside the mucosal immune system. *PLoS Biol*, *10*(9), e1001397.

Melvin, J. E., Park, K., Richardson, L., Schultheis, P. J., & Shull, G. E. (1999). Mouse down-regulated in adenoma (DRA) is an intestinal Cl(-)/HCO(3)(-) exchanger and is up-regulated in colon of mice lacking the NHE3 Na(+)/H(+) exchanger. *J Biol Chem*, *274*(32), 22855-22861.

Michlig, S., Harris, M., Loffing, J., Rossier, B. C., & Firsov, D. (2005). Progesterone down-regulates the open probability of the amiloride-sensitive epithelial sodium channel via a Nedd4-2-dependent mechanism. *J Biol Chem*, *280*(46), 38264-38270.

Moore, W. E., Holdeman, L. V., Cato, E. P., Smibert, R. M., Burmeister, J. A., Palcanis, K .G., & Ranney, R. R. (1985). Comparitive bacteriology of juvenile periodontitis. *Infect Immun*, *48*(2), 5017-19.

Morampudi, V., Graef, F. A., Stahl, M., Dalwadi, U., Conlin, V. S., Huang, T., Vallance, B. A., Yu, H. B., & Jacobson, K. (2017). Tricellular Tight Junction Protein Tricellulin Is Targeted by the Enteropathogenic Escherichia coli Effector EspG1, Leading to Epithelial Barrier Disruption. *Infect Immun*, *85*(1).

Morris, A. P., Kirk, K. L., & Frizzell, R. A. (1990). Simultaneous analysis of cell Ca^{2+} and Ca^{2+}-stimulated chloride conductance in colonic epithelial cells (HT-29). *Cell Regul*, *1*(12), 951-63.

Mousavi, S., Lobo de Sa, F. D., Schulzke, J. D., Bucker, R., Bereswill, S., & Heimesaat, M. M. (2019). Vitamin D in Acute Campylobacteriosis-Results From an Intervention Study Applying a Clinical Campylobacter jejuni Induced Enterocolitis Model. *Front Immunol*, *10*, 2094.

Mowat, A. M., & Bain, C. C. (2011). Mucosal macrophages in intestinal homeostasis and inflammation. *J Innate Immun*, *3*(6), 550-564.

Mozaffari Namin, B., & Soltan Dallal, M. M. (2018). Campylobacter Concisus and Its Effect on the Expression of CDX1 and COX2. *Asian Pac J Cancer Prev*, *19*(11), 3211-3216.

Mozaffari Namin, B., Soltan Dallal, M. M., & Ebrahimi Daryani, N. (2015). The Effect of Campylobacter concisus on Expression of IL-18, TNF-alpha and p53 in Barrett's Cell Lines. *Jundishapur J Microbiol*, *8*(12), e26393.

Mukhopadhya, I., Thomson, J. M., Hansen, R., Berry, S. H., El-Omar, E. M., & Hold, G. L. (2011). Detection of Campylobacter concisus and other Campylobacter species in colonic biopsies from adults with ulcerative colitis. *PLoS ONE*, *6*(6), e21490.

Musmano, R. A., Russi, M., Figura, N., Guglielmetti, P., Zanchi, A., Signori, R., Rossolini, A. (1998). Unusual species of campylobacters isolated in the Siena Tuscany area, Italy. *New Microbiol*, *21*(1), 15-22.

Nattramilarasu, P. K., Bucker, R., Lobo de Sa, F. D., Fromm, A., Nagel, O., Lee, I. M., Butkevych, E., Mousavi, S., Genger, C., Klove, S., Heimesaat, M. M., Bereswill, S., Schweiger, M. R., Nielsen, H. L., Troeger, H., & Schulzke, J. D. (2020). Campylobacter concisus Impairs Sodium Absorption in Colonic Epithelium via ENaC Dysfunction and Claudin-8 Disruption. *Int J Mol Sci*, *21*(2).

Nattramilarasu, P. K., Lobo de Sa, F. D., Schulzke, J. D., & Bucker, R. (2021). Immune-Mediated Aggravation of the Campylobacter concisus-Induced Epithelial Barrier Dysfunction. *Int J Mol Sci*, *22*(4).

Nickerson, C. A., Goodwin, T. J., Terlonge, J., Ott, C. M., Buchanan, K. L., Uicker, W. C., Emami, K., LeBlanc, C. L., Ramamurthy, R., Clarke, M. S., Vanderburg, C. R., Hammond, T., & Pierson, D. L. (2001). Three-dimensional tissue assemblies: novel models for the study of Salmonella enterica serovar Typhimurium pathogenesis. *Infect Immun*, *69*(11), 7106-7120.

Nielsen, H. L., Dalager-Pedersen, M., & Nielsen, H. (2020). High risk of microscopic colitis after Campylobacter concisus infection: population-based cohort study. *Gut*, *69*(11), 1952-1958.

Nielsen, H. L., Engberg, J., Ejlertsen, T., Bucker, R., & Nielsen, H. (2012). Short-term and medium-term clinical outcomes of Campylobacter concisus infection. *Clin Microbiol Infect*, *18*(11), E459-465.

Nielsen, H. L., Engberg, J., Ejlertsen, T., & Nielsen, H. (2013). Evaluation of fecal calprotectin in Campylobacter concisus and Campylobacter jejuni/coli gastroenteritis. *Scand J Gastroenterol*, *48*(5), 633-635.

Nielsen, H. L., Nielsen, H., Ejlertsen, T., Engberg, J., Gunzel, D., Zeitz, M., Hering, N. A., Fromm, M., Schulzke, J. D., & Bucker, R. (2011). Oral and fecal Campylobacter concisus strains perturb barrier function by apoptosis induction in HT-29/B6 intestinal epithelial cells. *PLoS ONE*, *6*(8), e23858.

Nielsen, H. L., Nielsen, H., & Torpdahl, M. (2016). Multilocus sequence typing of Campylobacter concisus from Danish diarrheic patients. *Gut Pathog*, *8*, 44.

Ogawa, M., Osada, H., Hasegawa, A., Ohno, H., Yanuma, N., Sasaki, K., Shimoda, M., Shirai, J., Kondo, H., & Ohmori, K. (2018). Effect of interleukin-1beta on occludin mRNA expression in the duodenal and colonic mucosa of dogs with inflammatory bowel disease. *J Vet Intern Med*, *32*(3), 1019-1025.

Ou, G., Rompikuntal, P. K., Bitar, A., Lindmark, B., Vaitkevicius, K., Wai, S. N., & Hammarstrom, M. L. (2009). Vibrio cholerae cytolysin causes an inflammatory response in human intestinal epithelial cells that is modulated by the PrtV protease. *PLoS ONE*, *4*(11), e7806.

Ousingsawat, J., Spitzner, M., Schreiber, R., & Kunzelmann, K. (2008). Upregulation of colonic ion channels in APC (Min/+) mice. *Pflugers Arch*, *456*(5), 847-855.

Pabst, R. (1987). The anatomical basis for the immune function of the gut. *Anat Empryol (Berl)*, *176*(2), 135-44.

Pastor, B. J., & Gibbons, R. J. (1986). Chemotactic response top formate by Campylobacter concisus and its potential role in gingival colonization. *Infect Immun*, *52*(2), 378-83.

Pope J. L., Ahamad, R., Bhat, A. A., Washington, M. K., Singh, A. B., & Dhawan, P. (2014). Claudin-1 overexpression in inteswtinal epithelial cells enhances susceptibility to adenamatous polyposis coli-mediated colon tumorigenesis. *Mol Cancer*, *13*, 167.

Prasad, S., Mingrino, R., Kaukinen, K., Hayes, K. L., Powell, R. M., MacDonald, T. T., & Collins, J. E. (2005). Inflammatory processes have differential effects on claudins 2, 3 and 4 in colonic epithelial cells. *Lab Invest*, *85*(9), 1139-1162.

Pulimood, A. B., Ramakrishna, B. S., Rita, A. B., Srinivasan, P., Mohan, V., Gupta, S., Perakath, B., Kang, G., Chandy, G., & Balasubramanian, K. A. (2008). Early activation of mucosal dendritic cells and macrophages in acute Campylobacter colitis and cholera: An in vivo study. *J Gastroenterol Hepatol*, *23*(5), 752-758.

Qi, Y., Wu, H. M., Yang, Z., Zhou, Y. F., Jin, L., Yang, M. F., & Wang, F. Y. (2021). New Insights into the Role of Oral Microbiota Dysbiosis in the Pathogenesis of Inflammatory Bowel Disease. *Dig Dis Sci*.

Rajendran, V. M., Geibel, J., & Binder, H. J. (2001). Characterization of apical membrane Cl-dependent Na/H exchange in crypt cells of rat distal colon. *Am J Physiol Gastrointest Liver Physiol*, *280*(3), G400-5.

Rajendran, V. M., & Sandle, G. I. (2018). Colonic Potassium Absorption and Secretion in Health and Disease. *Compr Physiol*, *8*(4), 1513-1536.

Raleigh, D. R., Marchiando, A. M., Zhang, Y., Shen, L., Sasaki, H., Wang, Y., Long, M., & Turner, J. R. (2010). Tight junction-associated MARVEL proteins marveld3, tricellulin, and occludin have distinct but overlapping functions. *Mol Biol Cell*, *21*(7), 1200-1213.

Richter, J. F., Hildner, M., Schmauder, R., Turner, J. R., Schumann, M., & Reiche, J. (2019). Occludin knockdown is not sufficient to induce transepithelial macromolecule passage. *Tissue Barriers*, *7*(2), 1612661.

Robinson, M. D., McCarthy, D. J., & Smyth, G. K. (2010). edgeR: a Bioconductor package for differential expression analysis of digital gene expression data. *Bioinformatics*, *26*(1), 139-140.

Rosenthal, R., Gunzel, D., Piontek, J., Krug, S. M., Ayala-Torres, C., Hempel, C., Theune, D., & Fromm, M. (2020). Claudin-15 forms a water channel through the tight junction with distinct function compared to claudin-2. *Acta Physiol (Oxf)*, *228*(1), e13334.

Rosenthal, R., Milatz, S., Krug, S. M., Oelrich, B., Schulzke, J. D., Amasheh, S., Gunzel, D., & Fromm, M. (2010). Claudin-2, a component of the tight junction, forms a paracellular water channel. *J Cell Sci*, *123*(Pt 11), 1913-1921.

Ruiz-Palacios, G. M., Torres, J., Torres, N. I., Escamilla, E., Ruiz-Palacios, B. R., & Tamayo, J. (1983). Cholera-like enterotoxin produced by Campylobacter jejuni. Characterization and clinical significance. *Lancet*, *2*(8344), 250-3.

Saitou, M., Furuse, M., Sasaki, H., Schulzke, J. D., Fromm, M., Takano, H., Noda, T., & Tsukita, S. (2000). Complex phenotype of mice lacking occludin, a component of tight juncion strands. *Mol Biol Cell*, *11*(12), 4131-42.

Sakaguchi, T., Köhler, H., Gu, X., McCormick, B. A., & Reinecker, H. C. (2002). Shigella flexneri regulates tight junction-associated proteins in human intestinal epithelial cellls. *Cell Microbiol*, *4*(6), 367-81.

Sandle, G. I. (1998). Salt and water absorption in the human colon: a modern appraisal. *Gut*, *43*(2), 294-9.

Sandle, G. I., Higgs, N., Crowe, P., Marsh, M. N., Venkatesan, S., & Peters, T. J. (1990). Cellular basis for defective electrolyte transport in inflamed human colon. *Gastroenterology*, *99*(1), 97-105.

Sassi, A., Wang, Y., Chassot, A., Komarynets, O., Roth, I., Olivier, V., Crambert, G., Dizin, E., Boscardin, E., Hummler, E., & Feraille, E. (2020). Interaction between Epithelial Sodium Channel gamma-Subunit and Claudin-8 Modulates Paracellular Sodium Permeability in Renal Collecting Duct. *J Am Soc Nephrol*, *31*(5), 1009-1023.

Schifferdecker, E., & Frömter, E. (1978). The AC impedence of Necturus gallbladder epithelium. *Pflugers Arch*, *377*(2), 125-33.

Schild, L., Schneeberger, E., Gautschi, I., & Firsov, D. (1997). Identification of amino acid residues in the alpha, beta, and gamma subunits of the epithelial sodium channel (ENaC) involved in amiloride block and ion permeation. *J Gen Physiol*, *109*(1), 15-26.

Schmidt, A. M., Escher, U., Mousavi, S., Tegtmeyer, N., Boehm, M., Backert, S., Bereswill, S., & Heimesaat, M. M. (2019). Immunopathological properties of the Campylobacter jejuni flagellins and the adhesin CadF as assessed in a clinical murine infection model. *Gut Pathog*, *11*, 24.

Schmidt, E., Kelly, S. M., & van der Walle, C. F. (2007). Tight junction modulation and biochemical characterisation of the zonula occludens toxin C-and N-termini. *FEBS Lett*, *581*(16), 2974-2980.

Schmitz, H., Rokos, K., Florian, P., Gitter, A. H., Fromm, M., Scholz, P., Ullrich, R., Zeitz, M., Pauli, G., & Schulzke, J. D. (2002). Supernatants of HIV-infected immune cells affect the barroer function of human HT-29/B6 intestinal epithelial cells. *AIDS*, *16*(7), 983-91.

Schneeberger, E. E., & Lynch, R. D. (1992). Structure, function, and regulation of cellular tight junctions. *Am J Physiol*, *262*(6 Pt 1), L647-61.

Schoen, H. F., & Candia, O. A. (1978). An inexpensive, high output voltage, voltage clamp for epithelial membranes. *Am J Physiol*, *235*(1), C69-72.

Schulthesis, P. J., Clarke, L. L., Meneton, P., Miller, M. L., Soleimani, M., Gawenia, L. R., Riddle, T. M., Duffy, J. J., Doetschmann, T., Wang, T., Giebisch, G., Aronson, P. S., Lorenz, J. N., & Shull, G. E. (1998). Renal and intestinal absorptive defects in mice lacking the NHE3 Na^+/H^+ exchanger. *Nat Genet*, *19*(39), 282-5.

Schulzke, J. D., Bojarski, C., Zeissig, S., Heller, F., Gitter, A. H., & Fromm, M. (2006). Disrupted barrier function through epithelial cell apoptosis. *Ann N Y Acad Sci*, *1072*, 288-299.

Schulzke, J. D., Gitter, A. H., Mankertz, J., Spiegel, S., Seidler, U., Amasheh, S., Saitou, M., Tsukita, S., & Fromm, M. (2005). Epithelial transport and barrier function in occludin-deficient mice. *Biochim Biophys Acta*, *1669*(1), 34-42.

Schulzke, J. D., Ploeger, S., Amasheh, M., Fromm, A., Zeissig, S., Troeger, H., Richter, J., Bojarski, C., Schumann, M., & Fromm, M. (2009). Epithelial tight junctions in intestinal inflammation. *Ann N Y Acad Sci*, *1165*, 294-300.

Schweinfest, C. W., Henderson, K. W., Suster, S., Kondoh, N., & Papas, T. S. (1993). Identification of a colon mucosa gene that is down-regulated in colon adenomas and adenocarconomas. *Proc Natl Acad Sci U S A*, *90*(9), 4166-70.

Shen, L., Su, L., & Turner, J. R. (2009). Mechanisms and functional implications of intestinal barrier defects. *Dig Dis*, *27*(4), 443-449.

Shen, L., Weber, C. R., Raleigh, D. R., Yu, D., & Turner, J. R. (2011). Tight junction pore and leak pathways: a dynamic duo. *Annu Rev Physiol*, *73*, 283-309.

Shifflett, D. E., Clayburgh, D. R., Koutsouris, A., Turner, J. R., & Hecht, G. A. (2005). Enteropathogenic E. coli disrupts tight junction barrier function and structure in vivo. *Laboratory Investigation*, *85*(10), 1308-1324.

Siegmund, B., Lehr, H. A., Fantuzi, G., & Dinarello, C. A. (2001). IL-1 beta-converting enzyme (caspase-1) in intestinal inflammation. *Proc Natl Acad Sci U S A, 98*(23), 1329-54.

Smith, P. D., Smythies, L. E., Shen, R., Greenwell-Wild, T., Gliozzi, M., & Wahl, S. M. (2011). Intestinal macrophages and response to microbial encroachment. *Mucosal Immunol, 4*(1), 31-42.

Soundrarajan, R., Melters, D., Shih, I. C., Wang, J., & Pearce, D. (2009). Epithelial sodium channel regulated by differential composition of a signaling complex. *Proc Natl Acad Sci U S A, 106*(19), 7804-9.

Staehelin, L. A., Mukherjee, T. M., & Williams, A. W. (1969). Fine structure of frozen-etched tight junctions. *Naturwissenschaften, 56*(3), 142.

Staehelin, L. A. (1972). Three types of gap junctions interconnecting intestinal epithelial cells visulaozed by freeze-etching. *Proc Natl Acad Sci U S A, 69*(5), 1318-21.

Staehelin, L. A. (1973). Further observations on the fine structure of freeze-cleaved tight junctions. *J Cell Sci, 13*(3), 763-86.

Stanfield, J. T., McCardell, B. A., & Madden, J. M. (1987). Campylobacter diarrhea in adult mouse model. *Microb Pathog, 3*(3), 155-65.

Staruschenko, A., Medina, J. L., Patel, P., Shapiro, M. S., Booth, R. E., & Stockand, J. D. (2004). Fluorescence resonance energy transfer analysis of subunit stoichiometry of the epithelial Na+ channel. *J Biol Chem, 279*(26), 27729-27734.

Stockmann, M., Schmitz, H., Fromm, M., Schmidt, W., Pauli, G., Scholz, P., Riecken, E. O., & Schulzke, J. D. (2000). Mechanisms of epithelial barrier impairment in HIV infection. *Ann N Y Acad Sci, 915*, 293-303.

Stockmann, M., Fromm, M., Schmitz, H., Schmidt, W., Riecken, E. O., Schulzke, J. D. (1998). Duodenal biopsies of HIV-infected patients with diarrrhoea exhibit epithelial barrier defects but no active secretion. *AIDS*, *12*(1), 43-51.

Sun, X., Threadgill, D., & Jobin, C. (2012). Campylobacter jejuni induces colitis through activation of mammalian target of rapamycin signaling. *Gastroenterology*, *142*(1), 86-95 e85.

Sun, Y., Zhang, J. N., Zhao, D., Wang, Q. S., Gu, Y. C., Ma, H. P., & Zhang, Z. R. (2011). Role of the epithelial sodium channel in salt-sensitive hypertension. *Acta Pharmacol Sin*, *32*(6), 789-797.

Tafazoli, F., Magnusson, K. E., & Zheng, L. (2003). Disruption of epithelial barrier integrity by Salmonella enterica serovar typhimurium requires geranylgeranylated proteins. *Infect Immun*, *71*(2), 872-881.

Takada, Y., Hisamatsu, T., Kamada, N., Kitazume, M. T., Honda, H., Oshima, Y., Saito, R., Takayama, T., Kobayashi, T., Chinen, H., Mikami, Y., Kanai, T., Okamoto, S., & Hibi, T. (2010). Monocyte chemoattractant protein-1 contributes to gut homeostasis and intestinal inflammation by composition of IL-10-producing regulatory macrophage subset. *J Immunol*, *184*(5), 2671-2676.

Tamura, A., Hayashi, H., Imasato, M., Yamazaki, Y., Hagiwara, A., Wada, M., Noda, T., Watanabe, M., Suzuki, Y., & Tsukita, S. (2011). Loss of claudin-15, but not claudin-2, causes Na+ deficiency and glucose malabsorption in mouse small intestine. *Gastroenterology*, *140*(3), 913-923.

Tanaka, H., Yamamoto, Y., Kashihara, H., Yamazaki, Y., Tani, K., Fujiyoshi, Y., Mineta, K., Takeuchi, K., Tamura, A., & Tsukita, S. (2016). Claudin-21 Has a Paracellular Channel Role at Tight Junctions. *Mol Cell Biol*, *36*(6), 954-964.

Tanner, A. C., Badger, S., Lai, C. H., Listgarten, M. A., Visconti, R. A., Socransky, S. S. (1981). Wolinella gen. nov., Wolinella succinogens (Vibrio suiccinogens Wlin et al.) comb. nov., and Disruption of Bacteroides gracilis sp. nov., Campylobacter concisus sp. nov., and Eikenella corrodens from Humans with Periodontal Disease. *Int J Syst Bacteriol*, *31*(4), 432-445.

Tanner, A. C., Strzempko, M. N., Belsky, C. A., & McKinley, G. A. (1985). API ZYM and API An-Ident reactions of fastidious oral gram-negative species. *J Clin Microbiol*, *22*(3), 333-5.

Tanner, A. C., Dzink, J. L., Ebersole, J. L., & Socransky, S. S. (1987). Wolinella recta, campylobacter concisus, bacteroides gracilis, and Eikenella corrodens from periodontal lesions. *J Periodontal Res*, *22*(4), 327-30.

Tominaga, H., Ishiyama, M., Ohseto, F., Sasamato, K., Hamamoto, T., Suzuki, K., & Watanabe, M. (1999). A water-soluble tetrazolium salt useful for colorimetric cell viability assay. *Anal Commun*, *36*, 47-50.

Treuting, P. M., & Dintzis, S. M. (2012). Lower Gastrointestinal Tract. In *Comparative Anatomy and Histology* (pp. 177-192).

Troeger, H., Epple, H. J., Schneider, T., Wahnschaffe, U., Ullrich, R., Burchard, G. D., Jelinek, T., Zeitz, M., Fromm, M., & Schulzke, J. D. (2007b). Effect of chronic Giardia lamblia infection on epithelial transport and barrier function in human duodenum. *Gut*, *56*(3), 328-335.

Troeger, H., Richter, J. F., Beutin, L., Gunzel, D., Dobrindt, U., Epple, H. J., Gitter, A. H., Zeitz, M., Fromm, M., & Schulzke, J. D. (2007a). Escherichia coli alpha-haemolysin induces focal leaks in colonic epithelium: a novel mechanism of bacterial translocation. *Cell Microbiol*, *9*(10), 2530-2540.

Tsai, C. L., Chiu, Y. M., Lee, Y. J., Hsieh, C. T., Shieh, D. C., Tsay, G. J., Bau, D. T., & Wu, Y. Y. (2018). Interleukin-32 plays an essential role in human calcified aortic valve cells. *Eur Cytokine Netw*, *29*(1), 36-47.

Tsukita, S., Furuse, M., & Itoh, M. (2001). Multifunctional strands in tight junctions. *Nat Rev Mol Cell Biol*, *2*(4), 285-93.

Underwood, A. P., Kaakoush, N. O., Sodhi, N., Merif, J., Seah Lee, W., Riordan, S. M., Rawlinson, W. D., & Mitchell, H. M. (2016). Campylobacter concisus pathotypes are present at significant levels in patients with gastroenteritis. *J Med Microbiol*, *65*(3), 219-226.

Van Etterijck, R., Breynaert, J., Revets, H., Devreker, T., Vandenplas, Y., Vandamme, P., & Lauwers, S. (1996). Isolation of Campylobacter concisus from feces of children with and without diarhhea. *J Clin Microbiol*, *34*(9). 2304-6.

Van Itallie, C. M., & Anderson, J. M. (2014). Architecture of tight junctions and principles of molecular composition. *Semin Cell Dev Biol*, *36*, 157-165.

Vandamme, P., Falsen, E., Pot, B., Hoste, B., Kersters, K., & De Ley, J. (1989). Identification of EF group 22 campylobacters from gastroenteritis cases as Campylobacter concisus. *J Clin Microbiol*, *27*(8), 1775-81.

Vandenberg, O., Cornelius, A. J., Souayah, H., Martiny, D., Vlaes, L., Brandt, S. M., & On, S. L. (2013). The role of Epsilonproteobacteria in children with gastroenteritis. *Pediatr Infect Dis J*, *32*(10), 1140-1142.

Verheyen, L., Degryse, F., Niewold, T., & Smolders, E. (2012). Labile complexes facilitate cadmium uptake by Caco-2 cells. *Sci Total Environ*, *426*, 90-99.

Waldström, T., Baloda, S. B., Krovacek, K., Faris, A., Bengston, S., & Walder, M. (1983). Swedish isolates of Campyloabcter jejuni/coli do not produce cytotonic or cytotoxic enterotoxins. *Lancet*, *322*(8355), 911.

Wang, Y., Liu, F., Zhang, X., Chung, H. K. L., Riordan, S. M., Grimm, M. C., Zhang, S., Ma, R., Lee, S. A., & Zhang, L. (2017). Campylobacter concisus Genomospecies 2 Is Better Adapted to the Human Gastrointestinal Tract as Compared with Campylobacter concisus Genomospecies 1. *Front Physiol*, *8*, 543.

Wassenaar, T. M. (1997). Toxin proiduction by Campylobacter spp. *Clin Microbiol Rev*, *10*(3), 466-76.

Weber, C. R., Nalle, S. C., Tretiakova, M., Rubin, D. T., & Turner, J. R. (2008). Claudin-1 and claudin-2 expression is elevated in inflammatory bowel disease and may contribute to early neoplastic transformation. *Lab Invest*, *88*(10), 1110-1120.

Welsh, M. J., Smith, P. L., Fromm, M., & Frizzell, R. A. (1982). Crypts are the site of intestinal fluid and electrolyte secretion. Science, *218*(4578), 1219-21.

Will, P. C., Lebowitz, J. L., & Hopfer, U. (1980). Induction of amiloride-sensitive sodium transport in the rat colon by mineralocorticoids. *Am J Physiol*, *238*(4), F261-8.

Yde Aagaard, M. E., Frahm Kirk, K., Linde Nielsen, H., Harder Tarpgaard, I., Bach Hansen, J., & Nielsen, H. (2020). Campylobacter concisus is prevalent in the gastrointestinal tract of patients with microscopic colitis. *Scand J Gastroenterol*, *55*(8), 924-930.

Yrios, J. W., & Balish, E. (1986). Colonization and infection of athymic and euthymic germfree mice by Campylobacter jejuni and Campylobacter fetus subsp. fetus. *Infect Immun*, *53*(2), 378-83.

Yu, A. S., Enck, A. H., Lencer, W. I., & Schneeberger, E. E. (2003). Claudin-8 expression in Madin-Darby canine kidney cells augments the paracellular barrier to cation permeation. *J Biol Chem*, *278*(19), 17350-17359.

Yu, A. S., McCarthy, K. M., Francis, S. A., McCormack, J. M., Lai, J., Rogers, R. A., Lynch, R. D., & Schneeberger, E. E. (2005). Knockdown of occludin expression leads to diverse phenotypic alterations in epithelial cells. *Am J Physiol Cell Physiol*, *288*(6), C1231-1241.

Zeissig, S., Bergann, T., Fromm, A., Bojarski, C., Heller, F., Guenther, U., Zeitz, M., Fromm, M., & Schulzke, J. D. (2008). Altered ENaC expression leads to impaired sodium absorption in the noninflamed intestine in Crohn's disease. *Gastroenterology*, *134*(5), 1436-1447.

Zeissig, S., Burgel, N., Gunzel, D., Richter, J., Mankertz, J., Wahnschaffe, U., Kroesen, A. J., Zeitz, M., Fromm, M., & Schulzke, J. D. (2007b). Changes in expression and distribution of claudin 2, 5 and 8 lead to discontinuous tight junctions and barrier dysfunction in active Crohn's disease. *Gut*, *56*(1), 61-72.

Zeissig, S., Fromm, A., Mankertz, J., Weiske, J., Zeitz, M., Fromm, M., & Schulzke, J. D. (2007a). Butyrate induces intestinal sodium absorption via Sp3-mediated transcriptional up-regulation of epithelial sodium channels. *Gastroenterology*, *132*(1), 236-248.

Zeissig, S., Fromm, A., Mankertz, J., Zeitz, M., Fromm, M., & Schulzke, J. D. (2006). Restoration of ENaC expression by glucocorticoid receptor transfection in human HT-29/B6 colon cells. *Biochem Biophys Res Commun*, *344*(4), 1065-1070.

Zhang, L., Danon, S. J., Greham, M., Chan, V., Lee, A., & Mitchell, H. (2005). Natural colonization with Helicabacter species and the development of inflammatory bowel disease in interleukin-10-deficient mice. *Helicobacter*, *10*(3), 223-30.

Zhang, L., Budiman, V., Day, A. S., Mitchell, H., Lemberg, D. A., Riordan, S. M., Grimm, M., Leach, S. T., & Ismail, Y. (2010). Isolation and detection of Campylobacter concisus from saliva of healthy individuals and patients with inflammatory bowel disease. *J Clin Microbiol*, *48*(8), 2965-2967.

I. Abbreviations

AJ	Adherens junction
APC	Adenomatous polyposis coli
APS	Ammonium persulfate
ATPase	adenosice triphosphatase
BALB/c	Bagg Albino/c
BCA	Bicinchoninic acid assay
BSA	Bovine serum albumin
bTJ	Bicellular TJ
ca.	Circa
CaCC	Calcium-activated chloride channel
cAMP	cyclic adenosine monophosphate
CBA	Cytometric bead array
CCK-8	Cell Counting Kit-8
CD	Crohn's Disease
CDT	cytolethal distending toxin
CFTR	Cystic fibrosis transmembrane conductance regulator
CFU	Colony forming unit
cGMP	cyclic guanosine monophosphate
CHO	Chinese hamster ovary cells
CLSM	Confocal laser scanning microscopy
Csep1	*Campylobacter concisu*s-secreted protein 1
CT	Cholera toxin
DANN	Deoxyribonucleic acid
DAPI	4′,6-diamidino-2-phenylindole
DMSO	Dimethyl sulfoxide
DRA	down regulated in adenoma
DRA	Down-regulated in adenoma
DSS	Dextran sulfate sodium
DTT	Dithiotheritol
ECL	Extracellular loop
EDTA	Ethylene diamine tetraacetic acid
EGTA	Ethylene glycol tetraacetic acid
ENaC	Epithelial sodium channel
FACS	Fluorescence-activated Cell Sorting
FCS	Fetal calf serum
FFEM	Freeze-fracture electron microscopy
FITC	Fluorescein isothiocyanate
FRET	Fluorescence Resonance Energy Transfer
GAPDH	Glyceraldehyde-3-Phosphate Dehydrogenase
GC	Glucocorticoids
GF	Germ-free
GJ	Gap junction
GR	Glucocorticoid receptor
IBD	Inflammatory Bowel Disease
IFN	Interferon

IL	Interleukin
IPA	Ingenuity pathway analysis
I_{SC}	Short-circuit current
JAM	junctional adhesion molecule
LOS	Lipooligosaccharide
LPS	Lipopolysaccharide
MAPK	Mitogen-activated protein kinase
MC	Mineralocorticoids
MDCK	Madin-Darby Canine Kidney
MOI	Multiplicty of infection
MR	Mineralocorticoid receptor
NEDD	Neuronally expressed developmentally downregulated
NF-κB	Nuclear factor 'kappa-light-chain-enhancer' of activated B-cells
NHE	Sodium-hydrogen antiporter
NKCC	Sodium Potassium Chloride co-transporter
OD	Optical density
P/S	Penicillin/Streptomycin
PAR-2	Protease-activated receptor-2
PBMC	Peripheral blood mononuclear cell
PBS	Phosphate-buffered saline
PFA	Paraformaldehyde
PGE_2	Prostaglandin E_2
PKC	protein kinase C
PLA2	Phospholipase A2
PMA	Phorbol 12-myristate 13-acetate
PMSF	Phenylmethylsulfonyl fluoride
PRR	Pattern recognition receptor
PVDF	Polyvinyldendifluoride
PVP-40	Polyvinylpyrrolidone
RNA	Ribonucleic acid
RNA-Seq	RNA sequencing
rpm	revolutions per minute
SDS	Sodium dodecyl sulphate
SPF	Specific pathogen-free
SRE	Steroid-responsive element
TdT	Terminal deoxynucleotidyl Transferase
TEMED	Tetramethylethylenediamine
TER	Transepithelial electrical resistance
TJ	Tight junction
TNF	Tumour necrosis factor
tTJ	Tricellular TJ
TUNEL	Terminal deoxynucleotidyl transferase dUTP nick end labeling
UC	Ulcerative colitis
WT	wild type
ZOT	Zonula occludens toxin

II. List of Figures

III. List of Tables

IV. List of publications

1. **Nattramilarasu, P. K., Bucker, R., Lobo de Sa, F. D., Fromm, A., Nagel, O., Lee, I. M., Butkevych, E., Mousavi, S., Genger, C., Klove, S., Heimesaat, M. M., Bereswill, S., Schweiger, M. R., Nielsen, H. L., Troeger, H., & Schulzke, J. D. (2020).** Campylobacter concisus Impairs Sodium Absorption in Colonic Epithelium via ENaC Dysfunction and Claudin-8 Disruption. *Int J Mol Sci*, *21*(2).

2. **Nattramilarasu, P. K., Lobo de Sa, F. D., Schulzke, J. D., & Bucker, R. (2021).** Immune-Mediated Aggravation of the Campylobacter concisus-Induced Epithelial Barrier Dysfunction. *Int J Mol Sci*, *22*(4).

3. **Lobo de Sa, F. D., Butkevych, E., Nattramilarasu, P. K., Fromm, A., Mousavi, S., Moos, V., Golz, J. C., Stingl, K., Kittler, S., Seinige, D., Kehrenberg, C., Heimesaat, M. M., Bereswill, S., Schulzke, J. D., & Bucker, R. (2019).** Curcumin Mitigates Immune-Induced Epithelial Barrier Dysfunction by Campylobacter jejuni. *Int J Mol Sci*, *20*(19).

4. **Butkevych, E., Lobo de Sa, F. D., Nattramilarasu, P. K., & Bucker, R. (2020).** Contribution of Epithelial Apoptosis and Subepithelial Immune Responses in Campylobacter jejuni-Induced Barrier Disruption. *Front Microbiol*, *11*, 344.

5. **Lobo de Sa, F. D., Heimesaat, M. M., Bereswill, S., Nattramilarasu, P. K., Schulzke, J. D., & Bucker, R. (2021).** Resveratrol Prevents Campylobacter jejuni-Induced Leaky gut by Restoring Occludin and Claudin-5 in the Paracellular Leak Pathway. *Front Pharmacol*, *12*, 640572.

V. Supplemental files

Upstream regulator	**Activation *Z*-score**	***P*-value of overlap**	**Target Molecule in dataset**
IFN-γ	1.225	8.43×10^{-4}	AQP1, ASNS, CEACAM5, CFTR, CHAC1, LAMP3, LCN2, **IL-32**, SLC7A11, SLC7A5
IL-1β	0.340	4.39×10^{-3}	CFTR, CRYAB, CYP1A1, FAM129A, **IL-32**, LCN2, SLC7A11
Lipopolysaccharide (LPS)	2.100	1.76×10^{-4}	AQP1, CFTR, CRYAB, CYP1A1, **IL-32**, LAMP3, LCN2, LYZ, S100A2, SLC7A11, TDO2, TRIB3, ULBP1
IL-5	2.000	3.68×10^{-3}	ASNS, HSPA6, PSAT1, SLC7A5
NF-κB complex	1.085	6.77×10^{-5}	AQP1, CD7, CFTR, **IL-32**, LCN2, SLC7A5, TDO2, TRIB3
Dexamethasone	1.720	5.83×10^{-6}	AQP1, ASNS, CEACAM5, CEACAM6, CEACAM7, CRYAB, CYP1A1, DNER, FAM129A, **IL-32**, HSPA6, LAMA1, LCN2, SPINK13, TDO2, TRIM31

Table S1. Upstream regulator analysis performed with Ingenuity Pathway Analysis (IPA) from RNA-Seq data to compare controls against *Campylobacter concisus*-infected HT-29/B6-GR/MR cells 48 hours post infection. The activation *Z*-score, overlap *P*-value and target molecules of different upstream regulators activated by *C. concisus* in DBA-stimulated HT-29/B6-GR/MR monolayers. The cytokine pathways of interferon-γ (IFN-γ) and interleukin-1β (IL-1β), and bacterial LPS were activated and target IL-32 (referring to the scheme, Figure 20). Interleukin-5 (IL-5) was another cytokine pathway found to be activated. In addition, other upstream regulators, NF-κB complex and dexamethasone which were activated, and target IL-32 are also displayed in the table. IL-32 is highlighted in the target molecule dataset. The overlap *P*-value calculated by Fisher's exact test measures whether there is a statistically significant overlap between the data set genes and the genes regulated by an upstream transcriptional regulator. The statistical significance is generally attributed to *P*-values < 0.01. *Z*-score determines whether an upstream transcriptional regulator has significantly more ''activated'' predictions than ''inhibited'' predictions ($z>0$) or vice versa ($z<0$). DBA = dexamethasone, butyrate and aldosterone (modified from Nattramilarasu et al., 2020).

Ion transporters	Gene name	Controls (mRNA)	*C. concisus* (mRNA)	Adjusted *P*-value
CFTR	***CFTR***	1290 ± 92	326 ± 24	0.003
NKCC1	***SLC12A2***	34296 ± 1812	16279 ± 619	0.001
NHE3	***SLC9A3***	142 ± 20	102 ± 3.8	0.841
Na^+/K^+-ATPase	***ATP1A1***	93251 ± 12562	81365 ± 986	0.954
CaCC	***CLCA1***	3 ± 1.5	0.7 ± 0.3	NA
DRA	***SLC26A3***	17 ± 8.3	6.3 ± 1.3	NA

Table S2. Gene expression changes of different absorptive and secretory transporters that influence the sodium absorption and ENaC function in controls and *Campylobacter concisus*-infected HT-29/B6-GR/MR monolayers after DBA stimulation. The mRNA expression changes were depicted as gene counts calculated by differential gene expression analysis using RNA-Seq (n = 3) and represented as mean ± SEM along with adjusted *P*-values (NA = not applicable). *P*-values were adjusted by Benjamin-Hochberg procedure. Adjusted *P*-values < 0.05 is considered as statistically significant. CFTR - cystic fibrosis transmembrane conductance regulator, NKCC1 - Na-K-Cl co-transporter 1, NEDD4-2 - neural precursor cell expressed developmentally downregulated protein 4-2, NHE3 - sodium-hydrogen antiporter 3, Na^+/K^+ATPase - sodium-potassium adenosine triphosphatase, CaCC - calcium-activated chloride channel, and DRA – Down-Regulated in Adenoma. DBA = dexamethasone, butyrate and aldosterone (modified from Nattramilarasu et al., 2020).

Declaration of independence:

I hereby confirm that I have written the present work independently and have not used any other aids than those specified. All statements taken from external sources in the wording or in the sense of the meaning are indicated by the origin.

This work has not been presented to any other examination committee in the same or a similar form and has not been published either.

Berlin,

[Praveen Kumar Nattramilarasu]